

DTIC FILE COPY

AD-A202 572



NONLINEAR FINITE ELEMENT ANALYSIS  
OF A GENERAL COMPOSITE SHELL

THESIS

Gregory S. Egan  
Captain, USAF

AFIT/GAE/AA/88D-12

**DISTRIBUTION STATEMENT A**

Approved for public release;  
Distribution Unlimited

DEPARTMENT OF THE AIR FORCE  
AIR UNIVERSITY

**AIR FORCE INSTITUTE OF TECHNOLOGY**

Wright-Patterson Air Force Base, Ohio

89 1 17 100

DTIC  
ELE.

JAN 17 1989

S

AD

1

AFIT/GAE/AA/88D-12

DTIC  
S JAN 17 1989  
CD

NONLINEAR FINITE ELEMENT ANALYSIS  
OF A GENERAL COMPOSITE SHELL

THESIS

Gregory S. Egan  
Captain, USAF

AFIT/GAE/AA/88D-12

DTIC  
CRA&I  
USA

Accession For	
NTIS CRA&I	<input checked="" type="checkbox"/>
DTIC TAB	<input type="checkbox"/>
Unannounced	<input type="checkbox"/>
Justification	
By	
Distribution	
Availability Codes	
Dist	Special
A-1	

Approved for public release; distribution unlimited

AFIT/GAE/AA/88D-12

NONLINEAR FINITE ELEMENT ANALYSIS  
OF A GENERAL COMPOSITE SHELL

THESIS

Presented to the Faculty of the School of Engineering  
of the Air Force Institute of Technology  
Air University  
in Partial Fulfillment of the  
Requirements for the Degree of  
Master of Science in Aeronautical Engineering

by

Gregory S. Egan  
Captain, USAF

December 1988

Approved for public release; distribution unlimited

### Acknowledgements

I wish to express my extreme gratitude to Dr. Anthony Palazotto for his patience, expert guidance, and sense of humor throughout this thesis.

I would like to thank Dr. James Olsen of the Air Force Wright Aeronautics Laboratory (AFWAL) for sponsoring this thesis work. Also, I would like to thank Dr. Narendra Khott, Vicki Tischler, and Holly Lowndes of the AFWAL and George Pearly of the 4950th ABW for technical support throughout the thesis.

Many thanks to the NASA Langley Research Center/ Structural Mechanics Branch for advise on running STAGS and in particular Dr. Gaylen Thurston for obtaining the latest version of STAGSC-1.

To Janet Mawhirter for her help on the VAX computer.

And last but definitely not least, to my wife Trisha, and kids, Dawn and Duke, for all the support and encouragement over the last 18 months.

## Table of Contents

	Page
Acknowledgements. . . . .	ii
List of Figures . . . . .	v
List of Tables. . . . .	viii
List of Symbols . . . . .	ix
Abstract. . . . .	xii
1. Introduction . . . . .	1
1.1 Objectives. . . . .	3
1.2 Scope . . . . .	3
2. Theory . . . . .	5
2.1 Nonlinear Shell Theory. . . . .	6
2.2 STAGSC-1 Theory . . . . .	9
2.2.1 Strain Displacement Relations. . . . .	9
2.2.2 Derivation of the Tangent Stiffness Matrix . .	11
2.2.3 Pressure Loading . . . . .	22
2.2.4 Plate Elements Representing a Shell. . . . .	23
2.2.5 Solution Techniques. . . . .	26
3. Finite Element Modeling. . . . .	32
3.1 Convergence Test. . . . .	40
3.2 Phase I Modeling. . . . .	50
3.3 Phase II Modeling . . . . .	57
3.4 Phase III Modeling. . . . .	70
4. Experimentation. . . . .	75
5. Comparison of Experimental and Finite Element Model Displacements. . . . .	88
6. Laminate Strength Analysis . . . . .	92
7. Conclusions. . . . .	97
Appendix A: Derivation of the STAGSC-1 Nonlinear Strain Displacement Equations . . . . .	99
Appendix B: Variational Formulation. . . . .	103
Appendix C: Classical Laminated Plate Theory . . . . .	106
Appendix D: Surface Normal Calculations. . . . .	112

Appendix E: Convergence Model: 1 to 1 Aspect Ratio. . . . .	114
Appendix F: UPRESS Subroutine for Convergence Test . . . . .	116
Appendix G: Finite Element Model (Model 6) . . . . .	118
Appendix H: UPRESS Subroutine for Finite Element Models 6 and 7. . . . .	156
Bibliography. . . . .	160
Vita. . . . .	162

## List of Figures

Figure	Page
2.1 Cylindrical Shell Section Showing Coordinate and Displacement Directions [4] . . . . .	8
2.2 STAGS QUA4 410 and 411 Quadrilateral Element [16] . . . . .	24
2.3 Flat Plate Element Representing a Curved Shell [13]. . . . .	25
2.4 Quadrilateral Element Local Reference System [17] . . . . .	28
3.1 Kevlar/Polyester Composite Shell. . . . .	33
3.2 Finite Element Model Side View. . . . .	34
3.3 Finite Element Model Front and Rear View. . . . .	35
3.4 Finite Element Model Angle View . . . . .	36
3.5 Finite Element Model and Loading Regions. . . . .	38
3.6 Ellipsoid Surface (X,Y) and Global (x,y,z) Reference System. . . . .	41
3.7 Convergence Test Finite Element Models with Loading Regions . . . . .	43
3.8 Convergence Test Results for $\sigma_x$ at X=75 degrees . . . . .	46
3.9 Convergence Test Results for $\sigma_x$ at X=105 degrees. . . . .	47
3.10 Convergence Test Results for $\sigma_y$ at X=75 degrees . . . . .	48
3.11 Convergence Test Results for $\sigma_y$ at X=105 degrees. . . . .	49
3.12 Shell Thickness Variation . . . . .	51
3.13 Node 168 Phase I Modeling: Isotropic Material, 410 Element, Clamped B.C. . . . .	55
3.14 Node 176 Phase I Modeling: Isotropic Material, 410 Element, Clamped B.C. . . . .	56
3.15 Shell Lower Boundary. . . . .	63
3.16 Modified Finite Element Boundary Condition. . . . .	66

3.17	Node 168 Phase II Modeling: Orthotropic Material Variable Thickness, 410 Element . . . . .	68
3.18	Node 176 Phase II Modeling: Orthotropic Material Variable Thickness, 410 Element . . . . .	69
3.19	Node 168 Phase III Modeling: Variable Thickness, Modified B.C.s. . . . .	73
3.20	Node 176 Phase III Modeling: Variable Thickness, Modified B.C.s. . . . .	74
4.1	Aluminum Frame. . . . .	75
4.2	Rubber Bladders . . . . .	76
4.3	Experimental Set-Up . . . . .	77
4.4	Close-Up of Displacement Transducers. . . . .	78
5.1	Deformed vs. Undeformed Finite Element Cross Section. . .	81
5.2	Shell and Finite Element Nodes Used for Comparison. . . .	82
5.3	Node 151: Experimental vs. Finite Element Surface Normal Displacement . . . . .	83
5.4	Node 159: Experimental vs. Finite Element Surface Normal Displacement . . . . .	84
5.5	Node 168: Experimental vs. Finite Element Surface Normal Displacement . . . . .	85
5.6	Node 176: Experimental vs. Finite Element Surface Normal Displacement . . . . .	86
5.7	Node 219: Experimental vs. Finite Element Surface Normal Displacement . . . . .	87
5.8	Node 227: Experimental vs. Finite Element Surface Normal Displacement . . . . .	88
5.9	Node 163: Experimental vs. Finite Element Surface Normal Displacement . . . . .	90
6.1	Tsai-Wu Composite Failure Analysis. . . . .	95
A.1	Line Element in Undeformed and Deformed State [7] . . . .	100
C.1	Coordinate System, Displacements, and Force and Moment Resultants. . . . .	107
C.2	Principal (x,y,z) and Material (1,2,3) Axis Systems . . .	109



C.3	Geometry of an N-Layered Laminate [14]. . . . .	110
D.1	Hypothetical Finite Element Surface . . . . .	112

## List of Tables

Figure	Page
3.1 Static Equivalent Loads . . . . .	37
3.2 Phase I Models. . . . .	50
3.3 Phase II Models . . . . .	57
3.4 Actual Shell Ply Lay Up . . . . .	61
3.5 Phase III Models. . . . .	71
4.1 Modified Static Equivalent Loads. . . . .	79

### List of Symbols

$d$	Variation
$E$	Young's modulus
$h$	Metric coefficients
$F$	Strength tensors
$G$	Shear modulus
$S$	Ultimate longitudinal shear strength
$t$	Thickness
$U$	Internal strain energy
$W$	External work due to applied loads
$u, v, w$	Displacements in the $x, y, z$ directions, respectively
$x, y, z$	Structural axis
$1, 2, 3$	Lamina principal axis
$M_x, M_y, M_{xy}$	Moment resultants
$N_x, N_y, N_{xy}$	Force resultants
$Q_{ij}$	Reduced stiffnesses
$\bar{Q}_{ij}$	Transformed reduced stiffnesses
$R_x, R_y$	Principal radii
$X_t, X_c$	Ultimate strength (tension/compression) in the 1-direction
$Y_t, Y_c$	Ultimate strength (tension/compression) in the 2-direction
$\alpha$	Metric coefficients
$\beta$	Average rotation
$\gamma$	Shear strain
$\epsilon$	Normal strain
$\nu$	Poisson's ratio

$\Pi$	Total potential energy
$\sigma$	Normal stress
$\tau$	Shear stress
$\phi$	Rotational terms
$\zeta_3$	Distance from midsurface
$\theta_x, \theta_y, \theta_z$	Rotations about the subscript axis
$\kappa_x, \kappa_y, \kappa_{xy}$	Curvatures
$\{a\}$	Nodal displacements (parameters)
$[A], [B], [D]$	Submatrices of the orthotropic material matrix
$[B]$	Product of $[L]$ and $[N]$
$[D]$	Material matrix
$\{f\}$	Nodal forces of the element
$[G]$	Matrix of coordinates after differentiating the shape functions
$[K]$	Stiffness matrix
$[L]$	Differential operator matrix
$[N]$	Shape functions
$[R]$	Matrix of derivatives
$[B_0]$	Constant $[B]$ matrix
$[B_L]$	$[B]$ matrix which is function of displacements
$[K_0]$	Linear portion of the tangent stiffness matrix
$[K_L]$	Nonlinear portion of the tangent stiffness matrix
$[K_T]$	Tangent stiffness matrix
$[K_\sigma]$	Initial stress matrix
$\{\epsilon\}$	Vector of strains
$\{\sigma\}$	Vector of stresses
$\{\theta\}$	Matrix of derivatives

$\{\Psi\}$  Sum of external and internal generalized forces  
 $\{\Psi(a)\}$  Sum of external and internal generalized forces as a function of displacements  
 $\{\epsilon_o\}, \{\sigma_o\}$  Initial strain and stress, respectively  
 Subscript "e" indicates element reference  
 Subscript "g" indicates global reference  
 Superscript "o" indicates midsurface values  
 Superscript "b" indicates bending terms  
 Superscript "p" indicates in-plane terms

### Abstract

2. An analytical study, using the STAGSC-1 computer code, was conducted on a Kevlar/Polyester composite shell of general shape with internal asymmetrical pressure loading. Experimentation was conducted on the shell ~~by the Air Force Wright Aeronautics Laboratory, Wright-Patterson AFB, Ohio~~ to find displacements in the shell due to this internal pressure loading.

Modeling of the composite structure was done in increments whereby each change in the finite element model better approximated the actual shell. Nonlinear computer runs were done at each model increment to compare against experimental results. Linear computer runs were also completed for comparison purposes.

It was found that accurate modeling of the shell to include thickness variations, boundary conditions, and materials is essential to obtain reasonable results. Also, the incorporation of the nonlinear analysis leads to displacement results that are within 15% of experimentation. Linear results from the same model are in error by over 75% due to large displacements in the shell. *Keywords:*

*Finite element analysis, Composite materials, Thesis. SBW/JES)*

# NONLINEAR FINITE ELEMENT ANALYSIS OF A GENERAL COMPOSITE SHELL

## 1. Introduction

In this thesis, a large laminated composite shell is analyzed using a finite element program. Since, under loading, large displacements occur in the shell, a nonlinear approach is used in the analysis. Shell research, in general, is important since this basic component is in many aerospace vehicles. For example, the fuselage, wings, and canopy on an aircraft or the skin on a missile. Furthermore, there is an increased use of composite materials in many of these shell components as in the use of composite wings on aircraft or the casing of a solid propellant rocket motor. This is primarily due to the ability of a designer to tailor the material properties in a structure to withstand the load environment. This material tailoring leads to, in general, a lighter structure than similar metal structure thereby reducing the overall weight of a vehicle; a critical factor in aerospace design.

The basic area of work on shells is very broad. A good portion of this work deals with geometrically linear problem solving. Ugural [1] shows a basic layout of linear shell theory. Other works such as Saada [2] and Sanders [3] deal with shells from a nonlinear point of view.

Fewer references consider composite shells modeled nonlinearly

and most of these deal with a standard geometric shape such as a cylinder. Bauld [4] and Dennis [5] work with shells of this type. Dennis [5] also has a very good introduction that outlines, in detail, other works (over 100) in shell analysis.

With the ever increasing capability of the modern computer, many shells are analyzed numerically. Most of the recent computer work is finite element based. Cook [6] has a very well written section on nonlinear solution techniques while the Structural Analysis for General Shells (STAGS) theory manual [7] and Zienkiewicz [8] have sections that deal specifically with shells and geometrically nonlinear finite element solutions.

Other references are concerned with the experimentation on composite shell structures. This is of particular importance in order to validate closed form and finite element solutions. References in this area include works by Knight and Starnes [9], Tisler [10], and Lee [11].

This thesis addresses all of these aspects of composite shells and includes another aspect that is not well documented. This other aspect is the comparison of a large scale nonlinear analysis with the experimental testing of a general composite shell. There is very little documentation on shells of the size (approximately 18 ft. long, 3 ft. wide, and 3 ft. high) and shape (not a standard geometric shape) considered in this thesis.



### 1.1 Objectives

The major purpose of this thesis was to determine if a nonlinear finite element analysis of a shell produces better results than a linear analysis of the same shell. The program used to do this analysis is the Structural Analysis for General Shells (STAGSC-1) computer program. The shell is loaded with an internal asymmetric pressure load. The second purpose was to investigate, the effect of modeling the shell as accurately as possible to see how changing different model parameters effect the overall shell response. A third purpose was to compare finite element results to experimental values. The final purpose was to carry out a stress analysis to check for composite failure. The results will be used to better understand the effects of large displacements on a finite element analysis.

### 1.2 Scope

A total of eight models were run on the shell to find displacements due to an internal asymmetric pressure load. The models were developed incrementally by starting with a constant thickness isotropic shell with clamped boundary conditions. Each model increment changed the basic model to better approximate the actual composite shell. These changes included modeling the thickness variation, modeling the composite material, and modeling the boundary conditions which are not a true clamped condition. During these increments the model was run nonlinearly using STAGSC-1

with linear runs for comparison purposes.

Next, the results were compared to experimental results. The experimental results were obtained by the Wright Aeronautics Laboratory, Wright-Patterson AFB, Ohio.

Finally, a Tsai-Wu failure analysis was carried out on the shell to determine if ply failure occurred in the composite.

## 2. THEORY

The Structural Analysis for General Shells (STAGS) computer program, developed by Lockheed Palo Alto Research Lab, was first operational in 1967. Its primary purpose, as evident in its name, is the analysis of thin shelled structures. From 1967-1976 the program was based on the finite difference method. In 1979 a new version of STAGS, STAGSC-1, was released and is based entirely on the finite element method [12]. The 1986 STAGSC-1 VAX Computer version is used in this thesis. Of the many capabilities in the STAGS program, the primary one used herein is the nonlinear static analysis. The basic finite element used in STAGSC-1 is the flat plate element that facets the shell surface to approximate its curvature. A look at the theory for this flat plate element and the theory used in STAGS is presented in the following sections. While this theory may not be the exact theory used in STAGSC-1, it is an attempt through research of documentation to give the reader some insight to STAGS' internal make-up to better understand the code.

Also, a review of Sanders' nonlinear shell theory is presented to better understand the kinematic relations needed in a plate element to approximate a shell surface. This does not imply the use of Sanders' nonlinear kinematic relations in STAGS; its is just a way of showing important relations in a true shell formulation that need to be incorporated in a plate type element.

## 2.1 Nonlinear Shell Theory

A review of Sanders' nonlinear shell theory is presented in order to understand the nonlinear strain displacement relations in a shell. This presentation will, in the subsequent section, provide an insight to the theory used in STAGSC-1.

The classical thin shell theory derived by Sanders assumes that the shell is thin, middle surface strains and rotations are small, and displacements away from the midsurface are restricted by the Kirchhoff-Love hypotheses [3]. With these assumptions in mind the equations for the midsurface and bending strains, respectively, are

$$\begin{aligned}\epsilon_x^o &= \frac{u_{,x}}{\alpha_x} + \frac{\alpha_{x,y}}{\alpha_x \alpha_y} v + \frac{w}{R_x} + \frac{1}{2} \phi_x^2 + \frac{1}{2} \phi^2 \\ \epsilon_y^o &= \frac{v_{,y}}{\alpha_y} + \frac{\alpha_{y,x}}{\alpha_x \alpha_y} u + \frac{w}{R_y} + \frac{1}{2} \phi_y^2 - \frac{1}{2} \phi^2 \\ \gamma_{xy}^o &= \frac{v_{,x}}{\alpha_x} + \frac{u_{,y}}{\alpha_y} - \frac{\alpha_{x,y}}{\alpha_x \alpha_y} u - \frac{\alpha_{y,x}}{\alpha_x \alpha_y} v + \phi_x \phi_y\end{aligned}\quad (2.1)$$

and

$$\begin{aligned}\kappa_x &= -\frac{\phi_{x,x}}{\alpha_x} + \frac{\alpha_{x,y} \phi_y}{\alpha_x \alpha_y} \\ \kappa_y &= -\frac{\phi_{y,y}}{\alpha_y} + \frac{\alpha_{y,x} \phi_x}{\alpha_x \alpha_y} \\ 2\kappa_{xy} &= \frac{\phi_{y,y}}{\alpha_y} + \frac{\phi_{x,x}}{\alpha_x} - \frac{\alpha_{y,x} \phi_x}{\alpha_x \alpha_y} - \frac{\alpha_{x,y} \phi_y}{\alpha_x \alpha_y} + \frac{\phi}{R_y} - \frac{\phi}{R_x}\end{aligned}\quad (2.2)$$

where  $u$  and  $v$  denote displacements tangent to the midsurface and  $w$  denotes displacement perpendicular to the shells midsurface,  $R_x$  and  $R_y$  are the principal radii of curvature,  $\phi_x$ ,  $\phi_y$ , and  $\phi$  are in-plane

rotational terms, and  $\alpha_x$  and  $\alpha_y$  are metric coefficients. The rotational terms are given by

$$\begin{aligned}\phi_x &= -\frac{w_{,x}}{\alpha_x} + \frac{u}{R_x} \\ \phi_y &= -\frac{w_{,y}}{\alpha_y} + \frac{v}{R_y} \\ \phi &= \frac{1}{2\alpha_x\alpha_y} \left[ (\alpha_y v)_{,x} - (\alpha_x u)_{,y} \right]\end{aligned}\tag{2.3}$$

The metric coefficients, written in a form similar to Saada [2], are

$$\begin{aligned}\alpha_x &= h_1 = \sqrt{E} \left( 1 + \frac{\xi_3}{R_x} \right) \\ \alpha_y &= h_2 = \sqrt{G} \left( 1 + \frac{\xi_3}{R_y} \right)\end{aligned}\tag{2.4}$$

where  $\xi_3$  is the distance from the midsurface and E and G are functions of the shell geometry (not material constants).

In order to simplify the presentation and get a better feel for the strain equations, a thin cylindrical shell will be used (see Figure 2.1). The reference surface for the shell is the midplane. For this cylindrical shell we let  $R_x \rightarrow \infty$ ,  $R_y = R$ ,  $\xi_3 = z$ , and assume that  $z \ll R$ . For this particular case Sanders' equations, (2.1) and (2.2), reduce to [4]

$$\begin{aligned}\epsilon_x^o &= u_{,x} + 1/2 \phi_x^2 + 1/2 \phi^2 \\ \epsilon_y^o &= v_{,y} + \frac{w}{R} + 1/2 \phi_y^2 - 1/2 \phi^2\end{aligned}\tag{2.5}$$

$$\gamma_{xy}^o = v_{,x} + u_{,y} + \phi_x \phi_y$$

and

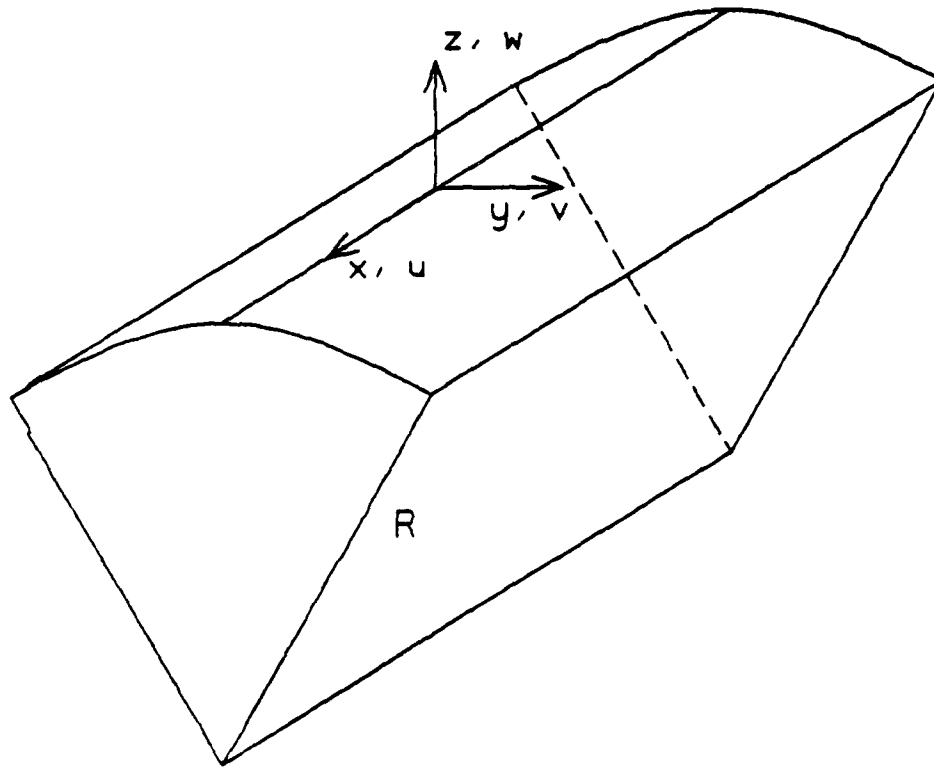
$$\kappa_x = \phi_{x,x}\tag{2.6}$$

$$\kappa_y = \phi_{y,y}$$

(2.6)

$$2\kappa_{xy} = 2\kappa_{yx} = \phi_{y,x} + \phi_{x,y} + \phi/R$$

(cont)



$$E = 1$$

$$G = 1$$

Figure 2.1 Cylindrical Shell Section Showing Coordinate and Displacement Directions [4]

Now, equations (2.5) and (2.6) can be written with the Kirchhoff-Love hypothesis to obtain the full strain expression:

$$\begin{Bmatrix} \epsilon_x \\ \epsilon_y \\ \gamma_{xy} \end{Bmatrix} = \begin{Bmatrix} \epsilon_x^0 \\ \epsilon_y^0 \\ \gamma_{xy}^0 \end{Bmatrix} - z \begin{Bmatrix} \kappa_x \\ \kappa_y \\ 2\kappa_{xy} \end{Bmatrix} \quad (2.7)$$

From equations (2.5), (2.6), and (2.7) it is much easier to understand the strain displacement relations for a simple shell while still appreciating the complexity of the formulation.

## 2.2 STAGSC-1 Theory

### 2.2.1 Strain Displacement Relations

As stated earlier, STAGS uses flat plates to approximate the curved surface of a shell. These plate elements are thin, therefore a state of plane stress can be assumed with  $\gamma_{xz}$ ,  $\gamma_{yz}$ ,  $\epsilon_z$ , and  $\sigma_z$  equal to zero, and the in-plane displacements,  $u$  and  $v$ , as well as the normal displacement,  $w$ , functionally depending on only two space variables [7]. As in Sanders' equations for a thin shell, STAGS uses the Kirchhoff-Love hypothesis for strains away from the midplane. With these assumptions in mind, an overview of STAGS' nonlinear kinematic relations can now begin. The complete derivation of the nonlinear kinematic relations is given in Appendix A.

To start the derivation, the midsurface strain,  $\epsilon_x^0$ , is given in a form which includes an in-plane rotation term,  $\phi$ , [7]:

$$\epsilon_x^0 = u_{,x} + 1/2(u_{,x}^2 + w_{,x}^2 + \phi^2) \quad (2.8)$$

In Sanders' nonlinear shell equations presented in the last section

$$\phi = 1/2(u_{,y} - v_{,x}) \quad (2.9)$$

which represent a rotation about a normal to the midplane. In a plate, the rotation of a line segment within the midplane will result

in a vector normal to this plane, similar to the rotation given in Equation (2.9). This normal rotation term for strain in a flat plate in the x-direction can be represented by  $v_{,x}$ . This does not imply keeping the  $v_{,x}$  term in Equation (2.9), dropping the  $u_{,y}$  term, and then substituting the results into Equation (2.8). What it says is that the normal rotation term is important for use in a plate in order for it to adequately model a shell. With this in mind the rotational term  $\phi$  for a flat plate is replaced directly by  $v_{,x}$  in Equation (2.8). Using this same line of reasoning, to adequately track midsurface normal rotations, the other strain terms,  $\epsilon_y^0$  and  $\gamma_{xy}^0$ , can be found. The final expressions for the midplane strains are [7]

$$\begin{aligned}\epsilon_x^0 &= u_{,x} + 1/2(u_{,x}^2 + v_{,x}^2 + w_{,x}^2) \\ \epsilon_y^0 &= v_{,y} + 1/2(u_{,y}^2 + v_{,y}^2 + w_{,y}^2) \\ \gamma_{xy}^0 &= u_{,y} + v_{,x} + (u_{,x}u_{,y} + v_{,x}v_{,y} + w_{,x}w_{,y})\end{aligned}\tag{2.10}$$

If the Kirchhoff-Love hypothesis is considered for out of plane strain terms (see Appendix A) and combined with the in-plane strain terms from Equation (2.10), the resulting expressions for strains in the plate are given by:

$$\begin{aligned}\epsilon_x &= \epsilon_x^0 - z w_{,xx} \\ \epsilon_y &= \epsilon_y^0 - z w_{,yy} \\ \gamma_{xy} &= \gamma_{xy}^0 - 2z w_{,xy}\end{aligned}\tag{2.11}$$

Equation (2.11) shows the nonlinear kinematic equations which appear to be used in STAGSC-1. These kinematic relations allow for large displacements and moderate rotations (due to the Kirchhoff-Love



hypothesis) and will be used in the following section to derive a general form of the tangent stiffness matrix.

### 2.2.2 Derivation of the Tangent Stiffness Matrix

The tangent stiffness matrix is a nonlinear stiffness matrix used in the Newton-Raphson method (see section 2.2.5) for solving a nonlinear set of equations. There are other techniques for solving these equations, but STAGSC-1 uses the Newton-Raphson (or modified Newton-Raphson), therefore, the derivation of the tangent stiffness matrix is of interest in this thesis. The tangent stiffness matrix is derived for a flat plate element, a STAGS type element, in a general way without reference to any specific shape functions. For the derivation of the specific shape functions used in the STAGS element see reference [13]. It must also be pointed out that STAGS uses an isoparametric formulation whereas this formulation is given in general coordinates to show the reader the steps involved in formulating a nonlinear stiffness matrix.

To start the derivation, a form of the tangent stiffness matrix is found from the energy expression. Consider  $\{\Psi\}$ , the sum of external and internal generalized forces (Appendix B, Equation (B.14)), which is given as [8]

$$\{\Psi\} = \int_v [B]^T \{\sigma\} dVol - \{f\} \quad (2.12)$$

where

$\{\sigma\}$  = vector of stresses

$\{f\}$  = nodal forces of the element

and  $[B]$  is defined as the product of the differential operator matrix,  $[L]$ , operating on the element shape functions,  $[N]$ . In an equilibrium state  $\{\Psi\}$  (Equation (2.12)) will equal zero. The strain displacement relations can be written (to include the  $[B]$  matrix) as

$$\{\epsilon\} = [L][N]\{a\} = [B]\{a\} \quad (2.13)$$

where  $\{a\}$  is the nodal displacement vector. In the case of a nonlinear stiffness matrix (i.e. tangent stiffness matrix),  $[B]$  is redefined as [8]

$$[B] = [B_0] + [B_L] \quad (2.14)$$

where

$$[B_0] = \text{constant}$$

$$[B_L] = \text{function of displacements}$$

In order to use the Newton-Raphson method, a relation between  $d\{a\}$  and  $d\{\Psi\}$  (see section 2.2.5) must be found. Taking the variation of Equation (2.12) with respect to  $d\{a\}$  gives the relation needed and is given as [8]

$$d\{\Psi\} = \int_V d[B]^T \{\sigma\} dVol + \int_V [B]^T d\{\sigma\} dVol = [K_T] d\{a\} \quad (2.15)$$

where  $[K_T]$  is the tangent stiffness matrix. In this derivation, strain is assumed small therefore the equation

$$\{\sigma\} = [D] (\{\epsilon\} - \{\epsilon_0\}) + \{\sigma_0\} \quad (2.16)$$

still applies, where  $[D]$  is the material matrix and the subscripts indicate initial values of stresses and strains (i.e. constants). With Equations (2.13), (2.14), and (2.16), the variational terms in Equation (2.15) can be rewritten as [8]

$$d\{\sigma\} = [D] d\{\epsilon\} = [D][B] d\{a\} \quad (2.17)$$

and

$$d[B]^T = d[BL]^T \quad (2.18)$$

With Equations (2.17) and (2.18), Equation (2.15) can be rewritten as

$$d(\Psi) = \int_V d[BL]^T \{\sigma\} dVol + \int_V [B]^T [D] [B] dVol d(a) \quad (2.19)$$

The first term in Equation (2.19) contains the initial stress matrix,  $[K\sigma]$ , while the last term turns out to be the linear and the nonlinear stiffness matrices,  $[K_0]$  and  $[K_L]$  respectively, after substituting Equation (2.14) in for  $[B]$  [8]. The three stiffness matrices contained in Equation (2.19) are

$$\begin{aligned} [K_0] &= \int_V [B_0]^T [D] [B_0] dVol \\ [K_L] &= \int_V \left( [B_0]^T [D] [BL] + [BL]^T [D] [BL] + \right. \\ &\quad \left. [BL]^T [D] [B_0] \right) dVol \\ [K\sigma]d(a) &= \int_V d[BL]^T \{\sigma\} dVol \end{aligned} \quad (2.20)$$

The full expression for the tangent stiffness matrix can now be written as

$$[K_T] = [K_0] + [K_L] + [K\sigma] \quad (2.21)$$

With an expression for the elements contained in the tangent stiffness matrix (Equation (2.21)), the derivation can now proceed toward finding the terms contained in the matrices that make up the tangent stiffness matrix.

The next steps in the derivation include formulating the kinematic relations, introducing the material matrix, and giving the displacement relations. Recalling the strain expression from the last section (Equation (2.11)) written in vector form and rearranged

to reflect in-plane and bending (out of plane) strains [8]

$$\{\epsilon\} = \begin{Bmatrix} \epsilon_o \\ \epsilon_x \\ \epsilon_y \\ \gamma_{xy} \\ -w_{,xx} \\ -w_{,yy} \\ -2w_{,xy} \end{Bmatrix} \quad (2.22)$$

where the distance from the midplane,  $z$ , has been incorporated in the material matrix (see Appendix C). If Equation (2.15) is rewritten, separating linear and nonlinear terms due to in-plane and bending strains, the results are [8]

$$\{\epsilon\} = \begin{Bmatrix} \epsilon_o^p \\ \epsilon_o^b \\ \epsilon_o^p \\ \epsilon_o^b \end{Bmatrix} + \begin{Bmatrix} \epsilon_L^p \\ 0 \end{Bmatrix} + \begin{Bmatrix} \epsilon_L^b \\ 0 \end{Bmatrix} \quad (2.23)$$

where

$\{\epsilon_o^p\}$  - linear in-plane strains

$\{\epsilon_o^b\}$  - linear bending strains

$\{\epsilon_L^p\}$  - nonlinear in-plane strains in  $u$  and  $v$

$\{\epsilon_L^b\}$  - nonlinear in-plane strains in  $w$

Incorporating the linear constitutive relationship, the material matrix  $[D]$ , for a composite material (derived in Appendix C), is given as

$$[D] = \begin{bmatrix} [A] & [B] \\ [B] & [D] \end{bmatrix} \quad (2.24)$$

Since the distance from the midplane,  $z$ , has been incorporated in this matrix, the integration indicated in Equation (2.20) for  $[K_o]$ ,  $[K_L]$ , and  $[K_\sigma]$  reduces to an area integral.

Finally, the displacements are defined in terms of nodal displacements using the shape functions for the plate element. If

for example, an element similar to the QUAF 410 is considered (see section 2.2.4), which has four corner nodes and six degrees of freedom per node, the displacements can be given as

$$\begin{Bmatrix} u \\ v \\ w \end{Bmatrix} = [N] \{a_i\} \quad (2.25)$$

The vector of element nodal displacements (parameters),  $\{a_i\}$ , can be subdivided into displacements that influence in-plane (superscript p) and bending (superscript b) as [8]

$$\begin{aligned} \{a_i^p\} &= \begin{Bmatrix} u_i \\ v_i \\ \beta_i \end{Bmatrix} \\ \{a_i^b\} &= \begin{Bmatrix} w_i \\ w_{,x_i} \\ w_{,y_i} \end{Bmatrix} \end{aligned} \quad (2.26)$$

where  $\beta$  represents an average rotation about the normal (similar to  $\phi$  in Equation (2.9)). The shape functions can also be divided in a similar manner as [8]

$$[N_i] = \begin{bmatrix} [N_i^p] & 0 \\ 0 & [N_i^b] \end{bmatrix} \quad (2.27)$$

In order to proceed further it is necessary to expand the expression for  $[B]$ . From Equation (2.14) it was shown that [8]

$$[B] = [B_0] + [B_L] \quad (2.28)$$

where

$$[B_0] = \begin{bmatrix} [B_0^p] & 0 \\ (3 \times 12) & [B_0^b] \\ (6 \times 24) & (3 \times 12) \end{bmatrix} \quad (2.29)$$

and

$$[B_L] = \begin{bmatrix} [B_L^p] & [B_L^b] \\ (3 \times 12) & (3 \times 12) \\ (6 \times 24) & 0 \end{bmatrix} \quad (2.30)$$

Note: The numbers in the parenthesis incate the matrix order.

The matrices  $[B_o^p]$  (linear in-plane) and  $[B_o^b]$  (linear bending) are standard matrices and are derived in reference [8] with the exception that in the derivation of  $[B_o^p]$  the normal rotation term,  $\beta$  (Equation (2.26)), must be included as a degree of freedom at each node. The matrix  $[B_L^p]$  and  $[B_L^b]$  are found by taking a variation of  $\{\epsilon_L^p\}$  and  $\{\epsilon_L^b\}$  (Equation (2.23)) respectively, with respect to the nodal degrees of freedom  $\{a\}$ .

In matrix form  $\{\epsilon_L^p\}$  can be written as

$$\{\epsilon_L^p\} = \frac{1}{2} \begin{bmatrix} u_{,x} & 0 & v_{,x} & 0 \\ 0 & u_{,y} & 0 & v_{,y} \\ u_{,y} & u_{,x} & v_{,y} & v_{,x} \end{bmatrix} \begin{Bmatrix} u_{,x} \\ u_{,y} \\ v_{,x} \\ v_{,y} \end{Bmatrix} \quad (2.31)$$

or [8]

$$\{\epsilon_L^p\} = 1/2 [R^p] \{\theta^p\} \quad (2.32)$$

The vector  $\{\theta^p\}$  can be related to the in-plane (u and v) nodal degrees of freedom as

$$\{\theta^p\} = \begin{Bmatrix} u_{,x} \\ u_{,y} \\ v_{,x} \\ v_{,y} \end{Bmatrix} = [G^p] \{a^p\} \quad (2.33)$$

(4x12) (12x1)

where  $[G^p]$  is a matrix of coordinates (i.e. the derivatives of the in-plane shape functions) and  $\{a^p\}$  is the vector of nodal displacements (Equation (2.26)). The next step involves taking the variation of  $\{\epsilon_L^p\}$ . To do this Equation (2.31) is rewritten as

$$\{\epsilon_L^P\} = \begin{Bmatrix} 1/2 u_{,x}^2 + 1/2 v_{,x}^2 \\ 1/2 u_{,y}^2 + 1/2 v_{,y}^2 \\ u_{,x} u_{,y} + v_{,x} v_{,y} \end{Bmatrix} \quad (2.34)$$

Taking the variation of Equation (2.34) gives

$$d\{\epsilon_L^P\} = \begin{Bmatrix} u_{,x} du_{,x} + v_{,x} dv_{,x} \\ u_{,y} du_{,y} + v_{,y} dv_{,y} \\ u_{,x} du_{,y} + u_{,y} du_{,x} + v_{,x} dv_{,y} + v_{,y} dv_{,x} \end{Bmatrix} \quad (2.35)$$

Rewriting Equation (2.35) results in

$$d\{\epsilon_L^P\} = \begin{bmatrix} u_{,x} & 0 & v_{,x} & 0 \\ 0 & u_{,y} & 0 & v_{,y} \\ u_{,y} & u_{,x} & v_{,y} & v_{,x} \end{bmatrix} d \begin{Bmatrix} u_{,x} \\ u_{,y} \\ v_{,x} \\ v_{,y} \end{Bmatrix} \quad (2.36)$$

where the first matrix on the right hand side equals  $[R^P]$  (Equation 2.32) and the last matrix can be written from Equation (2.33) as

$$d \begin{Bmatrix} u_{,x} \\ u_{,y} \\ v_{,x} \\ v_{,y} \end{Bmatrix} = [G^P] d\{a^P\} \quad (2.37)$$

(4x12) (12x1)

since  $[G^P]$  is a function of coordinates only.

Using the definition of  $[R^P]$  in Equation (2.32) along with Equation (2.37), Equation (2.36) can be written as

$$d\{\epsilon_L^P\} = [R^P][G^P]d\{a^P\} \quad (2.38)$$

From Equation (2.38) the resulting expression for  $[B_L^P]$  is, by definition,

$$[B_L^P] = [R^P][G^P] \quad (2.39)$$

(3x12) (3x4) (4x12)

Following the same line of reasoning used to find  $[B_L^p]$  from  $\{\epsilon_L^p\}$ , one can find from

$$\{\epsilon_L^b\} = \frac{1}{2} \begin{bmatrix} w_{,x} & 0 \\ 0 & w_{,y} \\ w_{,y} & w_{,x} \end{bmatrix} \begin{Bmatrix} w_{,x} \\ w_{,y} \end{Bmatrix} \quad (2.40)$$

or from [8]

$$\{\epsilon_L^b\} = 1/2 [R^b] \{\theta^b\} \quad (2.41)$$

that

$$\begin{matrix} [B_L^b] \\ (3 \times 12) \end{matrix} = \begin{matrix} [R^b] \\ (3 \times 2) \end{matrix} \begin{matrix} [G^b] \\ (2 \times 12) \end{matrix} \quad (2.42)$$

where  $[G^b]$  is composed of derivatives of the shape functions that are contained in the expression for  $w$ .

With the expressions for  $[B_0]$  and  $[B_L]$  determined (Equations (2.29) and (2.30) respectively), the material matrix defined (Equation (2.24)), and recalling that the volume integral has been reduced to an area integral (Equation (2.24)), the expressions for the linear and nonlinear stiffness matrices ( $[K_0]$  and  $[K_L]$ ) can be determined. If one uses Equation (2.20) and, after some manipulation,

$$\begin{matrix} [K_0] \\ (24 \times 24) \end{matrix} = \int_A \begin{bmatrix} [B_0^p]^T [A] [B_0^p] & [B_0^p]^T [B] [B_0^b] \\ [B_0^p]^T [B] [B_0^b] & [B_0^b]^T [D] [B_0^b] \end{bmatrix} dArea \quad (2.43)$$

and

$$\begin{matrix} [K_L] \\ (24 \times 24) \end{matrix} = \int_A \begin{bmatrix} [1] & [2] \\ [2] & [3] \end{bmatrix} dArea \quad (2.44)$$

where



$$\begin{aligned} [1]_{(12 \times 12)} &= [B_o^p]^T [A] [B_L^p] + [B_L^p]^T [A] [B_L^p] + [B_L^p]^T [A] [B_o^p] \end{aligned} \quad (2.45)$$

$$\begin{aligned} [2]_{(12 \times 12)} &= [B_o^p]^T [A] [B_L^b] + [B_L^p]^T [A] [B_L^b] + [B_L^p]^T [B] [B_o^b] \end{aligned} \quad (2.46)$$

$$\begin{aligned} [3]_{(12 \times 12)} &= [B_o^b]^T [B] [B_L^b] + [B_L^b]^T [A] [B_L^b] + [B_L^b]^T [B] [B_o^b] \end{aligned} \quad (2.47)$$

The final expression necessary for the tangent stiffness matrix is the initial stress matrix  $[K\sigma]$ . Recalling Equation (2.20), rewritten for convenience as

$$[K\sigma]d(a) = \int d[B_L]^T (\sigma') dVol \quad (2.48)$$

The stresses,  $(\sigma')$ , are defined in terms of the in-plane (superscript p) and bending (superscript b) stresses as [8]

$$(\sigma') = \left\{ \begin{matrix} N_x & N_y & N_{xy} & M_x & M_y & M_{xy} \end{matrix} \right\}^T = \left\{ \begin{matrix} \sigma & ,p \\ \sigma & ,b \end{matrix} \right\} \quad (2.49)$$

where the prime on the stresses indicates stress resultants, not true stresses, and the true stress resultants ( $N_x$ ,  $M_x$ , etc.) are given in Appendix C (Equation (C.11)). The stress resultants are average values over the element. This also implies that integration through the thickness has been completed thereby reducing the integration of Equation (2.48) to that of an area. Now, define the variation of  $[B_L]^T$  in Equation (2.48) from Equation (2.30) as

$$d[B_L]^T = \begin{bmatrix} d[B_L^p]^T & 0 \\ d[B_L^b]^T & 0 \end{bmatrix} \quad (2.50)$$

Substituting Equations (2.39) and (2.42) into Equation (2.50) and then substituting that result, as well as Equation (2.49), into Equation (2.48) gives [8]

$$[K\sigma]d(a) = \int_A \begin{bmatrix} [G^p]^T d[R^p]^T & 0 \\ [G^b]^T d[R^b]^T & 0 \end{bmatrix} \begin{Bmatrix} N_x \\ N_y \\ N_{xy} \\ M_x \\ M_y \\ M_{xy} \end{Bmatrix} dArea \quad (2.51)$$

Expanding Equation (2.51) and rewriting it in terms of in-plane (superscript p) and bending (superscript b) expressions results in

$$\begin{matrix} [K\sigma^p]d(a^p) \\ (12 \times 12)(12 \times 1) \end{matrix} = \int_A \begin{matrix} [G^p]^T d[R^p]^T \\ (12 \times 4)(4 \times 3) \end{matrix} \begin{Bmatrix} N_x \\ N_y \\ N_{xy} \end{Bmatrix} dArea \quad (2.52)$$

and

$$\begin{matrix} [K\sigma^b]d(a^b) \\ (12 \times 12)(12 \times 1) \end{matrix} = \int_A \begin{matrix} [G^b]^T d[R^b]^T \\ (12 \times 2)(2 \times 3) \end{matrix} \begin{Bmatrix} N_x \\ N_y \\ N_{xy} \end{Bmatrix} dArea \quad (2.53)$$

The following steps involve finding expressions for  $[K\sigma^b]$  and  $[K\sigma^p]$ .

Starting with Equation (2.52) and rewriting the last two matrices on the right hand side using Equation (2.31) gives

$$d[R^p]^T \begin{Bmatrix} N_x \\ N_y \\ N_{xy} \end{Bmatrix} = \begin{bmatrix} u_{,x} & 0 & u_{,y} \\ 0 & u_{,y} & u_{,x} \\ v_{,x} & 0 & v_{,y} \\ 0 & v_{,y} & v_{,x} \end{bmatrix} \begin{Bmatrix} N_x \\ N_y \\ N_{xy} \end{Bmatrix} \quad (2.54)$$

Expanding the right hand side of Equation (2.54) and also taking the variation, recalling that  $N_x$ ,  $N_y$ , and  $N_{xy}$  are constants (Equation (2.49)), results in

$$d[R^P]^T \begin{Bmatrix} N_x \\ N_y \\ N_{xy} \end{Bmatrix} = \begin{Bmatrix} N_x du_{,x} + N_{xy} du_{,y} \\ N_y du_{,y} + N_{xy} du_{,x} \\ N_x dv_{,x} + N_{xy} dv_{,y} \\ N_y dv_{,y} + N_{xy} dv_{,x} \end{Bmatrix} \quad (2.55)$$

Rewriting Equation (2.55) in matrix form gives

$$d[R^P]^T \begin{Bmatrix} N_x \\ N_y \\ N_{xy} \end{Bmatrix} = \begin{bmatrix} N_x & N_{xy} & 0 & 0 \\ N_{xy} & N_y & 0 & 0 \\ 0 & 0 & N_x & N_{xy} \\ 0 & 0 & N_{xy} & N_y \end{bmatrix} d \begin{Bmatrix} u_{,x} \\ u_{,y} \\ v_{,x} \\ v_{,y} \end{Bmatrix} \quad (2.56)$$

Recalling Equation (2.37) and substituting it into Equation (2.56) gives

$$d[R^P]^T \begin{Bmatrix} N_x \\ N_y \\ N_{xy} \end{Bmatrix} = \begin{bmatrix} N_x & N_{xy} & 0 & 0 \\ N_{xy} & N_y & 0 & 0 \\ 0 & 0 & N_x & N_{xy} \\ 0 & 0 & N_{xy} & N_y \end{bmatrix} [G^P] d(a^P) \quad (2.57)$$

Substituting Equation (2.57) into Equation (2.52) results in an expression for  $[K\sigma^P]$ :

$$[K\sigma^P]_{(12 \times 12)} = \int_A [G^P]^T_{(12 \times 4)} \begin{bmatrix} N_x & N_{xy} & 0 & 0 \\ N_{xy} & N_y & 0 & 0 \\ 0 & 0 & N_x & N_{xy} \\ 0 & 0 & N_{xy} & N_y \end{bmatrix} [G^P]_{(4 \times 12)} dArea \quad (2.58)$$

With the same type of derivation used to find  $[K\sigma^P]$ ,  $[K\sigma^b]$  can be found. The resulting expression for  $[K\sigma^b]$  is:

$$[K\sigma^p]_{(12 \times 12)} = \int_A [G^b]^T \begin{bmatrix} N_x & N_{xy} \\ N_{xy} & N_y \end{bmatrix} [G^b]_{(2 \times 12)} dArea \quad (2.59)$$

With Equations (2.58) and (2.59), the full expression for the initial stress matrix can be written as

$$[K\sigma]_{(24 \times 24)} = \begin{bmatrix} [K\sigma^p]_{(12 \times 12)} & 0 \\ 0 & [K\sigma^b]_{(12 \times 12)} \end{bmatrix} \quad (2.60)$$

### 2.2.3 Pressure Loading

Since STAGSC-1 is an energy based finite element program, the loading is restricted to conservative systems. In a conservative force system the work done by these forces is path independent [13]. In this thesis the loading is an internal pressure load, asymmetrically applied. A pressure load like this that remains normal to the surface during deformation (a live load) is not necessarily conservative [13]. An example of a conservative pressure system is a pressure acting on a closed body; the work equals the product of the pressure and the change in volume. For plates and shells, the pressure loading is conservative if, at the edge of the pressure field, the normal displacement or the product of the displacement vector (u,v) and the normal to the boundary in the tangent plane is zero [7,15].

From extensive research on STAGSC-1 theory and other related

articles on pressure loading, it would appear that the live pressure loading in STAGS is implemented as follows. The local reference frame of the element is established through the use of the updated Lagrangian formulation (see section 2.2.5). A normal is calculated to this local element reference frame and is established as the direction by which the pressure load is applied. Equivalent nodal loads are calculated for the element for the current pressure load (loads are incrementally applied). These loads are transformed into the global system and assembled with the other elements' equivalent nodal loads. A solution is then found for the displacements at this given load increment (the global force vector doesn't change within a load increment). Once these displacements are found, the element reference system as well as the element normal can be updated, an increment of pressure load added, and the process repeated.

#### 2.2.4 Plate Elements Representing a Shell

As stated earlier, STAGS uses plate elements to represent the surface of a shell. The quadrilateral plate elements primarily used in this thesis are the STAGS QUA4 410 and 411 elements. The QUA4 410 element has 24 degrees of freedom; three rotations and three displacements at each corner node. The QUA4 411 element has 32 degrees of freedom; four rotations and three displacements at each corner node and an in-plane tangent displacement at each of four side nodes. These Elements are shown in Figure 2.2.

From examining Figure 2.2 it is noted that a degree of freedom

not usually used in plate elements is included; the normal rotation  $\theta_z$ . This normal rotation, for the QUA4 410 and 411 elements, is the average in-plane rotation of the two adjacent edges of the plate element. This degree of freedom is necessary when two flat plate

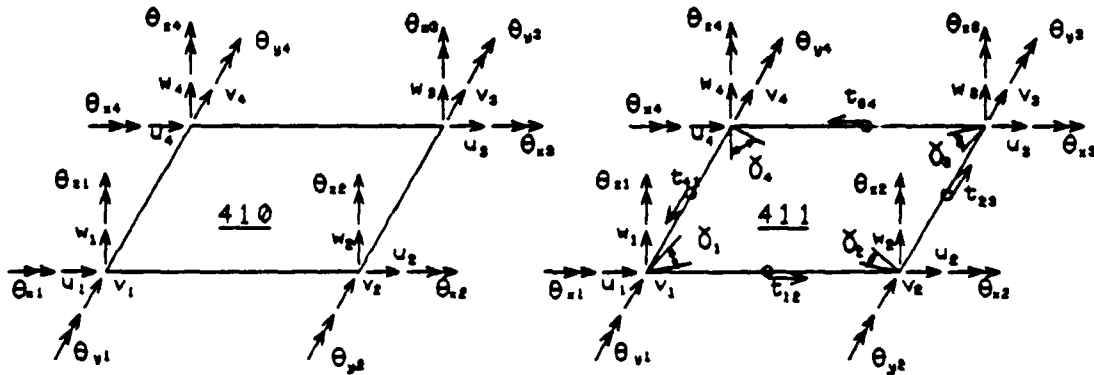


Figure 2.2 STAGS QUA4 410 and 411 Quadrilateral Element [16]

elements meet at an angle to represent a curved shell [13]. A problem with this rotation is that it does not appear in the strain energy expression for the element.

To illustrate, consider two flat plate elements joined together at an angle  $\alpha$  as in Figure 2.3. These plates represent the curved surface of a shell. Once the rotations of each element are transformed into the same reference system, compatibility is given as [13]

$$\begin{aligned} \left[ \begin{matrix} \theta_y^1 & -\theta_y^2 \end{matrix} \right] \cos(\alpha/2) - \left[ \begin{matrix} \theta_z^1 & +\theta_z^2 \end{matrix} \right] \sin(\alpha/2) &= 0 \\ \left[ \begin{matrix} \theta_z^1 & -\theta_z^2 \end{matrix} \right] \cos(\alpha/2) - \left[ \begin{matrix} \theta_y^1 & +\theta_y^2 \end{matrix} \right] \sin(\alpha/2) &= 0 \end{aligned} \quad (2.61)$$

where the superscripts 1 and 2 are the associated element numbers. As the angle between the elements,  $\alpha$ , becomes smaller the system of equations in Equation (2.61) becomes increasingly ill-conditioned and

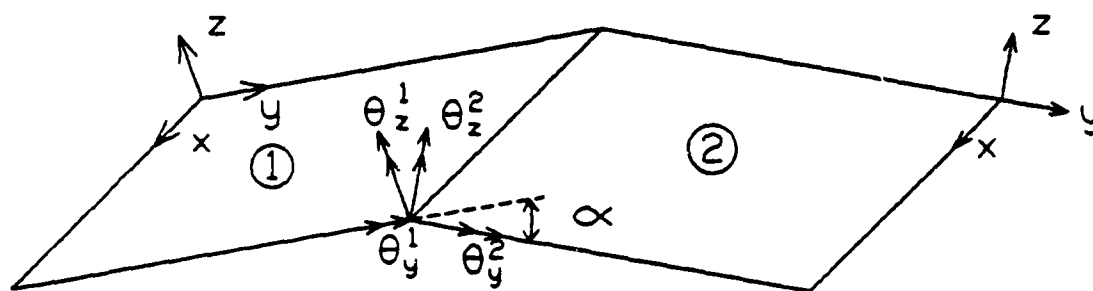


Figure 2.3 Flat Plate Element Representing a Curved Shell [13]

is singular at  $\alpha=0$  [13]. In order to overcome this difficulty a lower limit is set for the angle  $\alpha$ . Once this limit is reached  $\theta_z$  is omitted and Equation (2.61) is assumed as  $\theta_y^1 = \theta_y^2$ .

Another problem associated with the use of flat elements representing a curved surface has to do with displacement conformity at an interface of two flat elements. For a flat element the lateral deflection,  $w$ , is usually represented by at least a cubic polynomial in order to handle the second derivatives associated with bending strain. The in-plane displacements,  $u$  and  $v$ , are usually represented with either a linear or quadratic polynomial. If the compatibility relation for two adjacent flat elements is derived, the resulting expression is given as [13]

$$\left[ v^1 - v^2 \right] \cos(\alpha/2) - \left[ w^1 + w^2 \right] \sin(\alpha/2) = 0 \quad (2.62)$$

$$\left[ w^1 - w^2 \right] \cos(\alpha/2) - \left[ v^1 + v^2 \right] \sin(\alpha/2) = 0 \quad (2.62)$$

(cont)

If one examines Equation (2.62), it is evident that the displacement compatibility along the interface of the two elements cannot be satisfied (if  $v$  is a quadratic, it cannot fit the same curve as the cubic,  $w$ ) unless  $v$  and  $w$  are represented by polynomials of the same order. To overcome this displacement nonconformity the QUA410 uses a third order polynomial to represent  $u$  in the  $y$ -direction (linear in  $x$ ) and  $v$  in  $x$ -direction (linear in  $y$ ). The lateral deflection  $w$  is represented by a cubic polynomial in  $x$  and  $y$ . There are a total of twelve terms in polynomials representing  $u$  and  $v$  for the QUA410 element. This can be done since there are two displacements,  $u$  and  $v$ , and one rotation,  $\theta_z$ , at each node representing in-plane motion. The QUA411 element uses the same cubic polynomial to represent  $w$  but adds a shear term,  $\gamma$ , at each corner node and an in-plane tangent displacement,  $t$ , at midside nodes. This allows  $u$  to be cubic in  $y$  (quadratic in  $x$ ) and  $v$  to be cubic in  $x$  (quadratic in  $y$ ) [13]. Rotational compatibility is enforced only at the nodes, thus the QUA410 and 411 elements are nonconforming bending elements. The derivation of the shape functions associated with these assumed displacement fields is given in [13].

#### 2.2.5 Solution Techniques

The STAGSC-1 computer program uses a Newton-Raphson or modified Newton-Raphson (user defined) solution technique to solve the



nonlinear equilibrium equations. For a linear problem in STAGSC-1, the solution technique is much easier since the stiffness matrix is not a function of displacements. The linear set of equations is given as

$$[K]\{a\}=\{R\} \quad (2.63)$$

where  $[K]$  is the stiffness matrix (constant),  $\{a\}$  is the set of nodal degrees of freedom (nodal parameters), and  $\{R\}$  is the applied loads. STAGSC-1 uses a Cholesky triangular decomposition with forward and backward substitution to solve Equation (2.63) for  $\{a\}$  [12]. The solution for the nonlinear equilibrium equations is much more involved and will be looked at next.

Before starting the explanation of the Newton-Raphson solution technique, an explanation of the reference systems in STAGSC-1 is in order. There are basically two reference systems defined; a global reference system (subscript g) and a local element reference system (subscript e). The global reference system is fixed in space and does not move. The local reference system uses an updated Lagrangian approach. The local reference system, called a corotational system, is fixed to the element and moves with the element during rigid body motion [6]. This allows for the removal of rigid body motion in the element before calculating strain. The present version of STAGSC-1 (1986) also redefines the standard way of representing a rotation as a vector quantity. Rotations are defined by a triad (three mutually perpendicular unit vectors) to accurately map local rotations since they are dependent on order of rotation. The previous versions of STAGS used vectors to describe rotations which with large rotations gave spurious results (vectors cannot track order of rotation and are

only good for small rotations). This is the reason the QUA4 411 element was developed; to handle larger rotations, but with increased cost [18]. The reader is referred to [17] for a complete discussion on this rotational formulation. Finally, differentiation and integration within the element are done with respect to this corotational system [6].

For the STAGSC-1 quadrilateral element, the local reference system is defined as follows: An approximation of the warped element surface is made by crossing the principal diagonals of the element to form a vector and then establishing a plane normal to this vector such that one of the nodes lies on this plane. This node is where the local reference system is established by taking the z axis normal to the plane, the x or y axis is located along one of the element edges, and the remaining axis completes a cartesian right-handed system (see Figure 2.4) [17]. All local deformations of the element

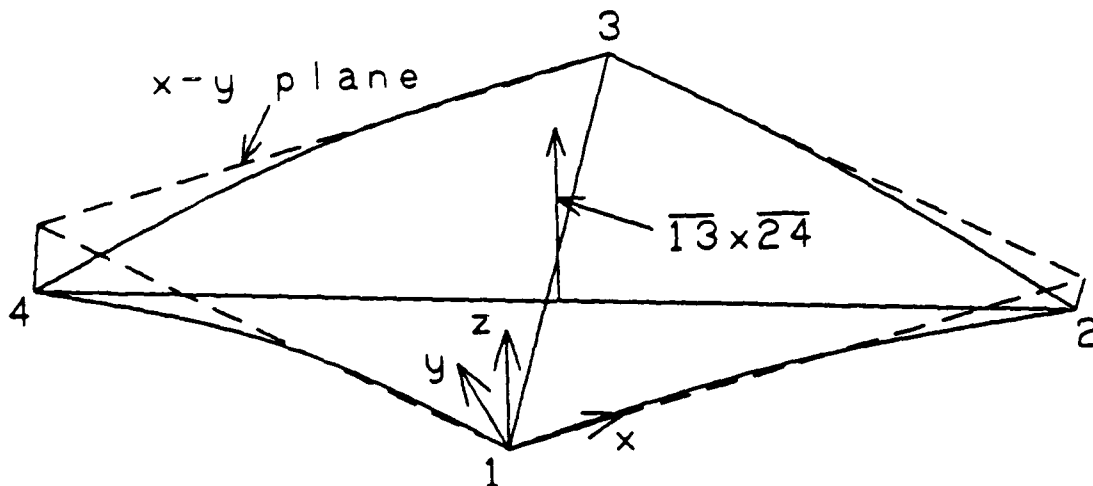


Figure 2.4 Quadrilateral Element Local Reference System [17]

are referenced to this local system during an iteration for a solution. Once a solution has been found in the global system the

local coordinates are updated and a new local reference system is established. This movement of the local reference system appears to be Eulerian except that the local coordinates of a point change [6]. Strains and rotations in the local reference system are usually small enough so as to ignore the nonlinear stiffness matrix  $[K_L]$  and sometimes even the initial stress matrix  $[K_0]$  that are part of the tangent stiffness matrix  $[K_T]$  [6]. This is only true for the local system, the global tangent stiffness matrix must, in general, contain all terms (see Equation (2.21)). From thorough research of STAGS documentation, it appears that STAGS uses the full tangent stiffness matrix in both the global and local systems to overcome difficulties in solutions due to highly nonlinear problems.

With the reference systems defined, the Newton-Raphson solution techniques can be explained. To start, expand the expression for the sum of external and internal forces,  $\{\Psi\}$  (see Appendix B), in a Taylor expansion

$$\left\{ \Psi(\{a\}^{n+1}) \right\} - \left\{ \Psi(\{a\}^n) \right\} + \left[ \frac{d\{\Psi\}}{d\{a\}} \right]_n (\Delta a)^n + \text{H.O.T.} = 0 \quad (2.64)$$

where H.O.T. means higher order terms and

$$\{a\}^{n+1} = \{a\}^n + \{\Delta a\}^n \quad (2.65)$$

From Equation (2.15) [8]

$$\frac{d\{\Psi\}}{d\{a\}} = [K_T] \quad (2.66)$$

where  $[K_T]$  is the tangent stiffness matrix; a function of displacements. If one uses the expression for  $\{\Psi\}$  in Equation (B.15) (Appendix B) and writes it as a function of displacements for the nonlinear problem one obtains [8]

$$\{\Psi(a)\} = [K(a)]\{a\} - \{f\} \quad (2.67)$$

where

$[K(a)]\{a\}$  - internal resisting forces of the element

$\{f\}$  - externally applied loads

Inserting Equations (2.66) and (2.67) into Equation (2.64) and eliminating the higher order terms results in

$$[K_T]\{\Delta a\}^n = \{f\} - [K(a)^n]\{a\}^n \quad (2.68)$$

The problem now is to find the the displacements within the element that balance the externally applied loads and the internal resisting forces (i.e. the sum of the right hand side of Equation (2.68) equaling zero). Since an updated Lagrangian approach is being used, the internal deformations are relative to the local reference system, therefore the last expression in Equation (2.68) needs to be written in terms of the local displacements. Rewriting Equation (2.68) in terms of the local (subscript e) and global (subscript g) displacements results in [6]

$$[K_T](\Delta a_e)^n = \{f\} - \sum [k(a_e)^n](a_e)^n \quad (2.69)$$

where

$\sum [k(a_e)^n](a_e)^n$  - internal resisting forces transformed into the global system and summed

The Newton-Raphson solution technique is given as follows [6]:

1. Increment the applied load  $\{f\}$ .
2. Establish the local coordinates for each element.
3. Formulate the element tangent stiffness matrices in terms of their local degrees of freedom.
4. Transform the local tangent stiffness matrices to the global

coordinate system and assemble them into the global stiffness matrix.

5. Compute the values of the local degrees of freedom  $\{a_e\}$  (zero for the first iteration within each load step) from the global degrees of freedom  $\{a_g\}$ .

6. Calculate the element internal forces  $[k(a_e)]\{a_e\}$ .

Transform these forces to the global system and assemble them with the other element internal forces.

7. Solve Equation (2.69) for  $\{\Delta a_g\}$ .

8. If the vector  $\{\Delta a_g\}$  is not small enough (i.e. converges) return to step 3.

After the solution converges (step 8) return to step 1 and repeat.

Once the solution has converged for the final load step ( $f$  has been incremented to equal the final load) the solution is complete.

An alternate solution technique is the modified Newton-Raphson method. In this method the tangent stiffness matrix is not reformulated at every iteration within a load step. The previously assembled stiffness matrix is used for successive iterations and is only refactored when the convergence rate dictates [6].

STAGS allows the user to control many of the parameters in the solution process to include: either using the full or modified Newton-Raphson method, control of the load step size, and the number of attempts at a solution if convergence difficulties arise.

### 3. Finite Element Modeling

The analysis carried out in this thesis consists of a linear and nonlinear static analysis using the Structural Analysis for General Shells, version C-1, (STAGSC-1) finite element computer program.

The structure modeled is a thin composite shell with the following characteristics:

1. Varying thickness over the shell.
2. Kevlar-49/F-141 Polyester Resin (Kevlar/Polyester) cloth composite.
3. Dimensions of approximately 216 in. long, 38 in. wide, and 34 in. high.
4. Unusual boundary conditions (not truly clamped or pinned).
5. Internal asymmetric pressure loading (see section 2.2.3).

These characteristics will be expanded upon in the following sections. The actual shell is shown in Figure 3.1. The primary area of concern in this analysis is the center section of the shell away from the boundaries; the area where experimental results were obtained (see section 4).

To model the structure, a finite element grid was developed to approximate the curved surface of the shell with flat quadrilateral and triangular plate elements. The basic model consists of 362 nodes and 362 elements. In areas where geometry dictates, smaller elements were used to better approximate the curvatures. The finite element model of the structure is shown in Figures 3.2, 3.3, and 3.4.

In order to model this kind of structure using STAGSC-1, individual node point locations had to be entered in the global

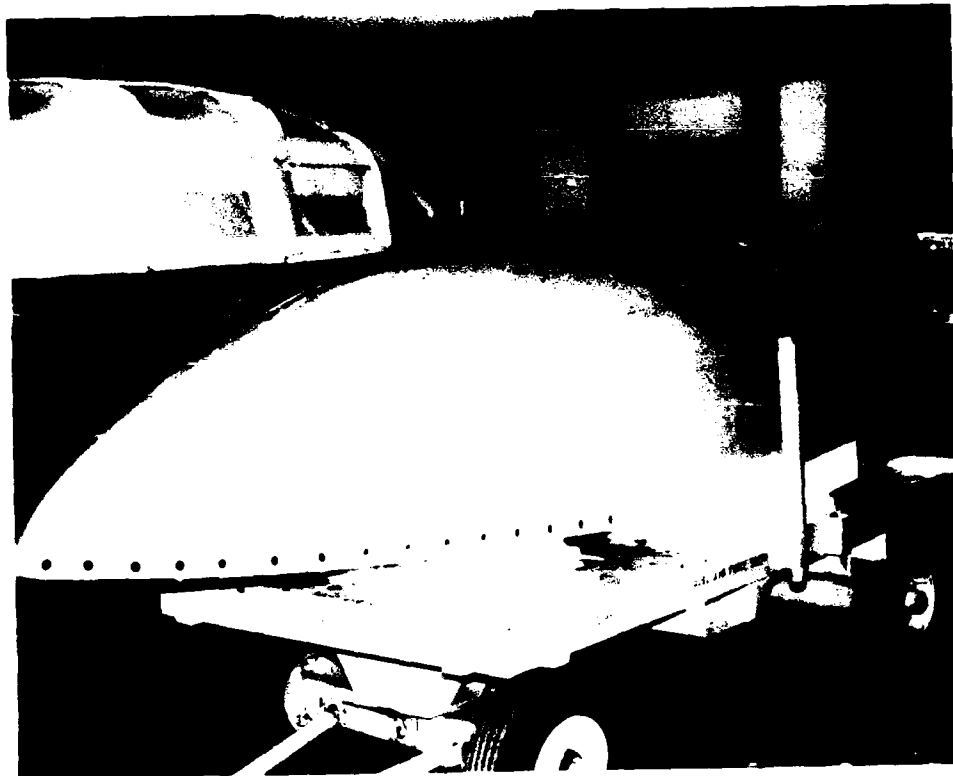


Figure 3.1 Kevlar/Polyester Composite Shell

system (reference located at the nose of the model). Also, element connectivity had to be entered by hand. This type of model is called an element unit in STAGS [16]. If the model was a standard geometric shape (e.g. cylinder, ellipsoid, etc.), STAGS would generate the finite element mesh.

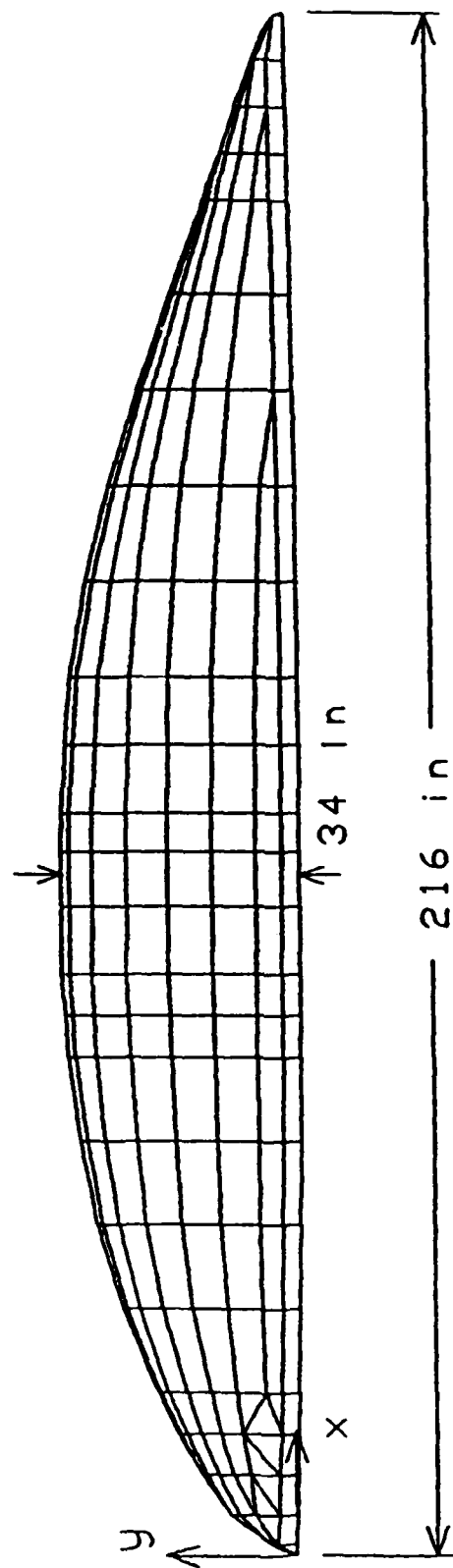


Figure 3.2 Finite Element Model Side View



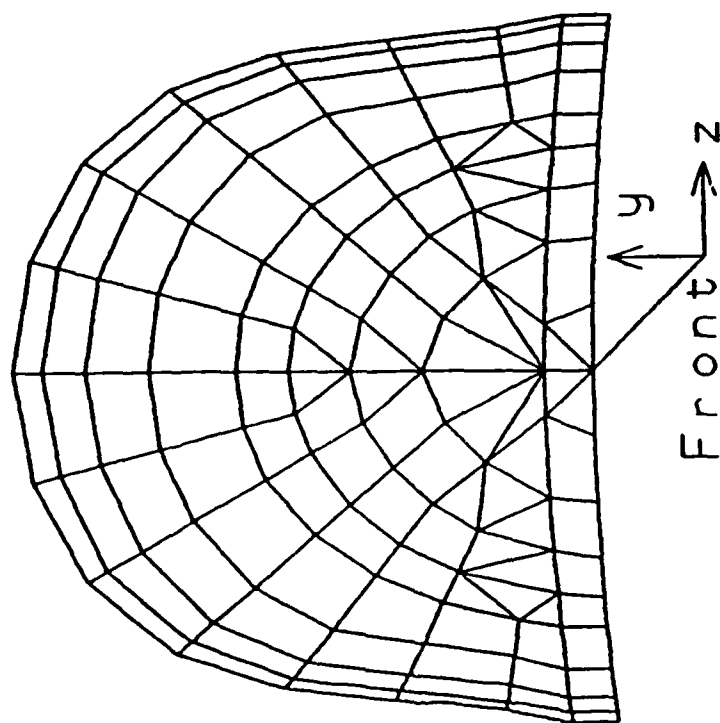
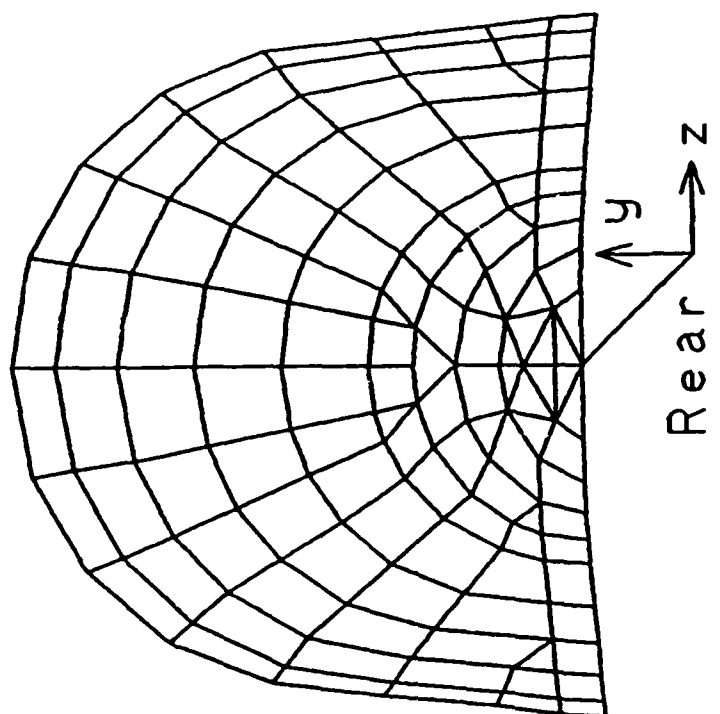


Figure 3.3 Finite Element Model Front and Rear View

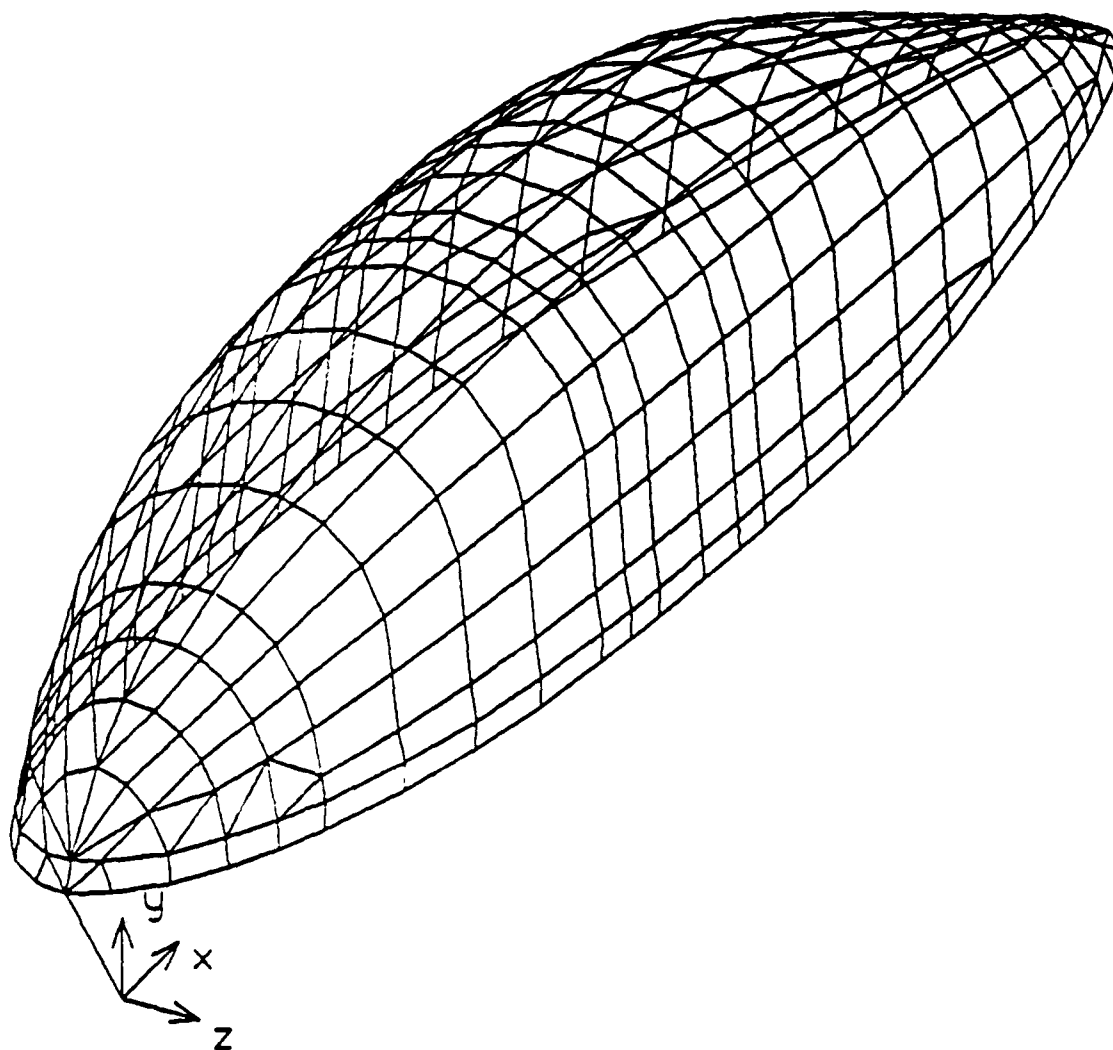


Figure 3.4 Finite Element Model Angle View

automatically and reduce the number of user inputs dramatically. This standard geometric shape in STAGS is called a shell unit [16].

The loading on the structure is an internal asymmetric pressure load over the surface of the shell. The loads are due to aerodynamic pressures on the shell and static equivalents were calculated by the 4950 Test Wing, Wright-Patterson AFB, Ohio. The static loads were divided into 20 loading regions on the shell; symmetric with respect to the x,y plane (see Figures 3.2, 3.3, and 3.4) in terms of location, but not in terms of load applied. Three different load conditions were calculated; the "worst case loading" is presented in this thesis. The loading regions are shown in Figure 3.5, superimposed on the finite element grid. The loading associated with these regions is presented in Table 3.1. This type of loading was achieved in STAGSC-1 by the use of a subroutine called UPRESS that is user generated. The user generates the code along the guidelines in

Load Region	1	2	3	4	5	6	7	8	9	10
Load (psi)	1.57	1.82	1.77	1.92	1.77	2.27	2.02	1.32	1.37	0.50
Load Region	11	12	13	14	15	16	17	18	19	20
Load (psi)	0.50	1.67	1.37	1.97	1.72	2.32	2.22	1.62	1.77	0.50

Table 3.1 Static Equivalent Loads

reference [16], compiles it, and links it with the STAGS program. Since the loading in this case is a live (remains normal to the surface) pressure load, the subroutine allows for a flag to the main program to calculate the loads as follower (live) loads (see section 2.2.3). The subroutine used on the final model is shown in

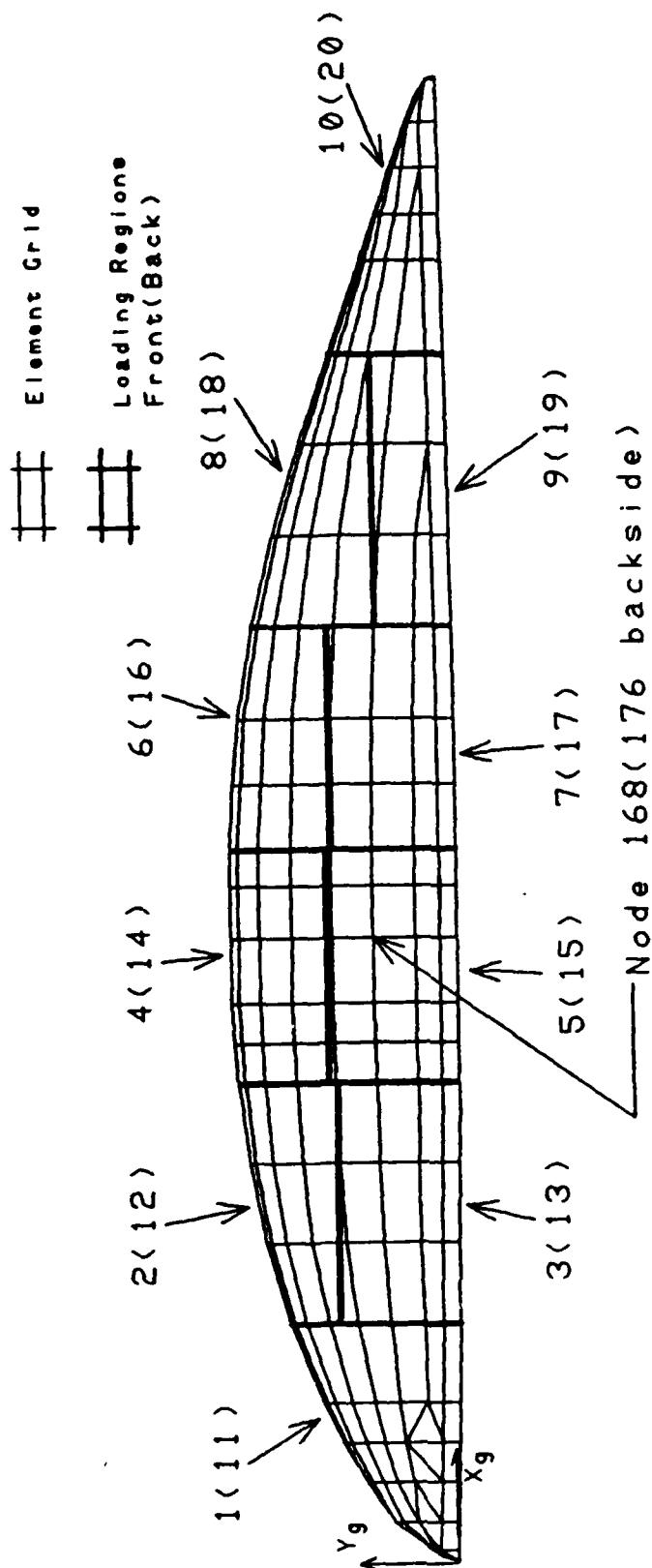


Figure 3.5 Finite Element Model and Loading Regions

Appendix H. The loads on the structure are applied in 0.1 increments of the total load for nonlinear runs.

The modeling of this shell structure was done in three phases. In each of these phases the previous model was modified to more closely approximate the actual shell. For example, changes in the first phase were kept for Phase II and improved upon. Some of the modeling parameters that were changed to more accurately model the shell and the phase in which they were changed include:

1. Thickness variation (Phase I).
2. Material modeling (Phase II and III).
3. Boundary conditions (Phase II).
4. Element type (Phase III).

The baseline model (starting model) consists of a constant thickness, isotropic shell with clamped boundary conditions and STAGS' QUAF 410 quadrilateral and TRINC 320 triangular elements (see section 2.2.4). The primary type of analysis during these phases is a static nonlinear analysis with linear static runs completed for comparison purposes. For the nonlinear runs a full Newton-Raphson solution technique (see section 2.2.5) was used to obtain the displacement solutions.

Load versus normal (to the shell surface) displacement plots are shown for Phase I through III models at nodes 163 and 176 (see Figure 3.5). In the element unit model the degrees of freedom coincide with global axis directions. In order to later compare the experimental displacements (normals) to the finite element displacements the finite element model displacements needed to be transformed into surface normals. The method used to transform the finite element

global displacements to surface normal displacements is shown in Appendix D.

To insure that the finite element model accurately models the shell, a convergence test was conducted to insure that the aspect ratios used in the model are acceptable. The aspect ratio is the length of the longest side of the element divided by its short side. In general, elongated (shaped like a rectangle) linear elements behave poorly, but quadratic elements are well behaved when elongated [6]. Since the STAGS QUA4 410 element is cubic in one direction and linear in the other (see section 2.2.4), it is not apparent whether the QUA4 410 element will behave correctly in this model.

In the center section of the model, away from the boundaries, the aspect ratios are approximately 1.5 to 1. A convergence test was done on a similar structure with aspect ratios of 2 to 1 and 1 to 1 to determine if the model is acceptable. The following section contains the results of this test.

The following sections detail the convergence test and Phases I-III modeling. With the basics of the model discussed, the explanation of the finite element modeling can proceed.

### 3.1 Convergence Test

The convergence test for the finite element model is done on a structure similar to the actual model. The reason the analysis was done on a similar model rather than the actual model is that in order to reduce the grid size for the actual model, new nodes, and element

connectivity would have to be defined and entered by hand (the basic model consists of approximately 750 lines of input while the final model has over 2000 lines). Using a STAGSC-1 ellipsoid shell unit (see reference [16]) on the other hand reduces the input dramatically (approximately 70 lines) while still being able to show the validity of the aspect ratio used in the real model. Convergence tests using 2 to 1 and 1 to 1 aspect ratios are used to validate the 1.5 to 1 aspect ratio used in the actual model.

Before showing the convergence test, an explanation of the STAGS shell unit reference system needs to be addressed. The reference system is based on a surface system where the shell is defined by surface coordinates  $X$  and  $Y$ . The global system coordinates are  $x$ ,  $y$  and  $z$ . Figure 3.6 shows the relation of the surface and global reference systems for the STAGSC-1 ellipsoid shell.

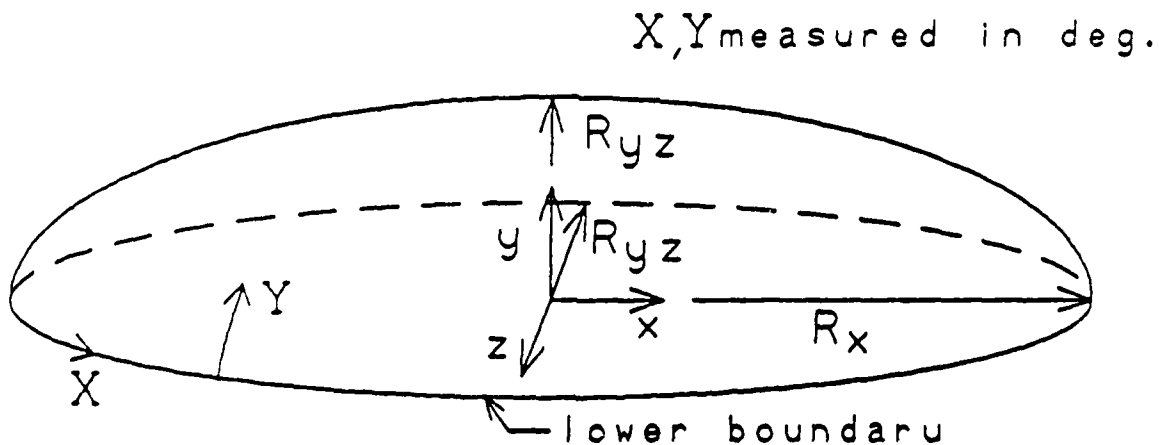


Figure 3.6 Ellipsoid Surface ( $X, Y$ ) and Global ( $x, y, z$ ) Reference Systems

For the convergence test  $R_x$  is 108.0 in. and  $R_y$  is 26.0 in. (see Figure 3.6) which will approximate the length of the shell but will make the convergence model wider than the actual model.

The thickness of the convergence model is taken to be constant over the entire shell and is 0.1455 in. This is the thickness used in the Phase I constant thickness model (see section 3.2).

Although the actual model is made of a Kevlar/Polyester composite fabric, the convergence model will treat the fabric as an orthotropic laminate with ply orientations of 0 and 90 degrees . There are a total of 40 plies used in this model that make up the thickness of the shell. The material properties for this material are:

$$E_1 = 4.89 \times 10^6 \text{ psi}$$

$$E_2 = 4.23 \times 10^5 \text{ psi}$$

$$\nu_{12} = 0.44$$

$$\nu_{21} = 0.038$$

$$G_{12} = 1.9 \times 10^5 \text{ psi}$$

This type of modeling treats the material orthotropically as in Phase II Modeling (section 3.3), and is explained in that section.

The finite element models for the convergence test are shown in Figure 3.7 with the loading regions superimposed on the grids. The loads used are the same as those shown in Table 3.1. The application areas of the loads varies from the actual model but is sufficiently close. Once again, the thrust of this convergence test is to validate the aspect ratio used in the actual model. The boundary conditions for the model are assumed clamped at the bottom edge.

The convergence models were ran using the nonlinear solution



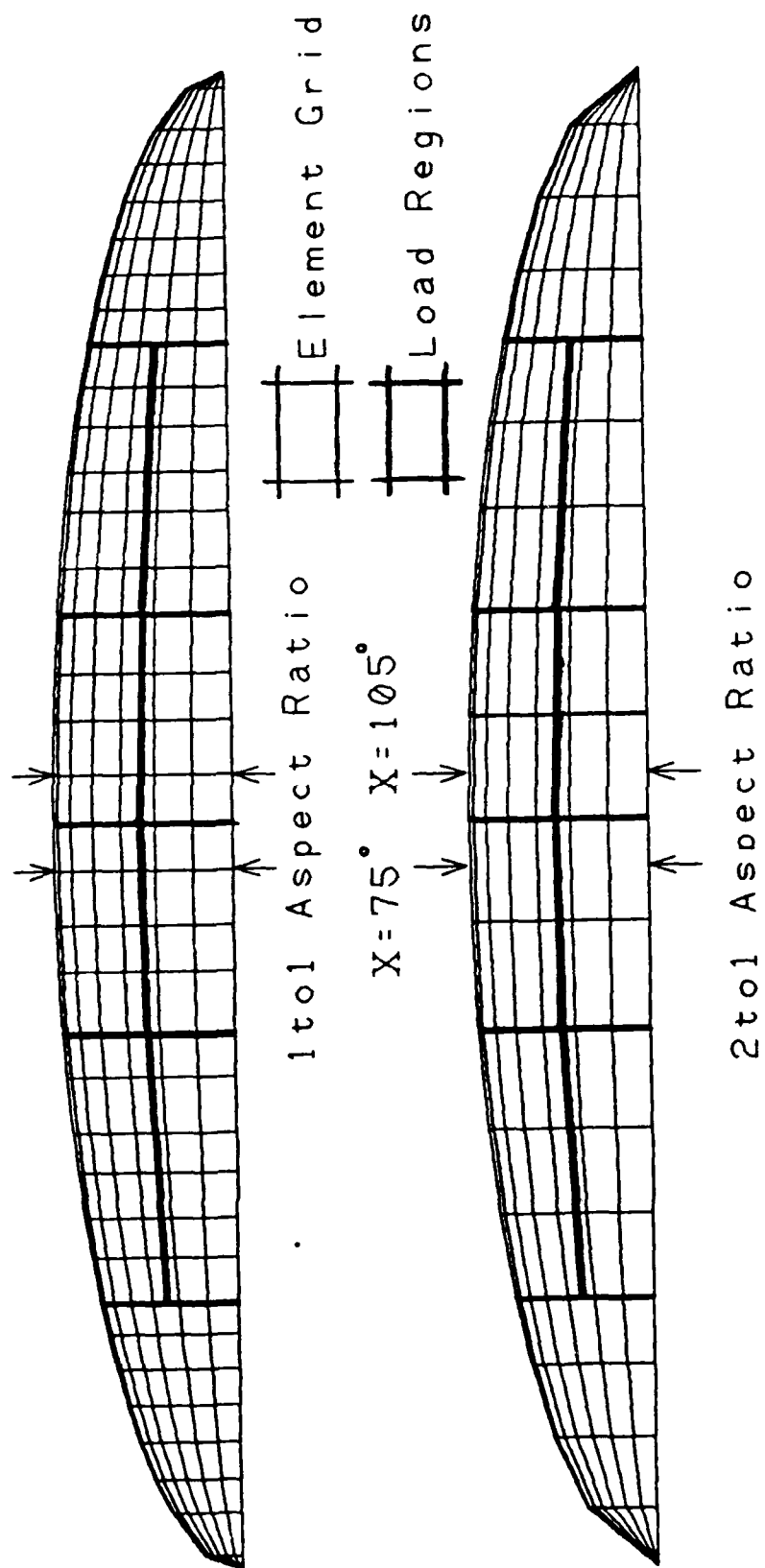


Figure 3.7 Convergence Test Finite Element Models with Loading Regions

option in STAGSC-1. The element used is a QUA4 410 (see section 2.2.4) STAGS element. The data deck used on the 1 to 1 convergence model is shown in Appendix E. The 2 to 1 model input deck is identical to the 1 to 1 model deck except for the N4 card where every other X value is omitted (see Appendix E). Loading on the structure is achieved by using the UPRSS subroutine option in STAGSC-1 [16]. The user creates the subroutine, compiles it, and then links it with the main program. The subroutine is shown in Appendix F.

The convergence test uses the stresses in the elements for model comparisons. Stresses were chosen since the strains are calculated from displacements, and stresses from the strains. If there is any discrepancies between models, they will be magnified in the stress calculations. Stresses in the X and Y directions (surface coordinates) were calculated at the element centroids for the innermost composite ply using the STAGSC-1 post processor (POSTP) [16].

To compare the 1 to 1 and 2 to 1 aspect ratio models, stresses in the X and Y directions (surface reference) were used at X equals 75 and 105 degrees. For the 2 to 1 aspect ratio model this X coordinate coincides with the centroid of the elements shown in Figure 3.7; the location where the stresses were calculated. For the 1 to 1 aspect ratio model the stresses at the centroids of the elements adjacent to X equals 75 and 105 degrees were averaged and used for comparison to the 2 to 1 aspect ratio model.

The results of this comparison for the stress in the X direction are shown in Figure 3.8 for X equals 75 degrees and in Figure 3.9 for X equals 105 degrees. The stresses in the Y direction are shown in

Figure 3.10 for X equals 75 degrees and in Figure 3.11 for X equals 105 degrees. The results in Figures 3.9 to 3.11 are shown for all elements in the Y direction (measured in degrees circumferentially) for the respective X value.

From examining Figures 3.8 to 3.11 it is evident that the aspect ratio of 1.5 to 1 used in the actual model should approximate the shell surface correctly. This conclusion is based on the fact that the stress results for the 1 to 1 and 2 to 1 models are extremely close in the both the X and Y directions over the entire area examined.

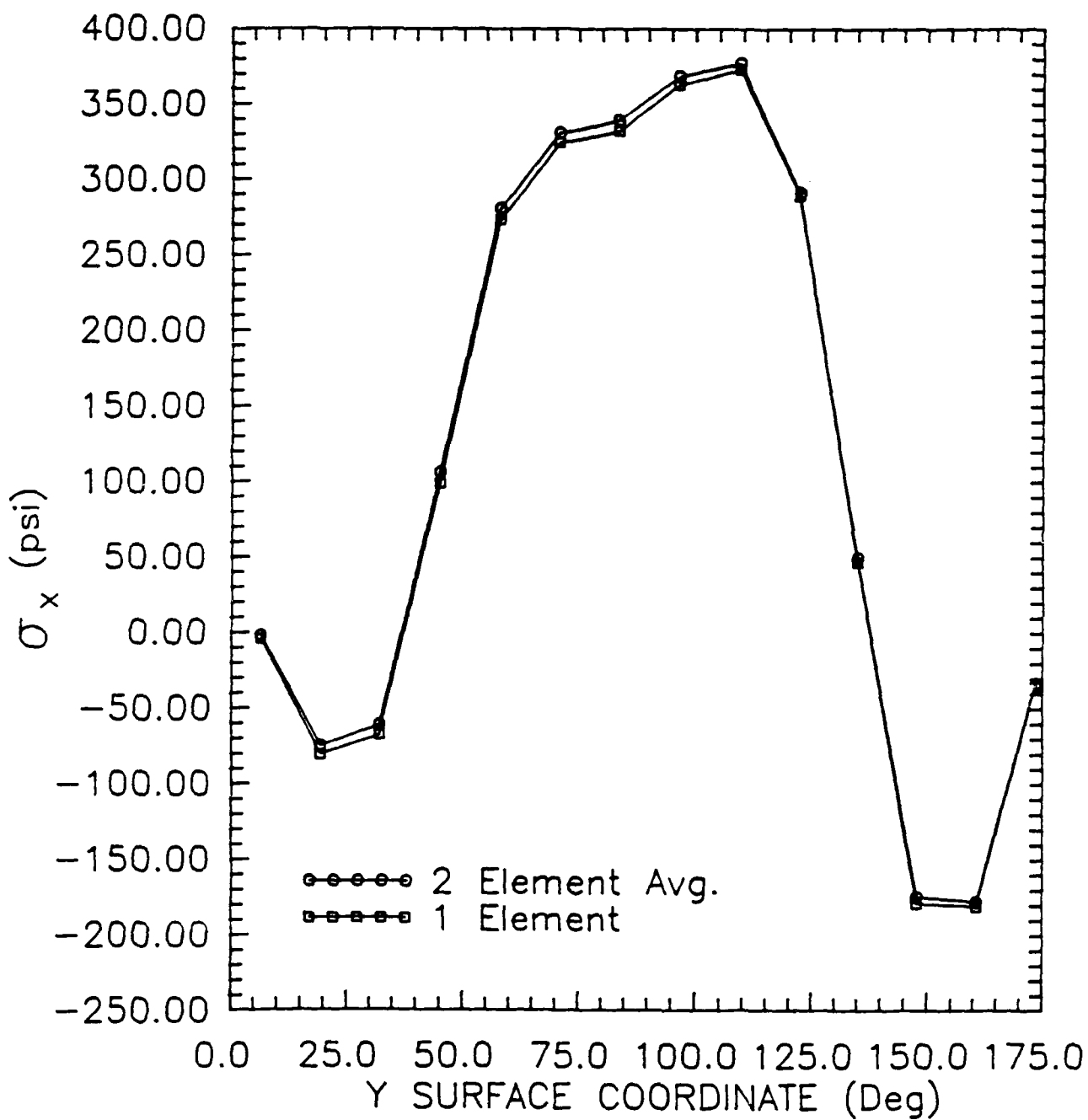


Figure 3.8 Convergence Test Results for  $\sigma_x$  at  $X=75$  degrees

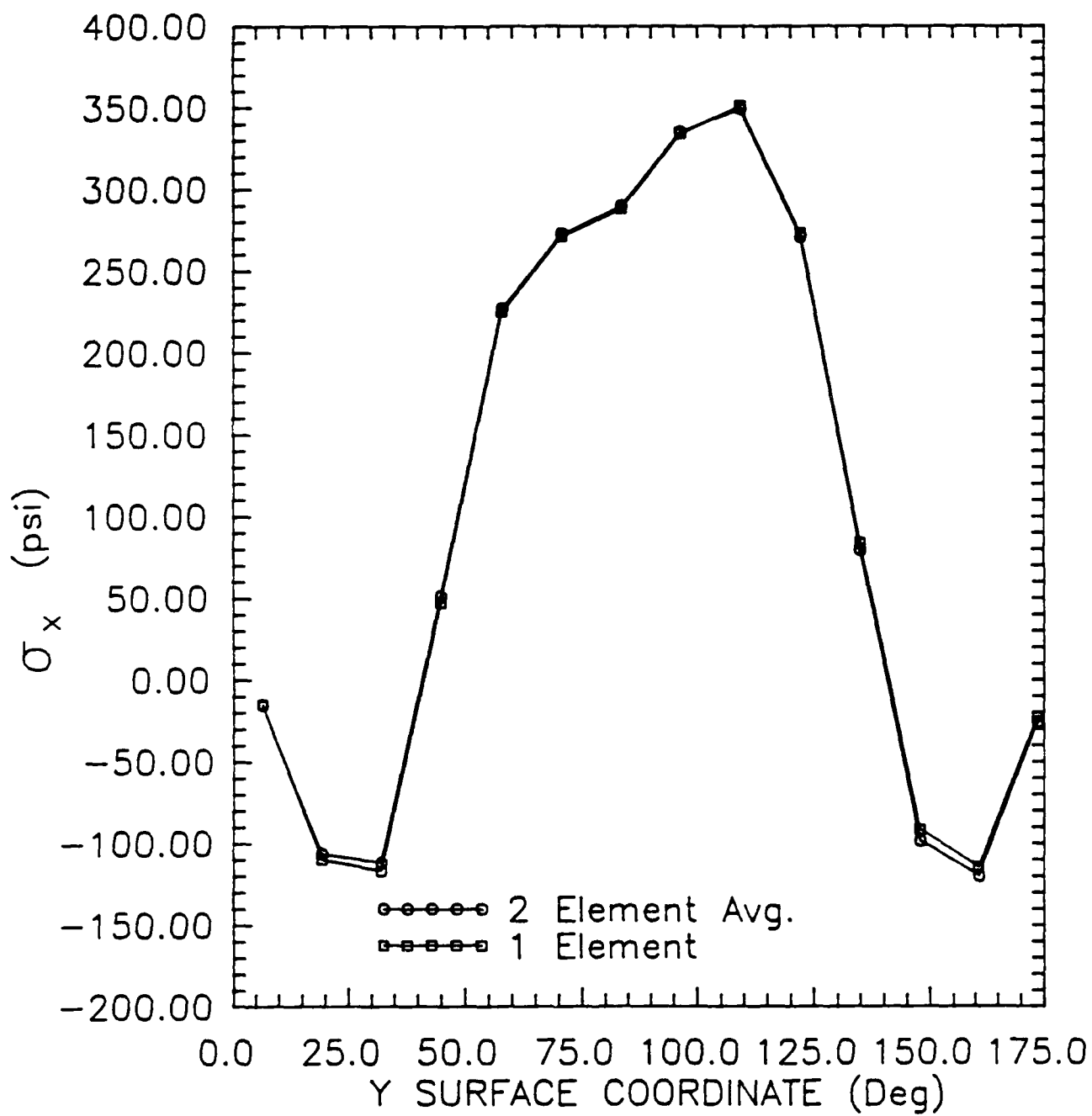


Figure 3.9 Convergence Test Results for  $\sigma_x$  at  $X=105$  degrees

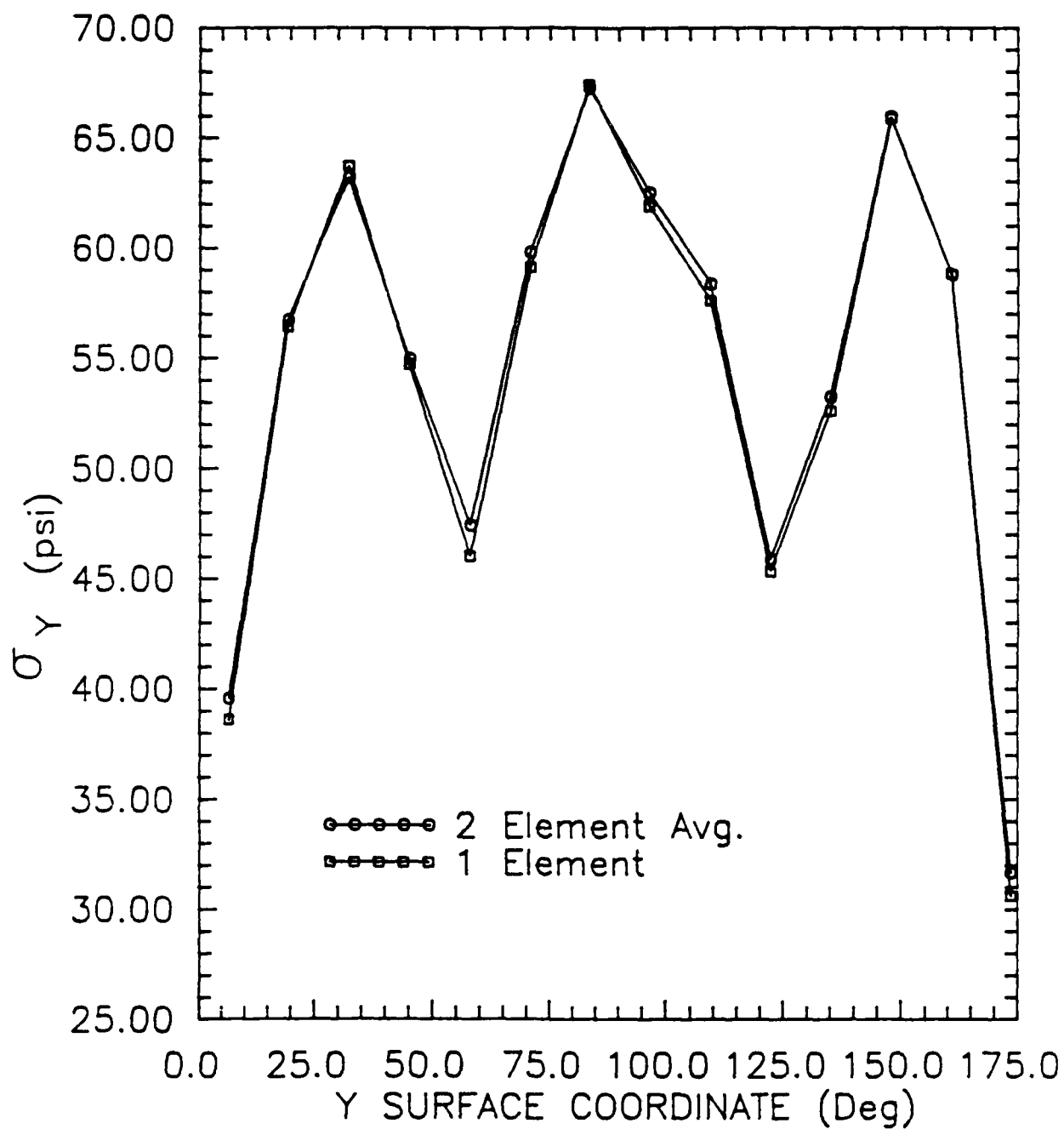


Figure 3.10 Convergence Test Results for  $\sigma_y$  at  $X=75$  degrees

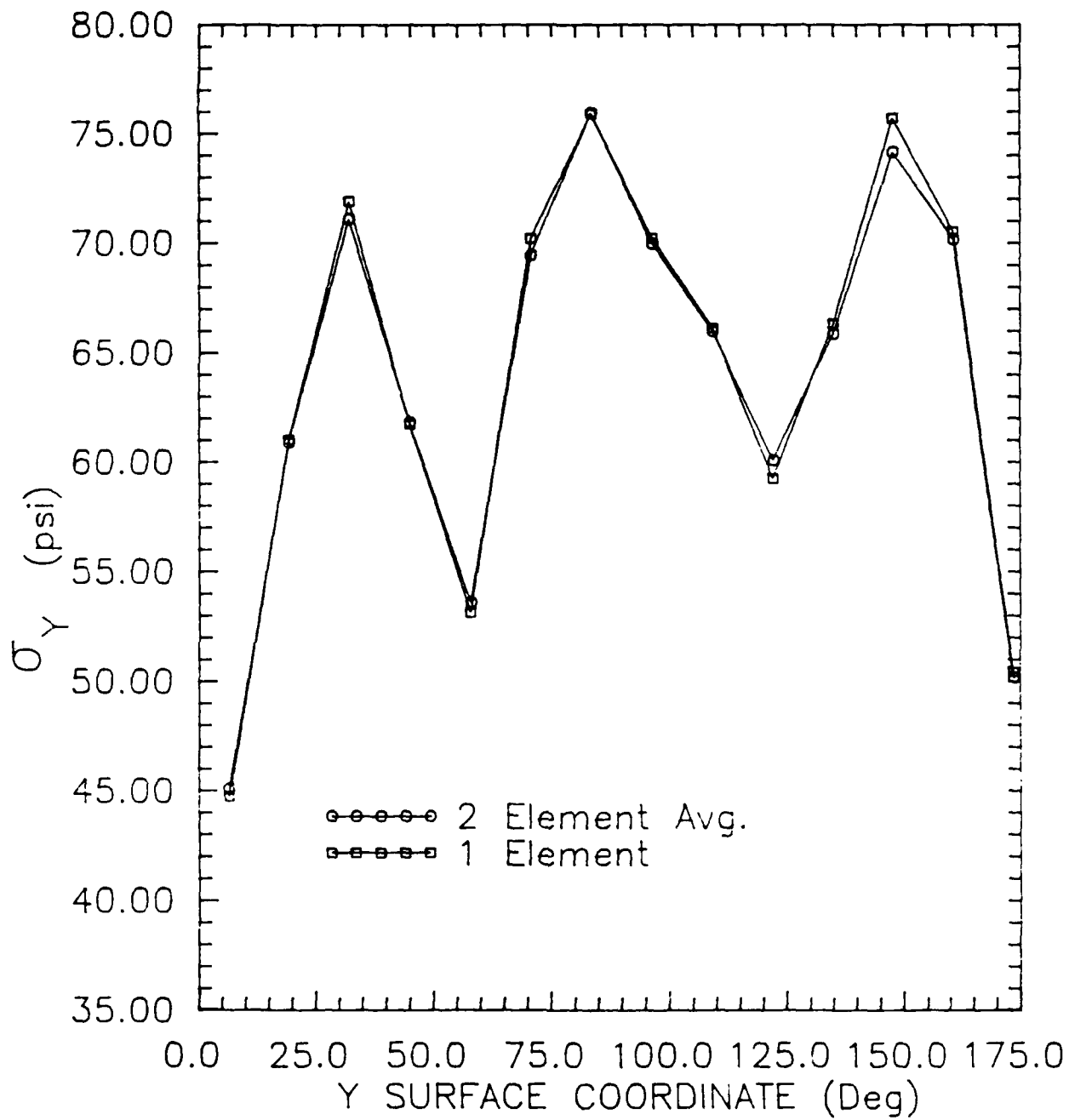


Figure 3.11 Convergence Test Results for  $\sigma_y$  at  $X=105$  degrees

### 3.2 Phase I Modeling

Phase I consists of three models, developed sequentially, to better understand the STAGSC-1 code and analysis involved. Table 3.2 presents the models developed in Phase I.

Mod	Solution	Thickness	Material	B.C.s	Type	DOF(ADOFF)*	Elem
1	Linear	Constant	Isotrop.	Clamp	410	2888(1908)	362
2	Nonlin.	Constant	Isotrop.	Clamp	410	2888(1908)	362
3	Nonlin.	Variable	Isotrop.	Clamp	410	2888(1908)	362

\* DOF= Degrees of Freedom

Elem= Total # of Elements

ADOFF= Active Degrees of Freedom    Type= Element Type

Table 3.2 Phase I Models

The starting model in the analysis is a constant thickness, isotropic model with clamped boundary conditions at the lower boundary. The model uses primarily QUA4 410 plate elements to approximate the surface with TRINC 320 triangular elements (see reference [16]) used where necessary.

The constant thickness model actually has two different thicknesses associated with it. The row of elements along the entire lower edge are 0.29 in. thick. The elements in the rest of the shell are 0.1455 in. thick.

The variable thickness model better approximates the actual thickness distribution in the shell. Figure 3.12 shows this thickness variation over the shell. A taper was built into the actual composite shell between thickness regions to gradually change



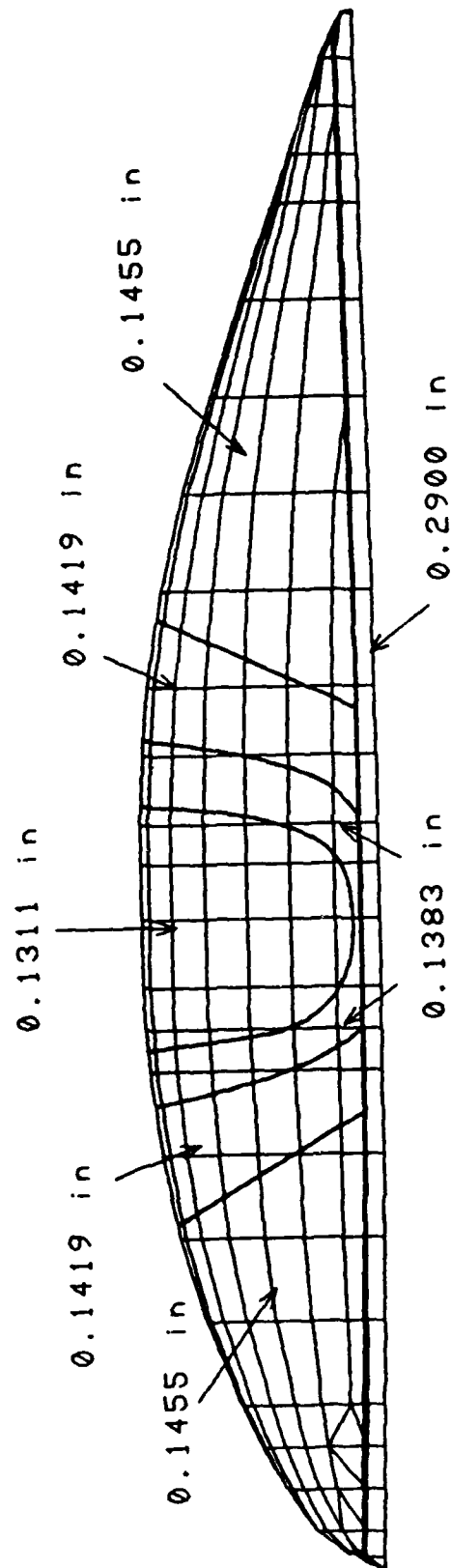


Figure 3.12 Shell Thickness Variation

the thickness variations; eliminating stress concentrations due to step transitions. To approximate this thickness variation, without refining the grid, an average element thickness was used based upon the element surface area. On a scale drawing similar to Figure 3.12, elements that had a thickness variation line cutting through them were given average thicknesses. For example, if an element was cut so that 60% of the element area was in the 0.1455 in. area and the remaining 40% was in the 0.1419 in area the resulting thickness would be:

$$t_{avg} = 0.6(0.1455 \text{ in.}) + 0.4(0.1419 \text{ in.}) = 0.144 \text{ in.}$$

Thicknesses were rounded to three decimal points except in areas where they are completely contained in a thickness region. In this case they were given the associated four decimal point thickness value. The thickness variation modeling resulted in 26 different thicknesses; 11 at the lower edge and 15 in the upper section of the model.

As stated earlier, the models in this phase were developed to better understand the STAGS program and the analysis in general. Therefore, all models in Phase I use an isotropic material modeling (orthotropic modeling is considered in sections 3.3 and 3.4) to simplify the analysis.

The material properties for the Kevlar/Polyester composite fabric were determined through testing by the Air Force Wright Aeronautics Laboratory (AFWAL) Materials Laboratory, Wright-Patterson AFB, Ohio. The results of tensile tests on the material gave:

$$E = 4.89 \times 10^6 \text{ psi}$$

$$G = 0.19 \times 10^6 \text{ psi}$$

$$\nu = 0.038$$

Since the Kevlar/Polyester composite weave is not an isotropic material, some assumptions were made. The value for Young's modulus, E, was used as shown. Poisson's ratio,  $\nu$ , was modified to approximate an isotropic material such as aluminum with a value of 0.33 [19]. The shear modulus, G, was also modified to fit its isotropic definition of [14]

$$G = \frac{E}{2(1+\nu)} \quad (3.1)$$

Using the value for E and the assumed  $\nu$  value gives, from Equation (3.1), a shear modulus of  $2.362 \times 10^6$  psi.

As shown in Table 3.2, the boundary conditions used in this phase of modeling was a clamped boundary condition around the entire bottom edge. Clamped means that all boundary degrees of freedom are constrained to zero displacement.

The QUAF 410 quadrilateral element and the TRINC 320 triangular element were used in this Phase due to their reduced degrees of freedom as compared to the QUAF 411 and TRINC 321 elements. Also, with the new rotational degree of freedom formulation (see section 2.2.5) the 410 element is better behaved under rotation [18].

The Phase I models were run on the VAX 11/785 computer using the STAGSC-1 program. One immediate result from the runs was the amount of computer time (Central Processing Unit (CPU) time) necessary to complete these runs. The linear run took only 11 minutes as opposed to the nonlinear runs which took 4 hours and 37 minutes each. As stated earlier, the nonlinear runs used the full Newton-Raphson method (as opposed to the modified Newton-Raphson method) as outlined

in section 2.2.5.

Load versus normal displacement plots are shown in Figures 3.13 and 3.14 for nodes 168 and 176 (Figure 3.5) respectively.

From examining Figures 3.13 and 3.14 it is evident that there is a difference between the linear and nonlinear constant thickness models. The nonlinear model is stiffer due to the coupling of in-plane and bending forces due to the higher order terms in the nonlinear kinematic relations.

The nonlinear models also show a difference due to the thickness variation. At the particular nodes graphed in Figures 3.13 and 3.14, the thickness difference is 0.0144 in. This effect is not as dramatic as the previously mentioned effect of a linear versus nonlinear run, but it does show a reduction in the stiffness of the model in this area due to the reduction of the bending moments; caused by the thinner model. There also is an interesting difference between the linear model and the nonlinear variable thickness model below about 0.4 of the total load. Initially the nonlinear model is not as stiff as the linear model, but this changes after about 0.4 of the total load due to the nonlinear coupling of membrane and bending forces.

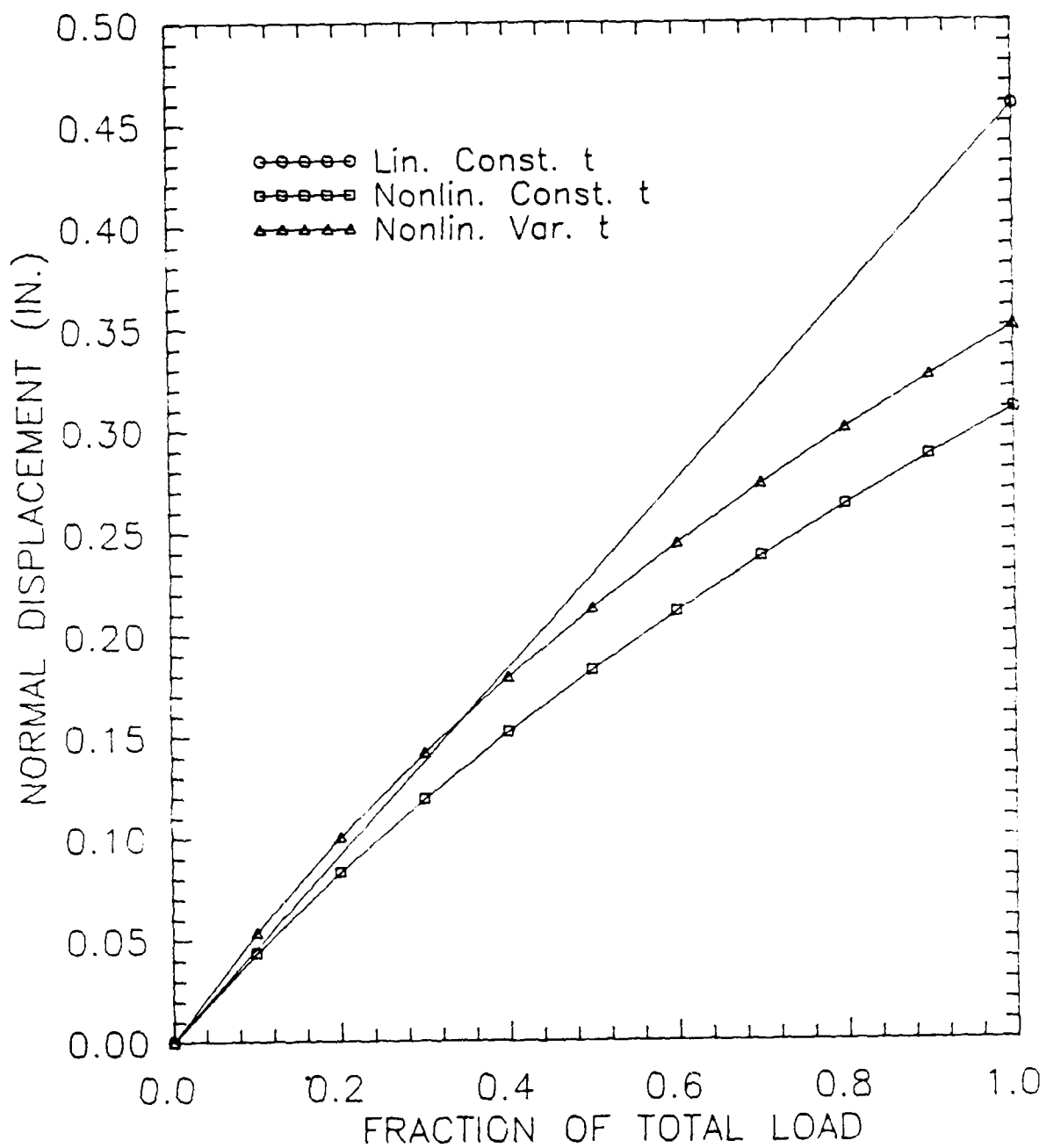


Figure 3.13 Node 168 Phase I Modeling: Isotropic Material, 410 Element, Clamped B.C.s

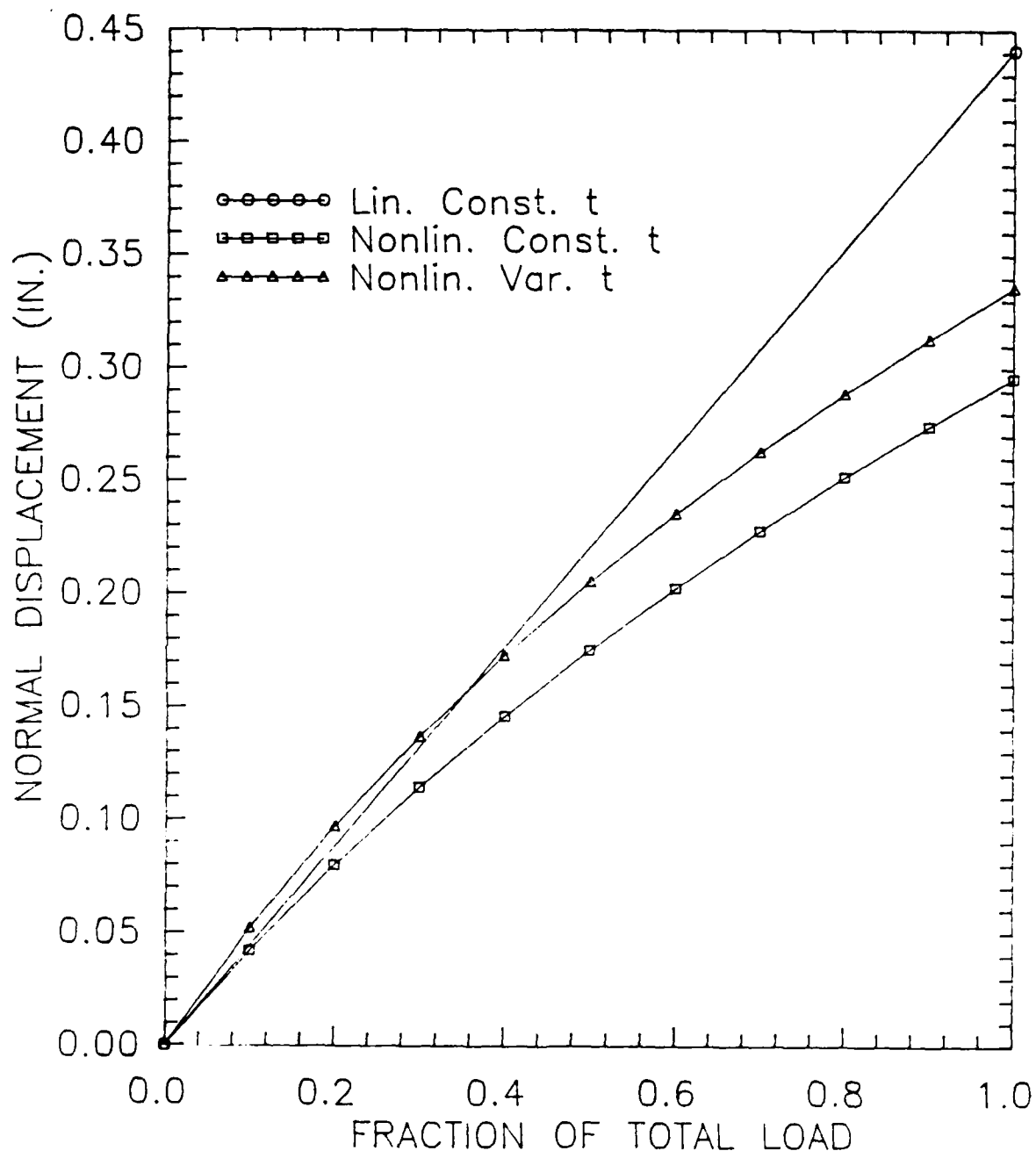


Figure 3.14 Node 176 Phase I Modeling: Isotropic Material, 410 Element Clamped B.C.s

### 3.3 Phase II Modeling

The basic model carried forward from the Phase I modeling is the nonlinear variable thickness model. All of the models in Phase I were modeled with an isotropic assumption, clamped boundary conditions, and QUA4 410 quadrilateral elements. The basic changes to this model include modifying the isotropic material assumption (modeling it as an orthotropic material) and modifying the boundary conditions. The three models developed in Phase II are shown in Table 3.3

Mod	Solution	Thickness	Material	B.C.s	Type	DOF(ADOFF)*	Elem
4	Nonlin.	Variable	Orthotrop	Clamp	410	2888(1908)	362
5	Linear	Variable	Orthotrop	Clamp	410	2888(1908)	362
6	Nonlin.	Variable	Orthotrop	Mod.	410	3616(2268)	466

\*DOF= Degrees of Freedom

Elem= Total # of Elements

ADOFF= Active Degrees of Freedom

Type= Element Type

Table 3.3 Phase II Models

The actual material used in the shell construction is a Kevlar-49/F-141 Polyester composite fabric (weave). The edge (0.29m thickness area in Figure 3.12) also includes a one ply inner and outer edge backup of Glass 7781/F-141 Polyester. STAGS is capable of handling composite materials through the thickness of the shell (the wall composition), but the specific types include a layered wall (orthotropic), a fiber wound wall, and a corrugated wall [16]. The shell material is a layered orthotropic material (composite weave)

but this is not the type of orthotropic material that STAGS is designed to handle (STAGS is designed for unidirectional composite materials).

After a thorough search on how to model this weave material, two solutions were found. The first was to model the weave as a layered isotropic material using all three of the material constants ( $E$ ,  $G$ , and  $\nu$ ) calculated by the AFVAL Materials Laboratory (see section 3.2). The second was to model the structure as a unidirectional orthotropic layered material which would involve modifying the ply lay-up and estimating a few material constants.

After examining a few test cases of modeling a simple structure with the same types of weave solutions as previously mentioned, it was found that the orthotropic (unidirectional and layered) material modeling was much more flexible than the isotropic modeling.

With the test cases in mind and from looking at preliminary experimental data in the same region (showing very large deflections) the orthotropic material modeling was used for the Kevlar/Polyester material.

To model the Kevlar/Polyester composite orthotropically, each lamina (ply) was split in half and modeled as two 0 and 90 degree plies (each having one-half the thickness of the original weave ply). At first glance this may not seem like a good approach since the lay-up will not be symmetric (the inner ply will always be at 0 degrees orientation and the outer ply at 90 degrees) and a coupling of in-plane and bending forces due to the material matrix  $[B]$  (see Appendix C) will result. This effect occurs but is very mild due to the number of plies in the lay-up and the thickness of the plies. In



order to model the shell this way the properties for an orthotropic material were found. For an orthotropic material (plane stress condition) the properties are [14]:

$E_1$  - Young's modulus in the 1-direction

$E_2$  - Young's modulus in the 2-direction

$\nu_{12}$  - Poisson's ratio in the 2-direction when loaded in the 1-direction

$\nu_{21}$  - Poisson's ratio in the 1-direction when loaded in the 2-direction

$G_{12}$  - Shear modulus in the 1-2 plane

where the subscripts 1 and 2 indicate material coordinates as shown in Figure C.2, Appendix C. In order to find these values, some approximations were made.

From the Phase I modeling section, the results of the AFWAL tests on the Kevlar/Polyester composite were:

$E = 4.89 \times 10^6$  psi

$G = 0.19 \times 10^6$  psi

$\nu = 0.038$

The Young's modulus,  $E$ , from above can be assumed as  $E_1$  since it is the modulus in the fiber direction and for a weave this is 0 or 90 degrees. From examining Poisson's ratios for composite materials in references [14] and [20] it would appear that the Poisson's ratio given would correspond to  $\nu_{21}$  due to its extremely low value.

Therefore the given Poisson's ratio will be used as  $\nu_{21}$ . The shear modulus,  $G$ , is the in-plane shear therefore it will be used as  $G_{12}$ .

The only value left to find is  $E_2$ ; since for an orthotropic material  $\nu_{12}$  can be found from [14]

$$\nu_{12} = \nu_{21} \frac{E_1}{E_2} \quad (3.2)$$

Orthotropic material properties could not be found for Kevlar/Polyester, however Graphite/Epoxy values are readily available. To estimate a value of  $E_2$  for Kevlar/Polyester a ratio of  $E_1$  to  $E_2$  for Graphite/Epoxy was used along with the assumed Kevlar/Polyester  $E_1$  value. From reference [20] a ratio of  $E_1$  to  $E_2$  for Graphite/Epoxy is approximately

$$\frac{E_1}{E_2} = \frac{18.5 \times 10^6 \text{ psi}}{1.6 \times 10^6 \text{ psi}} = 11.56 \quad (3.3)$$

With the ratio found in Equation (3.3) and the Kevlar/Polyester  $E_1$  value,  $E_2$  becomes

$$E_2 = \frac{E_1}{11.56} = \frac{4.89 \times 10^6 \text{ psi}}{11.56} = 4.23 \times 10^5 \quad (3.4)$$

Now if one uses Equation (3.2) a value for  $\nu_{12}$  can be found resulting in

$$\nu_{12} = 0.038 \left( \frac{4.89 \times 10^6 \text{ psi}}{4.23 \times 10^5 \text{ psi}} \right) = 0.44 \quad (3.5)$$

Properties for the edge backup material (Glass/Polyester cloth) used on the shell were not determined experimentally, therefore approximate values were used.

The glass plies were treated as an isotropic material, as in Phase I for Kevlar/Polyester, since they only make up about six percent of the edge thickness. A value for Young's modulus for Glass/Polyester cloth was found in reference [21] and was  $3.24 \times 10^6$  psi. A Poisson's ratio could not be found for a cloth material so a Poisson's ratio was estimated, as in Phase I modeling, as 0.33. The

shear modulus was calculated from Equation (3.1) as  $1.22 \times 10^6$  psi.

In order to model the shell as a laminate of composite plies the specification for the ply lay-up was used. A listing for the ply lay-up is shown in Table 3.4 for the different thickness areas shown in Figure 3.12. This table is for the actual shell; the model is

Ply No.†	t/ply	total t	Mat.	Region Thicknesses (Figure 3.12)				
				0.1311	0.1383	0.1419	0.1455	0.2900
A‡	.0085	.0085	G					X
1	.0036	.0036	K	X	X	X	X	X
2-16	.0085	.1275	K	X	X	X	X	X
17-18	.0036	.0072	K		X	X	X	X
19	.0036	.0036	K			X	X	X
20-34‡	.0085	.1275	K					X
35	.0036	.0036	K				X	X
B‡	.0085	.0085	G					X
Total Plies				16	18	19	20	37

\* K-Kevlar/Polyester    † Numbered from outer ply inward  
 G-Glass/Polyester    ‡ Used only on the edge  
 (Dimensions in inches)

Table 3.4 Actual Shell Ply Lay Up

laid up the same way except that each ply in the finite element model is made up of two 0 and 90 degree plies each having half the thickness of the actual shell ply.

As an example of the lay-up used in the finite element model consider an element in the 0.1419 in. thickness region (see Figure 3.12). Doubling the number of plies and halving each ply thickness in Table 3.4 gives the lay-up in this thickness region, for the finite element model, as follows:

- 2 layers of 0.0018 in. Kevlar/Polyester

- 30 layers of 0.00425 in. Kevlar/Polyester
- 4 layers of 0.0018 in. Kevlar/Polyester
- 2 layers of 0.0018 in. Kevlar/Polyester

where all plies alternate between 0 and 90 degrees orientation.

Thicknesses that lie between the actual shell thicknesses (see Figure 3.12) due to the variable thickness approximation (see section 3.2) are modeled as in the following example of a hypothetical 0.144 in. thick element. This thickness lies between the 0.1419 in. and 0.1455 in. thickness regions in Table 3.4. The model is first given the total lay-up of the 0.1419 in. region as in the previous example. The remaining thickness (0.0021 in.) is divided into two 0 and 90 degree plies (corresponding to ply no. 35, Table 3.4) of Kevlar/Polyester.

All thicknesses above 0.1455 in. in the variable thickness model correspond to edge thicknesses. These approximated thicknesses for the edge elements vary from 0.231 to 0.29 in. From Table 3.4 the total number of plies in the actual shell edge is 37 which corresponds to 74 plies in the orthotropic approximation for the model. After trying a 74 ply run on the computer it was found after several attempts that STAGS is limited to approximately 50 plies. With this in mind the edges were modeled with 42 plies. Plies 1, 17-18, and 35 were left as shown in Table 3.4 (modified as before by halving each shell ply). Plies A and B were left at full thickness and treated isotropically. Plies 2-16 in Table 3.4 were modeled as 20 plies at 0.006375 in. each. Plies 20-34 in Table 3.4 are where the variable thicknesses on the edge were taken into account. They were modeled as 10 plies with variable thicknesses to accommodate

thicknesses on the edge other than 0.29 in.

All of the models in Phase I and models 4 and 5 in Phase II have clamped boundary conditions at the lower edge. A cross section of the actual boundary (continuous around the entire lower edge) on the lower edge of the shell is shown in Figure 3.15. The lower edge of the finite element model is shown in the figure and this is where the clamped models (Models 1-5) were assumed fixed. The angle  $\theta$  shown in Figure 3.15 is zero degrees over much of the boundary except at each end of the shell where it approaches ten degrees.

By examining Figure 3.15 it is obvious that the clamped boundary condition that was originally assumed is too stiff. The 0.5 in. aluminum plate will allow lateral deflection due to bending, and the rubber washer in the plane of the shell will allow vertical deflection. These two components are changed in the modified

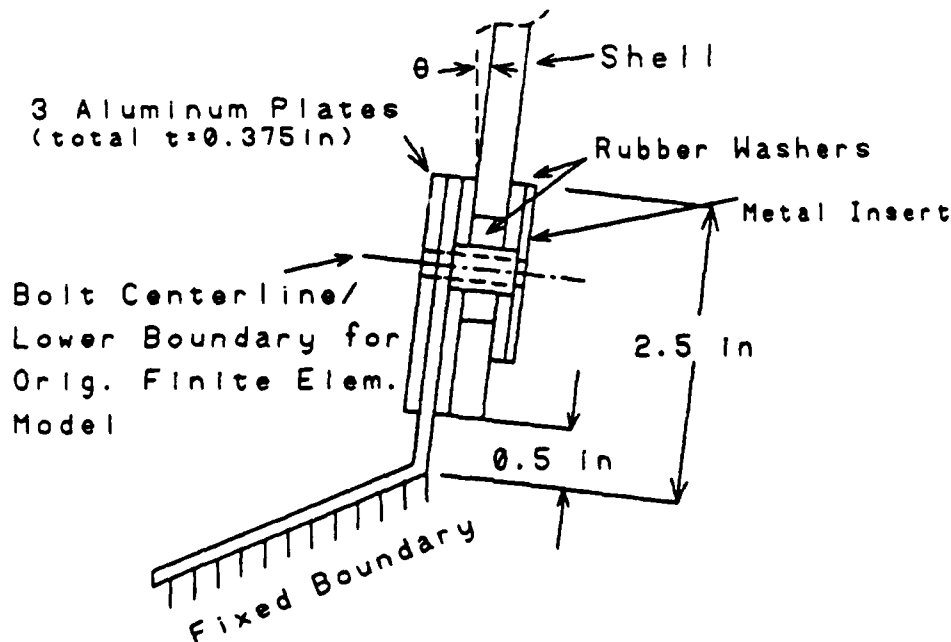


Figure 3.15 Shell Lower Boundary

boundary conditions.

To model the aluminum plate, a 0.5 in. high by 0.125 in. thick plate element was added to the finite element model at the lower edge (see Figure 3.16). The lengths of the elements were determined by the original lower boundary elements directly above the aluminum plate elements. Degrees of freedom at the interface of the shell and plate were assumed free. The material properties of the aluminum plate are [22]

$$E = 10.7 \times 10^6 \text{ psi}$$

$$\nu = 0.33$$

$$G = 4.0 \times 10^6 \text{ psi}$$

To simulate the rubber washer a STAGS general beam element (GSBM2 220) was used. These beam elements were attached to the lower nodes of the aluminum plate element and are oriented vertically (see Figure 3.16). Since material properties for the actual rubber could not be found and even if they could be found, an analytic analysis of the equivalent stiffness of the washers would be extremely difficult. Therefore, an estimate had to be made for the equivalent beam stiffness necessary to model the washers.

This approximation was done using the force (F), stiffness (k), and displacement (x) relation for a spring as in

$$F = kx \tag{3.6}$$

If the displacements due to the rubber washers could be found in the actual model due to the applied forces, the stiffness could be found. This stiffness would then have to be related to the equivalent stiffness in a linear beam as in

$$k = \frac{AE}{L} \quad (3.7)$$

where A is the cross-sectional area, E is the Young's modulus, and L is the length of the beam.

During experimental testing of the shell (see section 4) rough measurements were made at the lower edge of the shell to see how much vertical displacement was caused by the rubber washers. Vertical equilibrium forces were then found from the linear model 5 (see Table 3.3), using the STAGS post processor, at the locations where the rough measurements were taken experimentally. Using these experimental displacements and the finite element forces an approximation of the stiffnesses in the rubber washers could be found from Equation (3.6). The average stiffness found from Equation (3.6) was 6,292 lb./in.

The beam used in the model could then be designed with any combination of variables shown on the right hand side of Equation (3.7) equaling the estimated rubber washer stiffness. The values used for the "rubber beam" in the analysis were

$$A = 1.15 \text{ in}^2$$

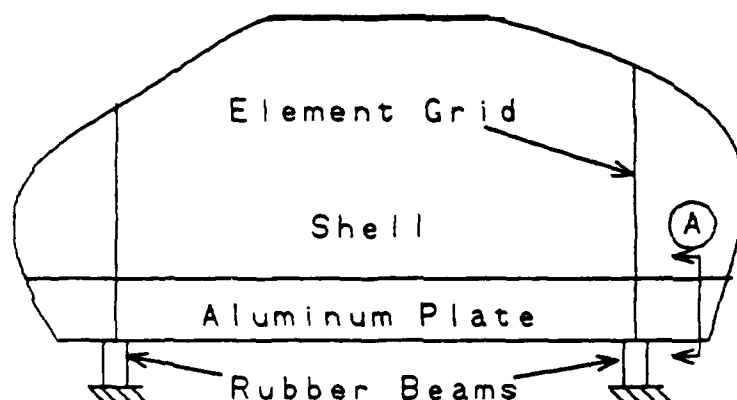
$$E = 2.07 \times 10^4 \text{ psi}$$

$$L = 0.377 \text{ in.}$$

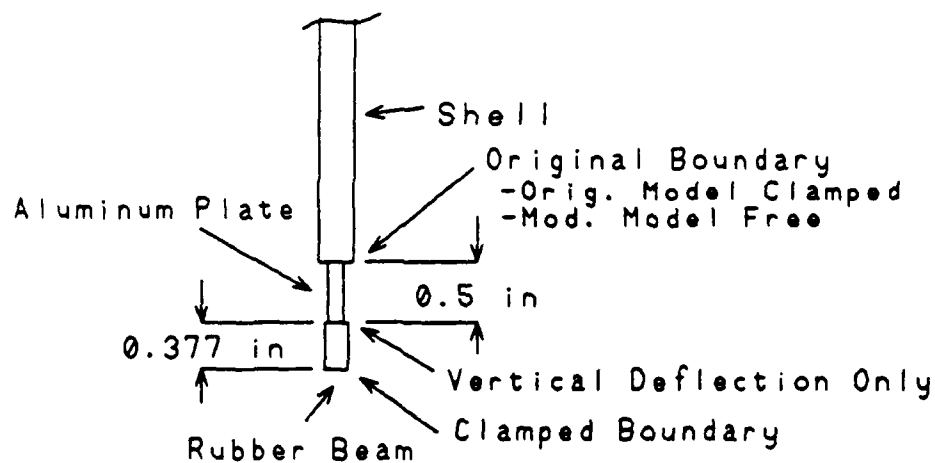
Finally, the beam was modeled in STAGS with a linear kinematic relation since the stiffnesses were calculated linearly. The beam is clamped at the bottom and only allowed vertical deflection at the top; to simulate the vertical deflection of the washer.

Figure 3.16 shows the modified finite element boundary condition in a side and cross section view. The figure shows the relation in

the model between the shell, the aluminum plate, and the "rubber beam." The additional elements (aluminum plate and "rubber beam") do not have an applied load; the shell is loaded as in the clamped models.



Side View



View (A)

Figure 3.16 Modified Finite Element Boundary Condition



As in Phase I modeling, all models in this Phase were ran on the VAX 11/785 computer. The CPU time for the nonlinear clamped model (Model 4) was about 5 hours, 29 minutes. The same model in a linear run (Model 5) took about 15 minutes. The orthotropic model with the modified boundary conditions (Model 6) took about 6 hours, 34 minutes.

Load versus normal displacement plots are shown in Figures 3.17 and 3.18 for nodes 168 and 176 (Figure 3.5) respectively.

From examining Figures 3.17 and 3.18 there is more than a 100 percent difference in the linear versus nonlinear runs for the clamped models. The linear run is assumed in error due to its displacement as compared to the thickness of the shell (0.1311 in.) in the area surrounding the node points 168 and 176. Linear plate (STAGS "shell" element) theory assumes that the displacements are much smaller than the thickness of the shell [1]. For this particular area the opposite is true; the displacements are much larger than the shell thickness. Because of this violation in the thin plate assumption for linear theory, and the tendency in this shell for large displacements under the given loading, Model 5 was the last linear run attempted.

The difference between the clamped and modified boundary condition runs (Figure 3.17 and 3.18) shows a slight but pronounced reduction of stiffness in the modified boundary condition model. The clamped boundary condition obviously is stiffer.

Finally, by going back to Phase I and examining Figures 3.13 and 3.14 for the same nodes, there is a dramatic difference between modeling the structure isotropically versus orthotropically. The

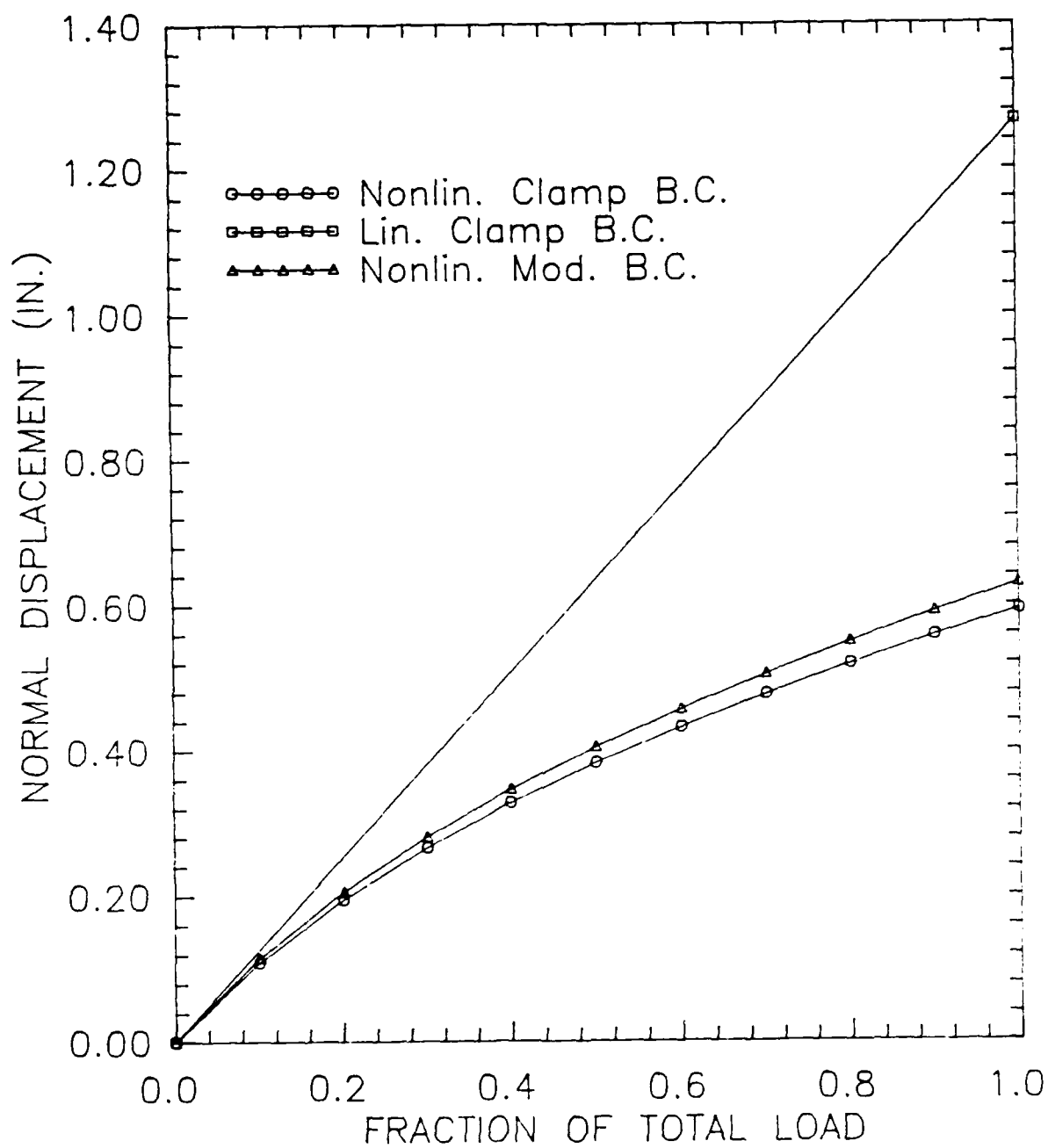


Figure 3.17 Node 168 Phase II Modeling: Orthotropic Material  
Variable Thickness, 410 Element

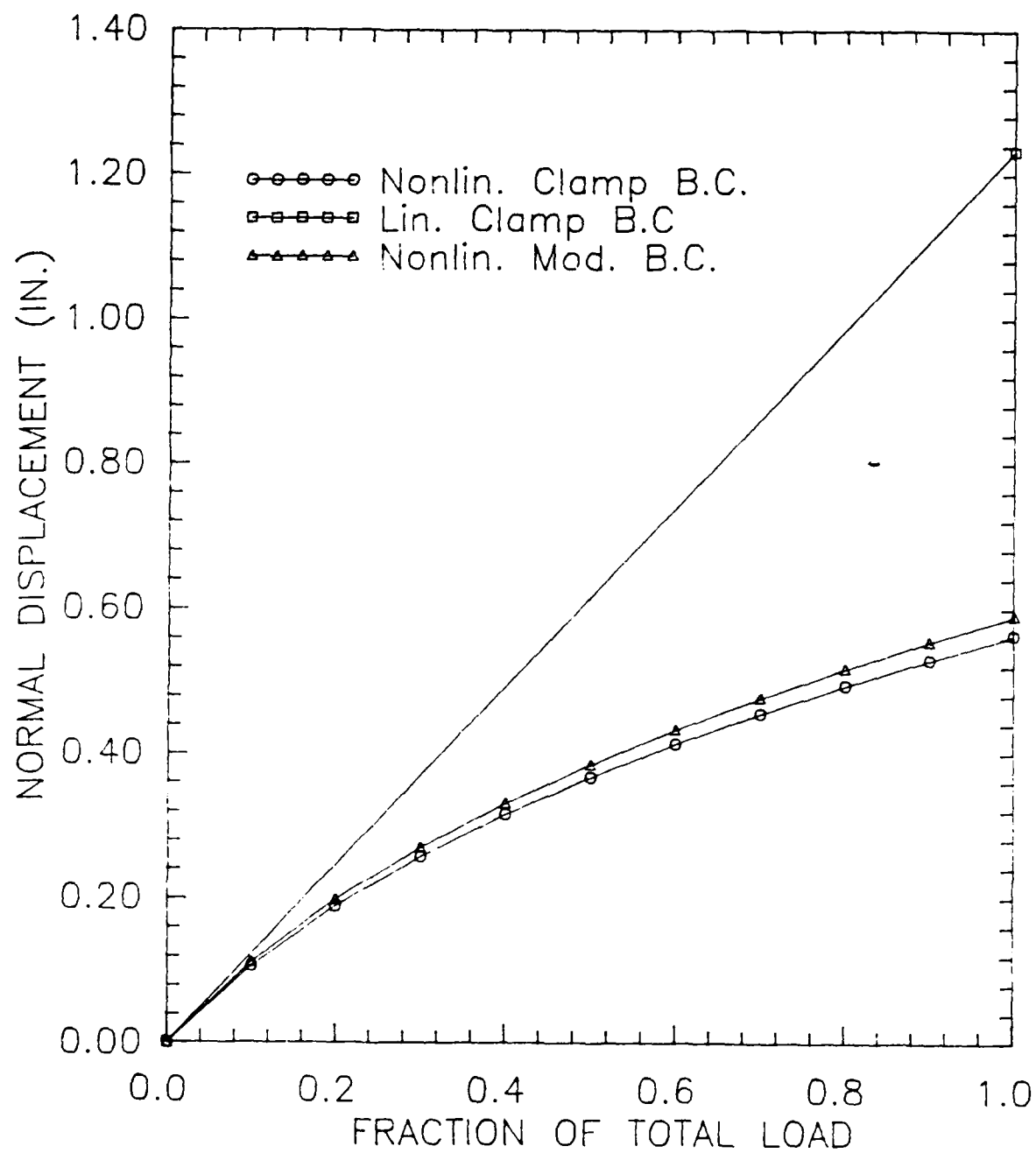


Figure 3.18 Node 176 Phase II Modeling: Orthotropic Material  
Variable Thickness, 410 Element

displacements in the orthotropic model nearly double those of the isotropic model. From this comparison it is a possibility that the material assumption used in Phase I is much too stiff since only one of the actual material constants (Young's Modulus) was actually used. In Phase II all of the actual material constants were used and two were assumed from the relation of another orthotropic material (Graphite/Epoxy). Comparisons of finite element solutions versus experimental results (section 5) will show if the orthotropic assumption is valid.

#### 3.4 Phase III Modeling

In this phase the sixth model (Phase II) in the analysis is used for comparison to the two models developed in this stage. Both of the models developed in Phase III are similar to Model 6 with the exception that one model is changed to model the Kevlar/Polyester material as a layered isotropic material (to compare against the orthotropic material model of section 3.3) and the other model changes the STAGS element types. A summary of these finite element models is shown in Table 3.5 along with Model 6 from Phase II modeling.

The layered isotropic model (Model 7) uses the same lay-up as in Model 6. The only change to the model is that all of the material constants calculated by the AFWAL Materials Laboratory are used. They are written here again for convenience as

$$E = 4.89 \times 10^6 \text{ psi}$$

$$G = 0.19 \times 10^6 \text{ psi}$$

$$\nu = 0.038$$

Mod	Solution	Thickness	Material	B.C.s	Type	DOF(ADOFF) *	Elem
6	Nonlin.	Variable	Orthotrop	Mod.	410	3616(2268)	466
7	Nonlin.	Variable	Isotropic	Mod.	410	3616(2268)	466
8	Nonlin.	Variable	Orthotrop	Mod.	411	5899(3506)	466

\*DOF= Degrees of Freedom

Elem= Total # of Elements

ADOFF= Active Degrees of Freedom

Type= Element Type

Table 3.5 Phase III Models

The ply orientation in the model is left at 0 and 90 degrees since in an isotropic material the material constants are the same in either direction.

The final model in the analysis, Model 8, is the same as Model 6 with the exception that the QUA4 410 quadrilateral element (see section 2.2.4) is replaced by the QUA4 411 element, the TRINC 320 triangular element with the TRINC 321, and the GSBM2 220 beam element with the GSBM2 221.

Models 7 and 8 were ran on the VAX 11/785 computer in the same manner as the other runs. The CPU time for the layered isotropic model (Model 7) was 6 hours and 9 minutes which was close to the 6 hours and 43 minutes it took to run Model 6. A dramatic difference in CPU time was found in Model 8. Model 8 took 26 hours and 51 minutes to run. It was anticipated that the Model 8 run would take longer due to the increased number of degrees of freedom (see Table 3.5), but not as long as it actually did.

Load versus normal displacement plots are shown in Figures 3.19 and 3.20 for nodes 168 and 176 (see Figure 3.5) respectively.

From examining Figures 3.19 and 3.20 it is evident that the layered isotropic material model (Model 7) is a much stiffer model than the orthotropic model (Model 6). From examining experimental data it is also evident that the orthotropic model gives better results in terms of displacements.

Finally from Figures 3.19 and 3.20 the change to a higher degree of freedom element (QUAF 411 Element) was not necessary. In fact, given the CPU time necessary to complete the Model 8 (411 Element) run versus the time for the Model 6 (410 Element), the QUAF 411 element seems to be very impractical for mild nonlinearities (as opposed to a shell collapse which is highly nonlinear).

Since the QUAF 410 Element model (Model 6) was much more economical and gave essentially the same results as the QUAF 411 model (Model 8) and since the displacement results for Model 6 are much better than those for Model 7, Model 6 was used for comparison with the experimental results (see section 5). The STAGS input deck for Model 6 is shown in Appendix G. The UPRESS loading subroutine used to apply the pressure loading in this model is shown in Appendix H.

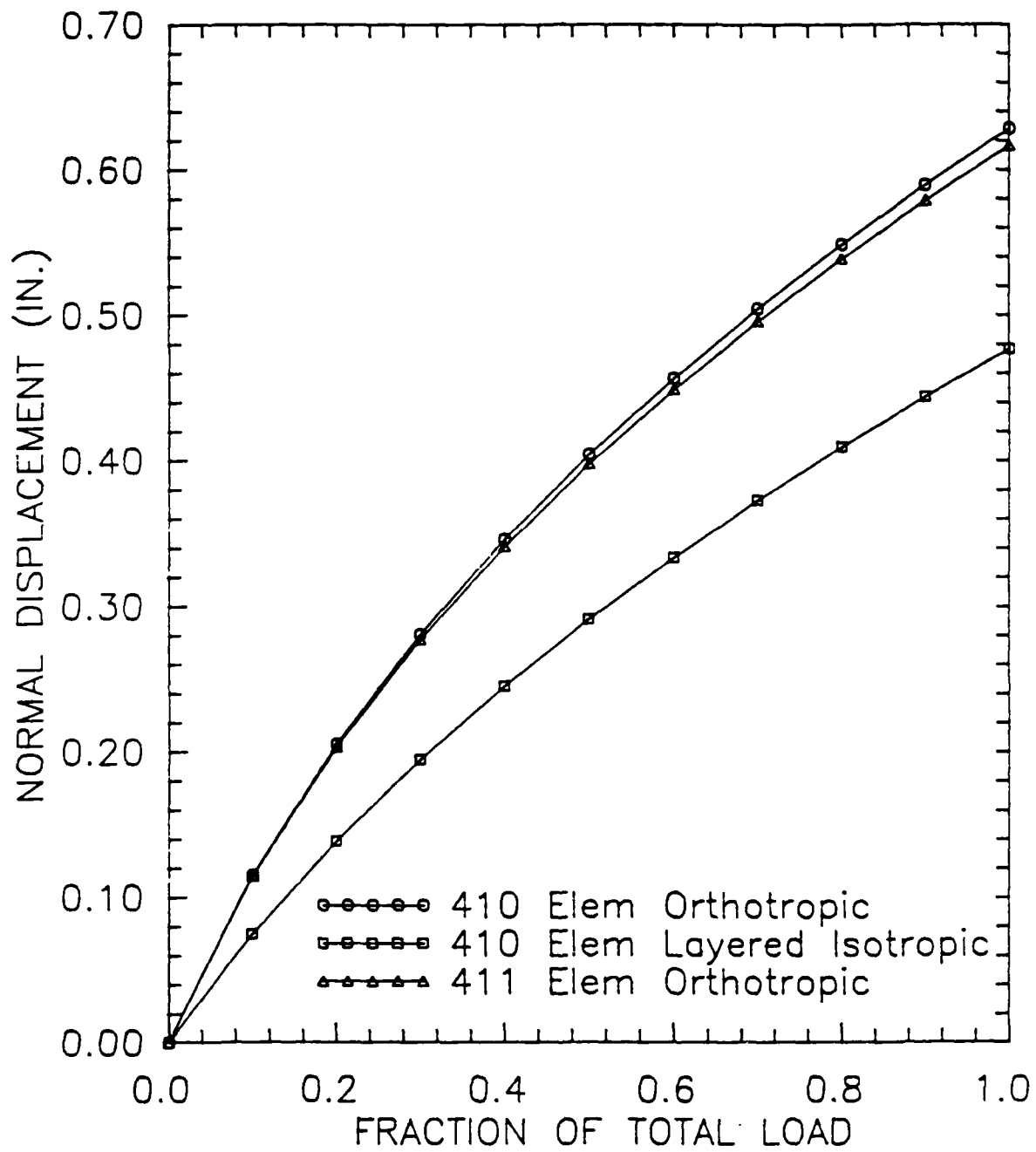


Figure 3.19 Node 168 Phase III Modeling: Variable Thickness, Modified B.C.s

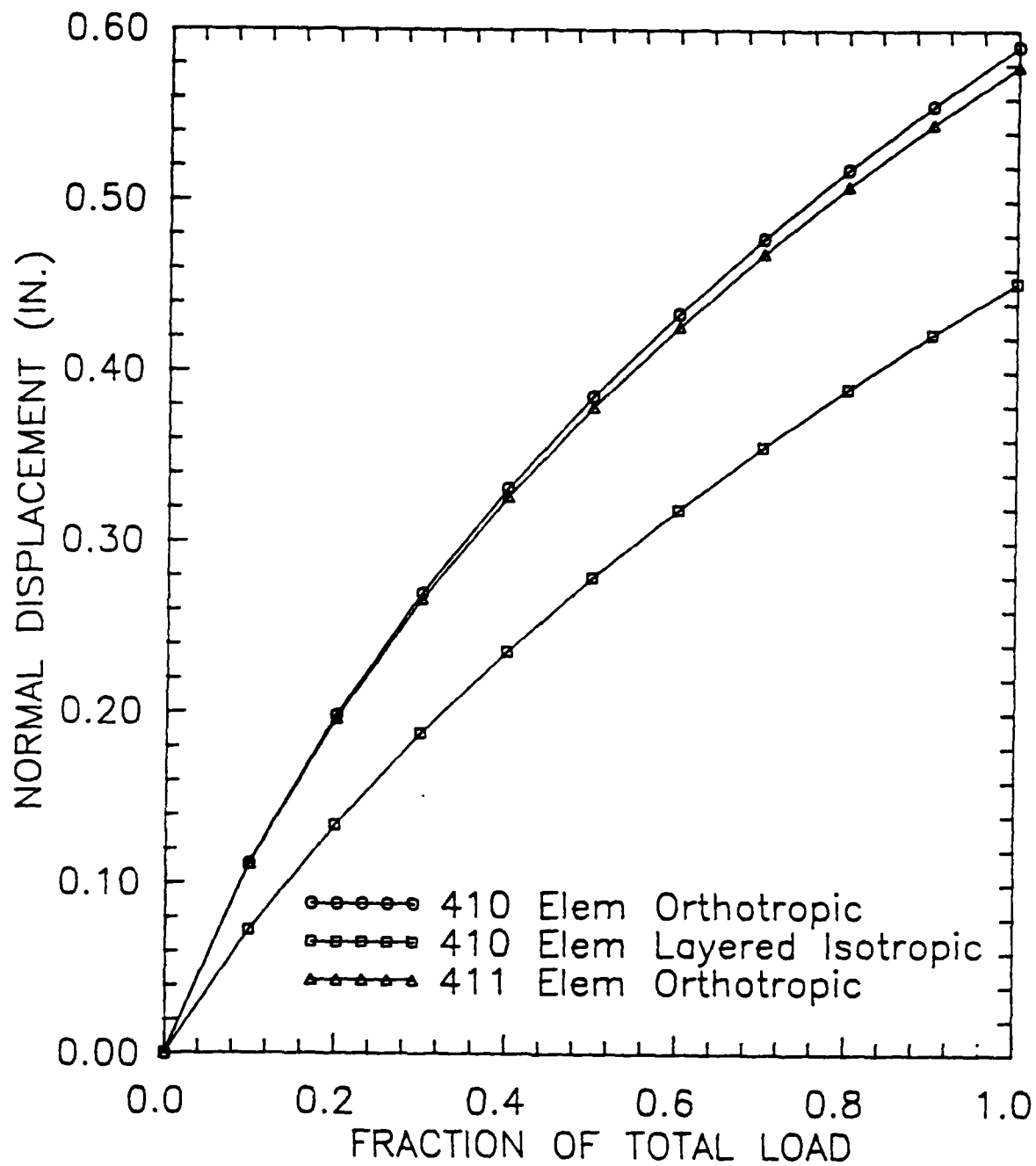


Figure 3.20 Node 176 Phase III Modeling: Variable Thickness, Modified B.C.s



#### 4. Experimentation

The experimentation on the actual shell was done by the Air Force Wright Aeronautics Laboratory, Wright-Patterson AFB, Ohio. The test simulated the actual aerodynamic loading on the shell by using inflatable bladders within the shell to provide internal pressure loading.

The steps necessary to devise a test fixture that can produce this type of pressure loading is as follows. First, an aluminum frame (Figure 4.1) was built that was the same shape as the shell but

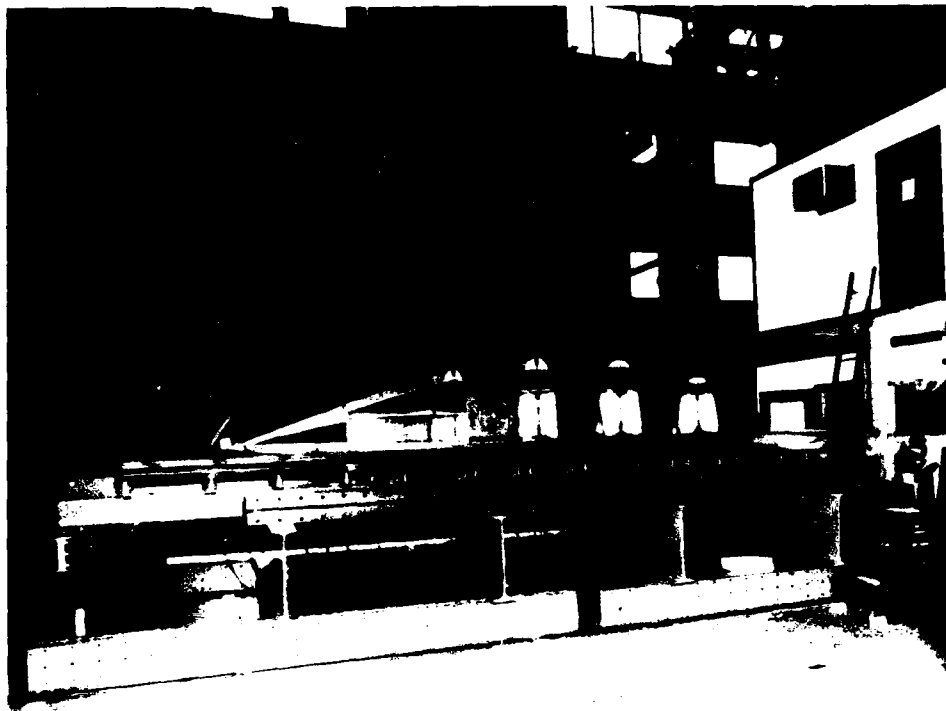


Figure 4.1 Aluminum Frame

was smaller so that the shell would fit over the frame and leave about 1 1/2 in. between the two. The frame also had spaces in it that coincide with the load regions shown in Figure 3.7. Next, holes were drilled into each load area of the test frame. Rubber hoses, extending from electronically controlled pressure valves, were inserted into each hole and the gap around the hoses sealed. This entire assembly was then bolted to a test stand.

Rubber sheets were then glued to the frame with contact cement; covering each load region and forming the basic loading bladder (Figure 4.2). A border of one inch thick closed cell foam was

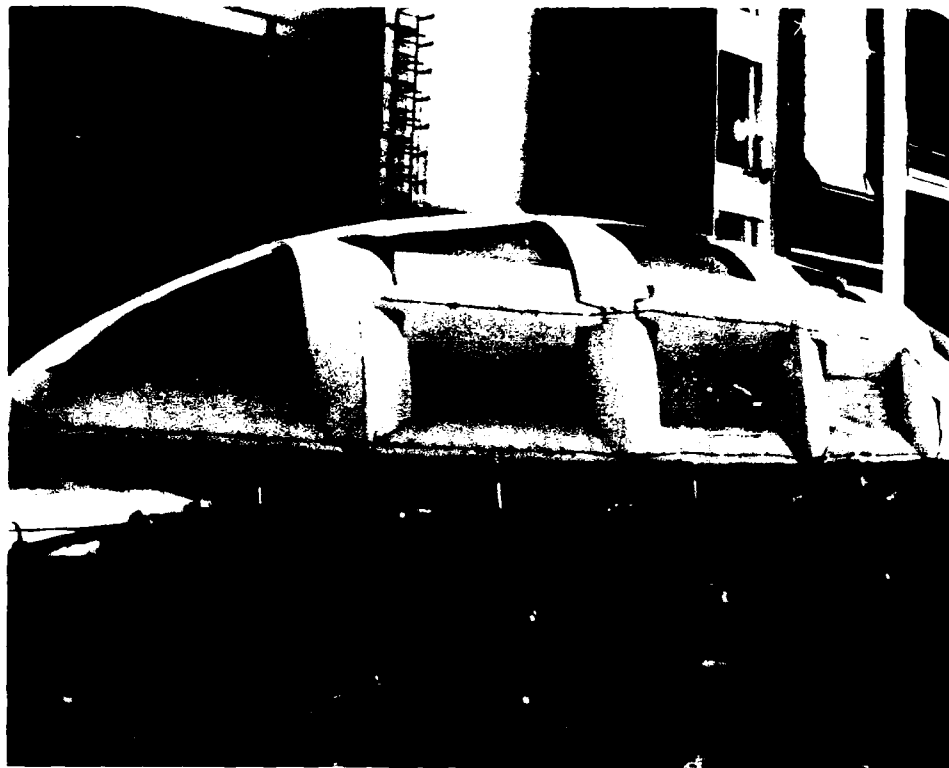


Figure 4.2 Rubber Bladders

attached (glued to the rubber and tied to the aluminum frame) to

the intersection of each load region. This foam border was about twelve inches wide (extending six inches into each region) tapered from one inch thick at its midpoint (the load region boundary) to a zero thickness at the edges. This foam border kept the bladder in one region from bulging into another region. The taper kept the inner edges of the closed cell foam from touching the shell before the bladder contacts the shell.

The shell was then placed over the frame and bolted to the test stand (Figure 4.3) with same type of boundary restraint as shown in

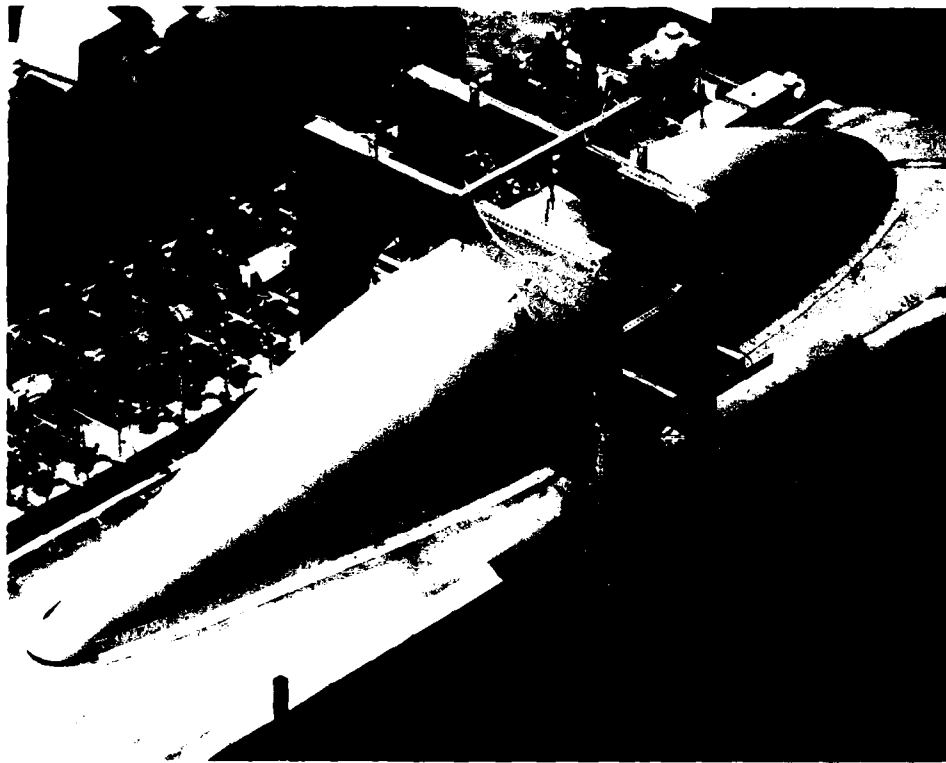


Figure 4.3 Experimental Set-Up

Figure 3.15. Finally, linear variable differential transducers (LVDTs) were placed around the mid-section of the shell (Figure 4.4). The

LVDTs were oriented so as to measure normal displacements of the

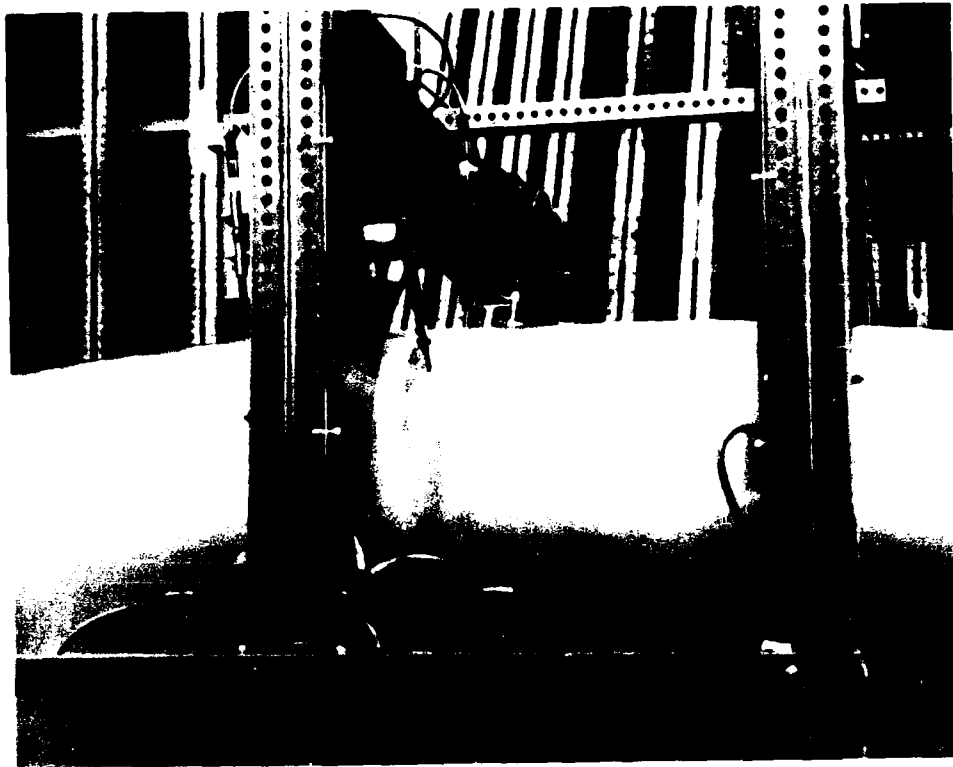


Figure 4.4 Close-Up of Displacement Transducers

shell at specified points that coincide with node points on the finite element model.

During loading it was anticipated that the bladders would tend to bulge more toward the center of a load region; reducing the contact area of the pressure load. To compensate for this, the 4950 Test Wing recalculated the loading (Table 3.1) on the shell to account for the reduced contact area of the bladder as compared to the true pressure values. Table 4.1 shows modified loads used in the

finite element modeling (Figure 3.5).

Load Region	1	2	3	4	5	6	7	8	9	10
Load (psi)	1.57	1.82	2.13	1.92	2.12	2.27	2.42	1.32	2.08	0.50
Load Region	11	12	13	14	15	16	17	18	19	20
Load (psi)	0.50	1.67	1.65	1.97	2.06	2.32	2.66	1.62	2.41	0.50

Table 4.1 Modified Static Equivalent Loads

A computer was used to control the loading on the shell. The computer would open and close individual valves that controlled the air pressure to each load region. Pressure transducers provided feedback to the computer to insure that the regions were loaded properly.

During testing the shell was loaded in increments (10% of total load) up to the total load and back down to an unloaded condition. The computer that controlled the load on the shell also took readings from all of the measuring devices on the shell at predetermined time steps. Displacement results obtained during testing are shown along with finite element solutions in the following section.

## 5. Comparison of Experimental and Finite Element Model Displacements

As stated in the Phase III Modeling section (section 3.4), the finite element model used for comparison to experimental results is the variable thickness, orthotropic material model with modified boundary conditions (Model 6) and a QUA4 410 element. In order to show a general deformation pattern for the shell a cross-section view of the undeformed and deformed shape of the shell is shown at the same cross-section (constant x value) as the nodes that were shown in the Phase I-III modeling sections (see Figure 3.5).

From Figure 5.1 a general deformation pattern is apparent. The shell is bulging at the sides and the top is deflecting down. Also from examining the data from the model and experimentation, the displacements on the sides of the shell at a y value of approximately eleven inches are the largest. These displacements are an order of magnitude larger than the displacements at the top of the shell. There also seems to be a lack of consistency in the experimental deflections at the top of the shell. Because of the large difference in displacements and the inconsistency in the experimental displacements at the top of the shell, the side node displacements will be compared. Finally, a node on the top of the shell is shown for general trends in this area.

Comparison of load versus displacement are made for the nodes shown in Figure 5.2. The load versus displacement curves for these nodes are shown in Figures 5.3 to 5.9.

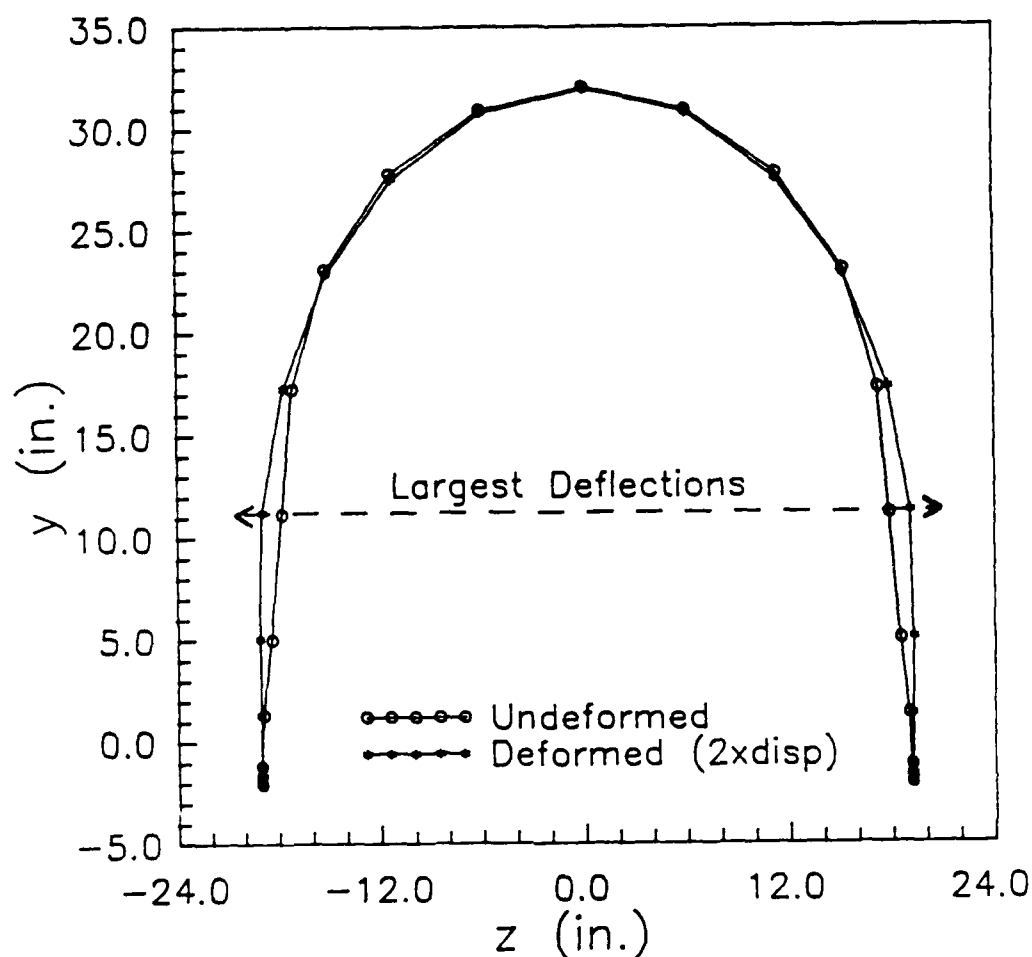


Figure 5.1 Deformed vs. Undeformed Finite Element Cross Section

From examination of Figures 5.3 to 5.8 for the side nodes, the finite element solutions are within 12.5% of the experimental results at maximum load. The Figures also show a "hysteresis" type effect for the experimental results. This effect is not a true hysteresis (plastic deformation); it is caused by the shell moving at the boundaries because of the rubber washers (see section 3.4) and not settling completely back into the boundary attachment.

These nodes also show very large displacements (greater than 0.5

in.) which are much larger than the thickness of the shell. For

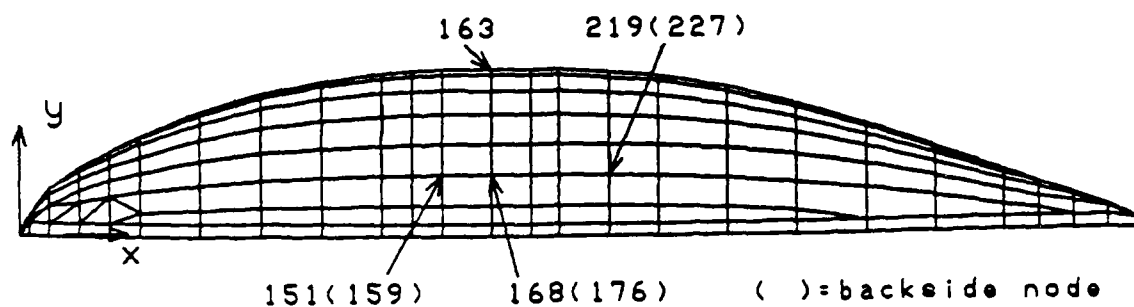


Figure 5.2 Shell and Finite Element Nodes Used for Comparison

example the displacement at node 168 is greater than 0.6 in. and the thickness is only 0.1311 in. This type of displacement justifies the use of a nonlinear finite element model since the basic assumption behind a linear analysis is that the displacements must be much smaller than the thickness of the shell [1].



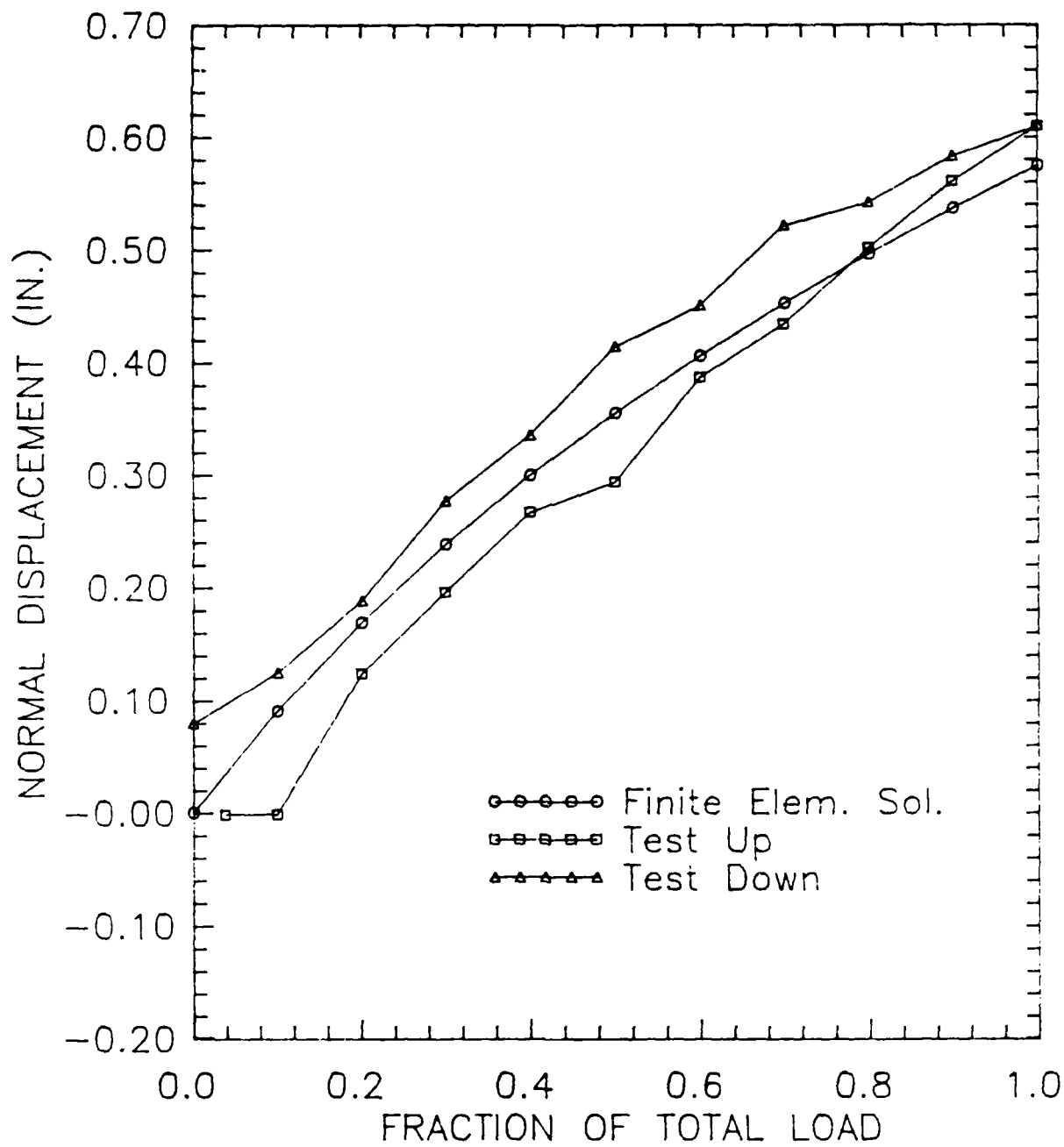


Figure 5.3 Node 151: Experimental vs. Finite Element Surface Normal Displacement

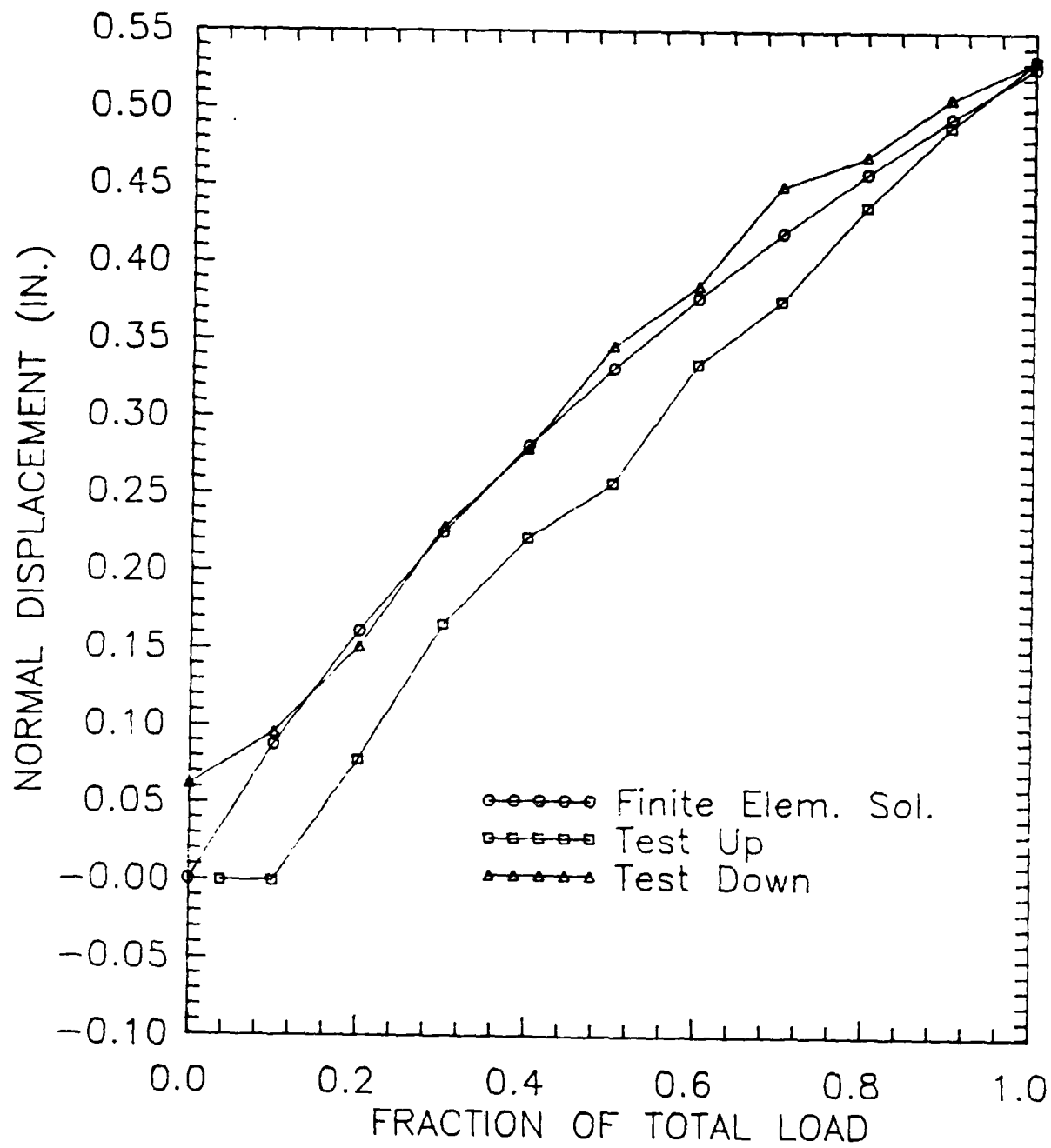


Figure 5.4 Node 159: Experimental vs. Finite Element Surface Normal Displacement

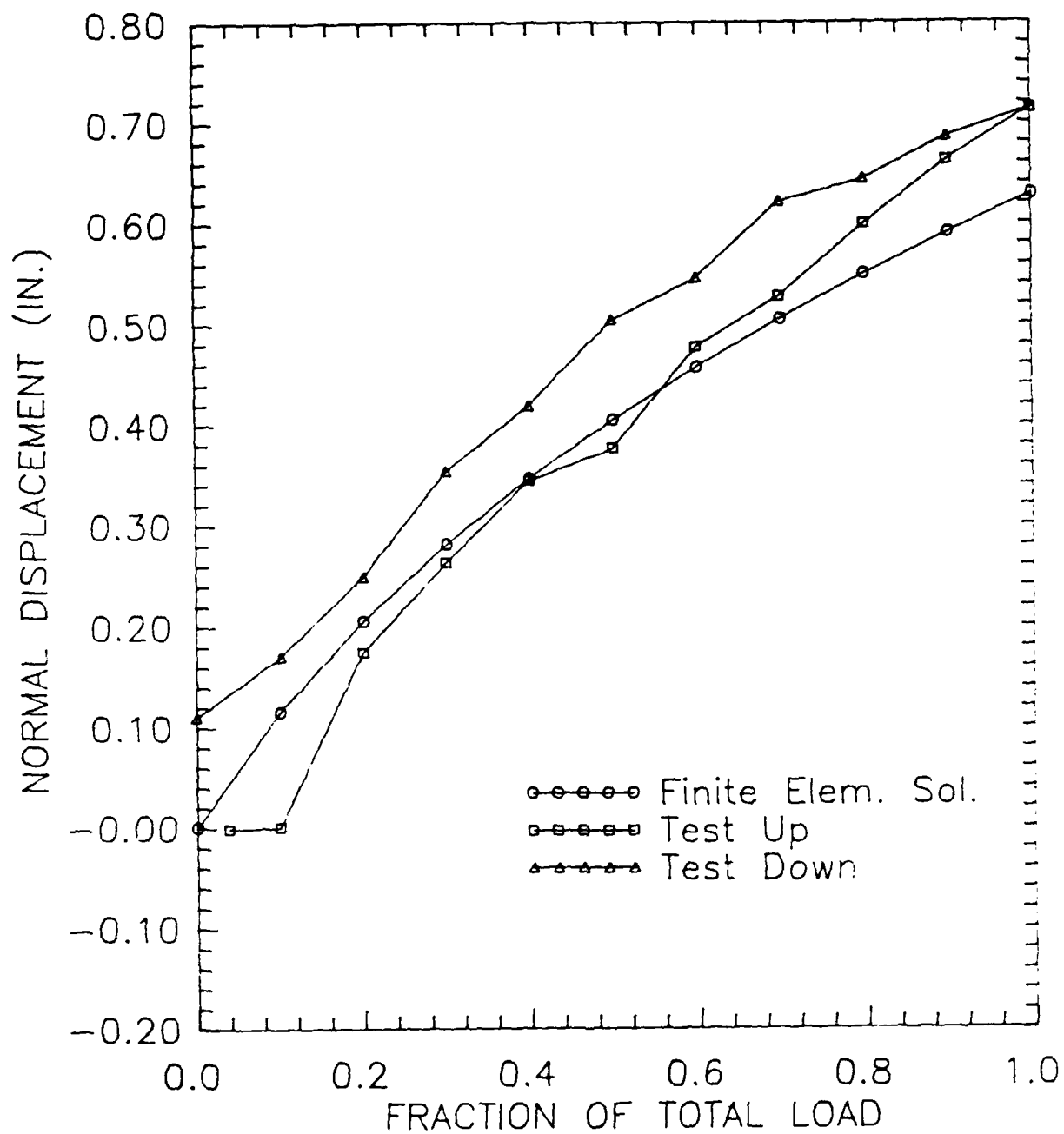


Figure 5.5 Node 168: Experimental vs. Finite Element Surface Normal Displacement

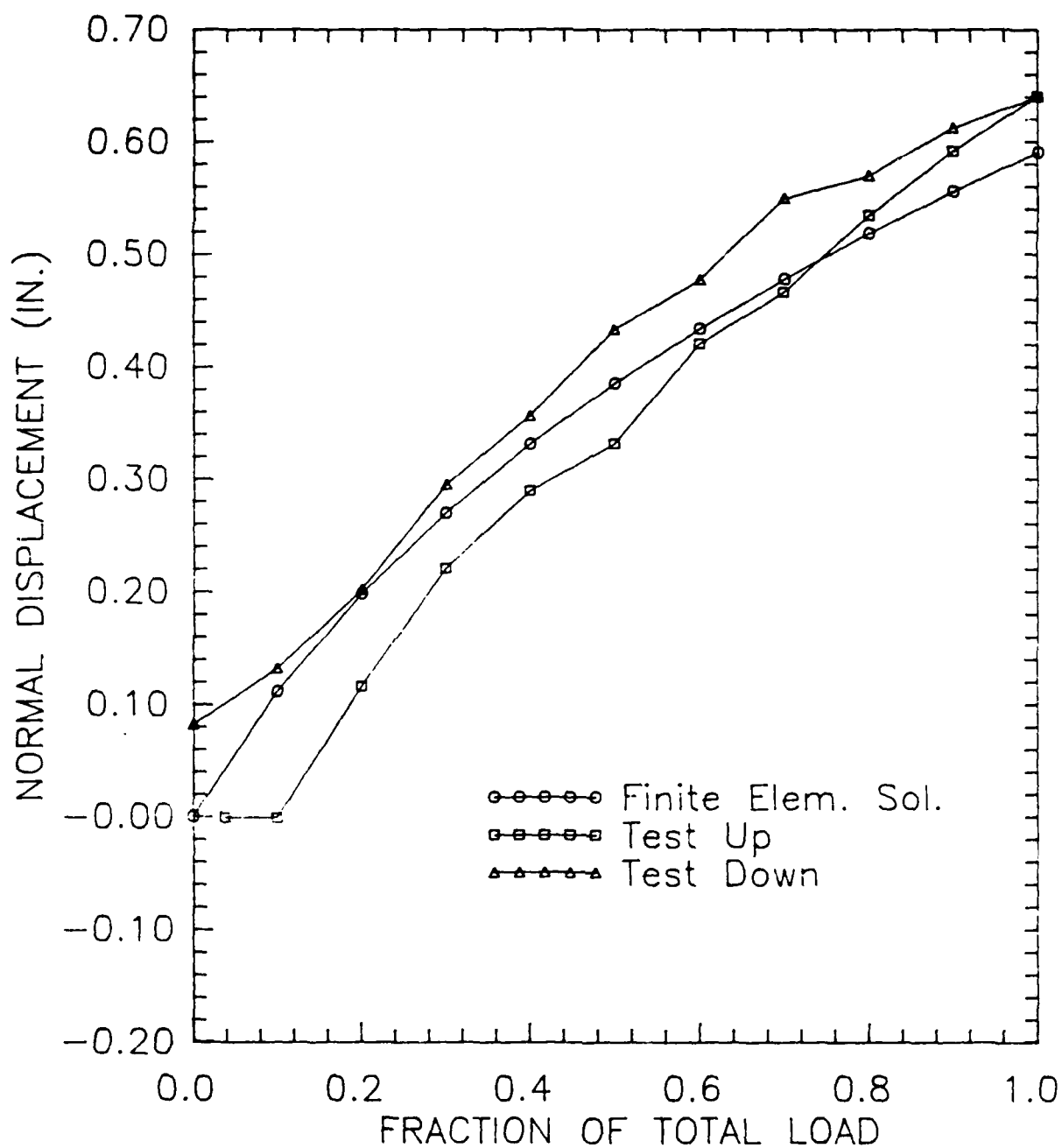


Figure 5.6 Node 176: Experimental vs. Finite Element Surface Normal Displacement

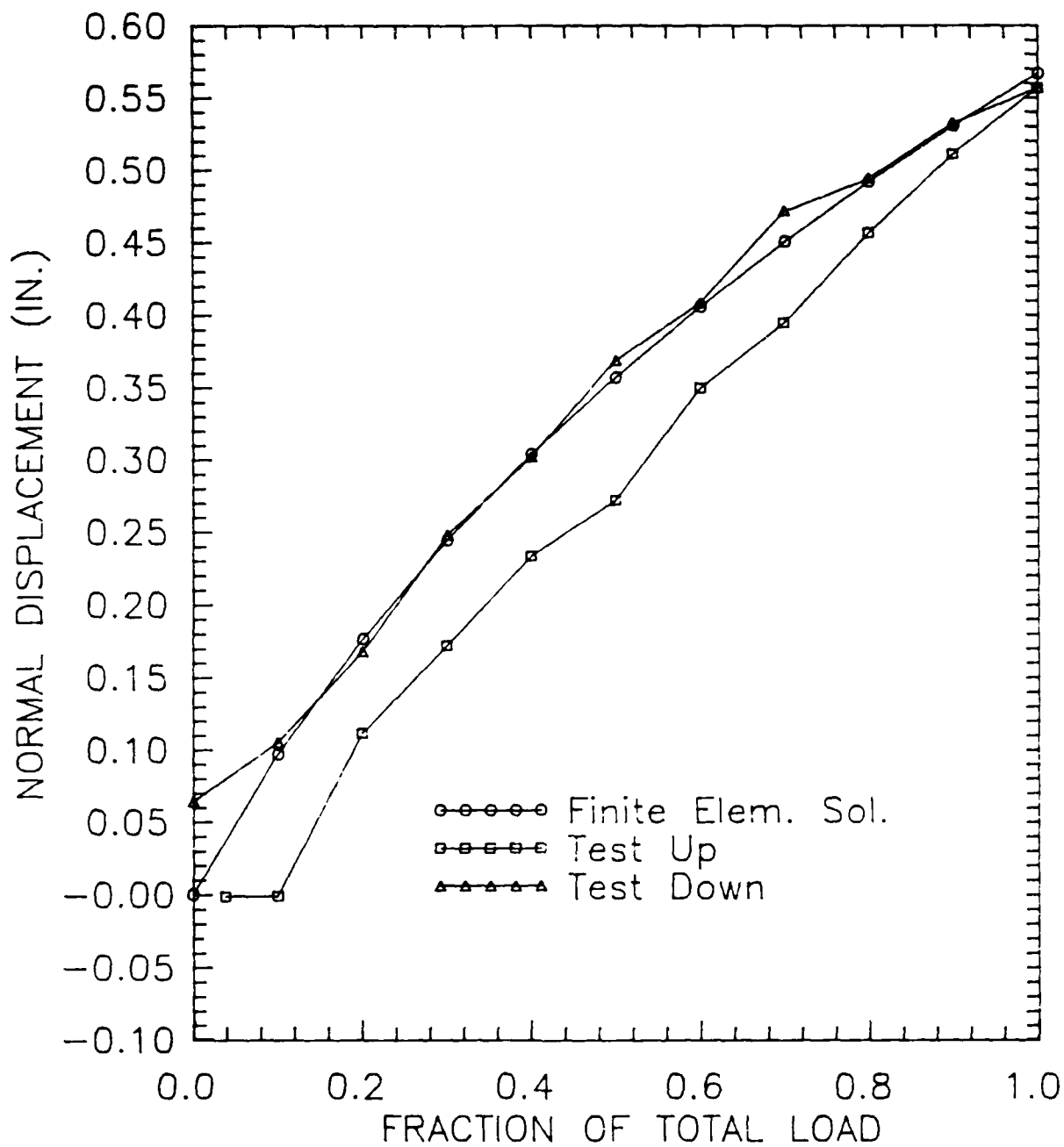


Figure 5.7 Node 219: Experimental vs. Finite Element Surface Normal Displacement

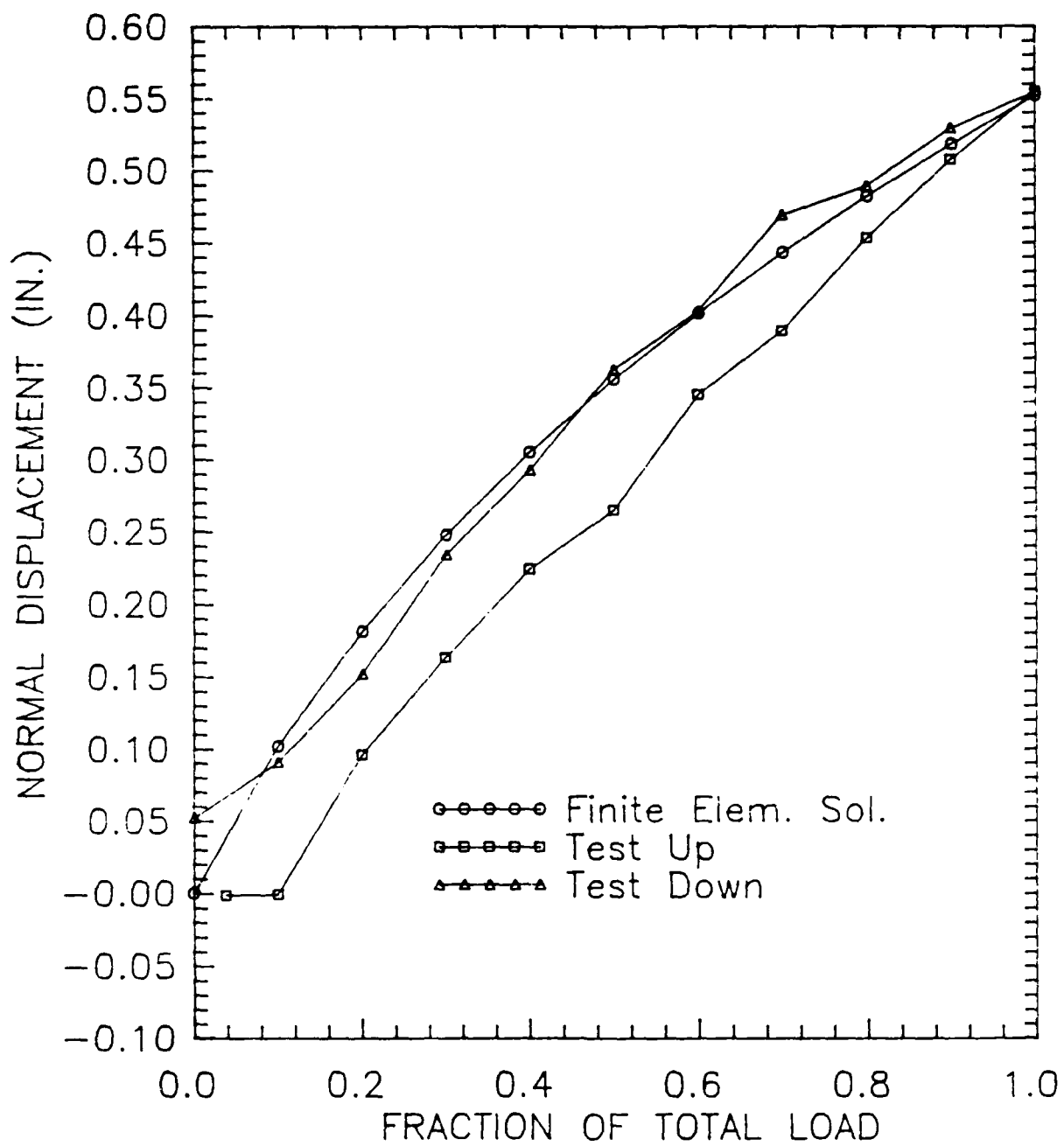


Figure 5.8 Node 227: Experimental vs. Finite Element Surface Normal Displacement

From looking at Figure 5.9 for node 163 on the top of the shell the experimental value at maximum load is much smaller than the finite element solution. But, the experimental displacements show a very erratic behavior at this and other top node locations. The only part of this loading curve that makes sense is the section from approximately 0.0 to 0.2 of the total load. The curve shows an upward movement of the shell due to the rubber washer until full compression of the washer at about 0.2 of the total load. This phenomenon was noted during testing; a general upward movement of the shell at the beginning and then movement of the shell due to kinematics. This general pattern is also evident in the side nodes (Figures 5.3 to 5.8). Up until about 0.1 of the total load there is no lateral displacement (the side node normal) at the side nodes. Above this point the side nodes start deflecting outward causing the bulging of the shell as depicted in Figure 5.1. What this also says is that the modeling of the rubber washers using "rubber beams" (see section 3.4), that deflect during the entire load process, will not accurately model this type of movement; essentially rigid body motion. Above about 0.2 of the total load the curve does not follow a definite load path and is considerably different from that of the unloading path. After discussion with the Wright Aeronautics Laboratory, there does not seem to be any definite reason for this load behavior. However, it must be emphasized, once again, that these displacements are extremely small (in the hundredths of inches) and are of an order of magnitude less than the side displacements. Therefore, the writer feels that they are not important relative to the displacements on the side of the shell.

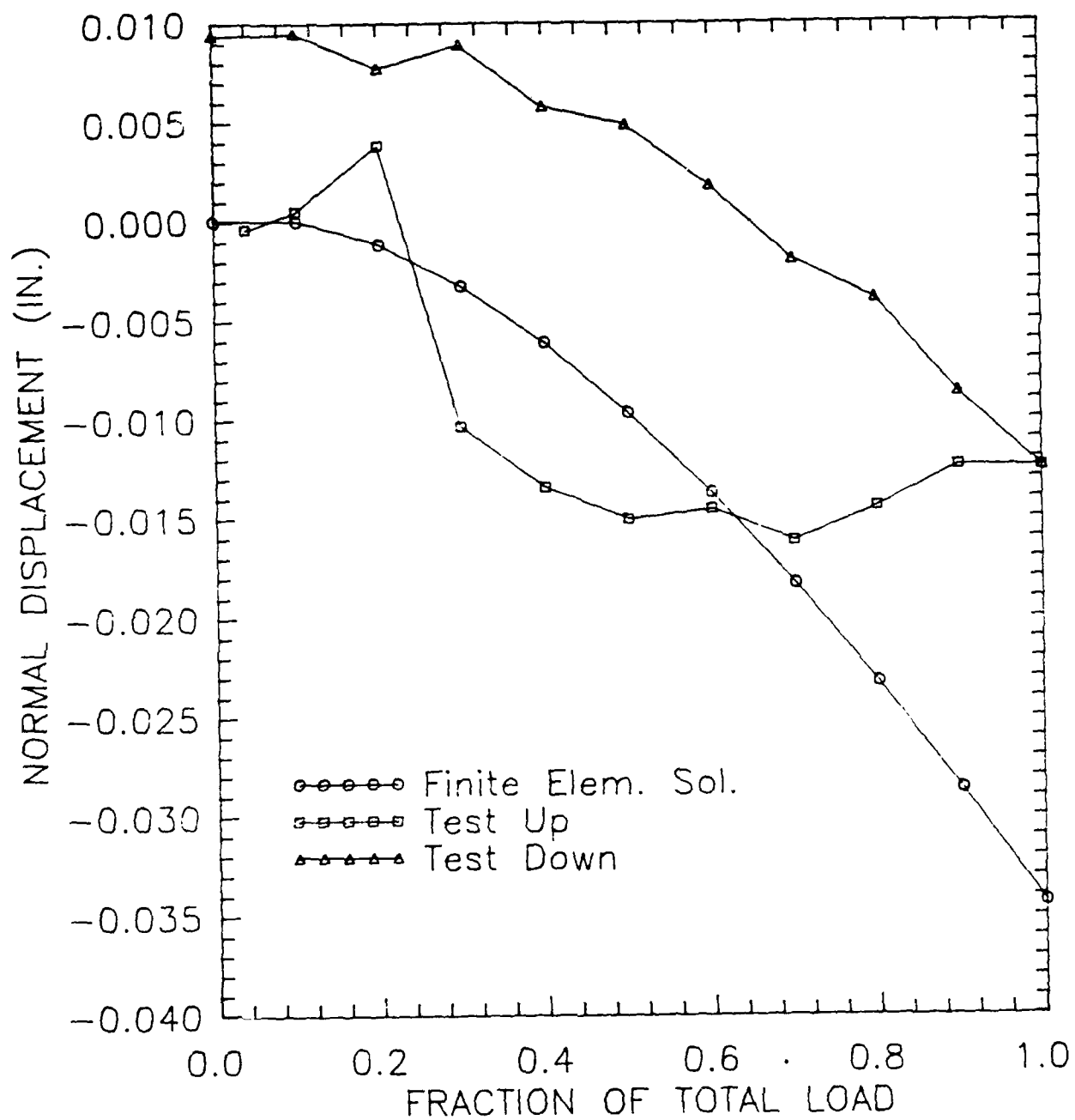


Figure 5.9 Node 163: Experimental vs. Finite Element Surface Normal Displacement



Overall the results from the finite element model using STAGSC-1 are very good. They also show that for a shell as large and flexible as the one considered in this thesis that a nonlinear analysis is essential in accurate modeling.

## 6. Laminate Strength Analysis

An important factor in the post processing of a finiteelement analysis is the determination of whether the loads on the structure are large enough to cause failure. This is especially true in composite materials since they are usually used in areas that require a tailoring of material properties in a particular direction to meet a load requirement. Simply looking at the stresses in the structure from a computer printout and comparing them to uniaxial material properties is inadequate due to, in general, a biaxial if not triaxial stress state in the actual structure [6]. To analyze a structure for possible failure under these conditions, biaxial strength theories have been developed. One such strength theory is the Tsai-Wu theory that deals with failure in an individual ply [6].

In the Tsai-Wu theory, failure in a ply occurs if the combination of strength tensors ( $F_1$ ,  $F_2$  etc.) and the stresses on the ply in the material coordinates ( $\sigma_1$ ,  $\sigma_2$ , and  $\tau_{12}$ ) are greater than unity. In equation form, for an orthotropic ply under plane stress conditions, failure occurs if [6]

$$F_1 \sigma_1 + F_2 \sigma_2 + F_{11} \sigma_1^2 + F_{22} \sigma_2^2 + F_{66} \tau_{12}^2 + 2F_{12} \sigma_1 \sigma_2 > 1 \quad (6.1)$$

where

$$F_1 = \frac{1}{X_t} + \frac{1}{X_c} \quad (6.2)$$

$$F_2 = \frac{1}{Y_t} + \frac{1}{Y_c} \quad (6.3)$$

$$F_{11} = -\frac{1}{X_t X_c} \quad (6.4)$$

$$F_{22} = \frac{1}{Y_t Y_c} \quad (6.5)$$

$$F_{ss} = \frac{1}{S^2} \quad (6.6)$$

$$F_{12} = \frac{1}{2\sigma^2} \left[ 1 - \left( \frac{1}{X_t} + \frac{1}{X_c} + \frac{1}{Y_t} + \frac{1}{Y_c} \right) \sigma + \left( \frac{1}{X_t X_c} + \frac{1}{Y_t Y_c} \right) \sigma^2 \right] \quad (6.7)$$

and

$X_t$  = ultimate tensile strength in the 1-direction

$X_c$  = ultimate compressive strength in the 1-direction

$Y_t$  = ultimate tensile strength in the 2-direction

$Y_c$  = ultimate compressive strength in the 2-direction

$S$  = ultimate longitudinal shear strength

To find  $F_{12}$  it is necessary to find the biaxial tensile failure stress,  $\sigma$ . Since this property is difficult to find experimentally reference [23] suggests that

$$F_{12} = \frac{1}{2(X_t X_c Y_t Y_c)^{1/2}} \quad (6.8)$$

To use this theory for the Kevlar/Polyester shell analyzed, a few assumptions need to be made since the shell was modeled as an orthotropic material even though it was a composite weave. The Air Force Wright Aeronautics Laboratory calculated ultimate strengths for the Kevlar/Polyester material in tension, compression, and shear. These values were used for  $X_t$ ,  $X_c$ , and  $S$  respectively and are given as

$$X_t = 70,400 \text{ psi}$$

$$X_c = 13,000 \text{ psi} \quad (6.9)$$

$$S = 8,690 \text{ psi}$$

The other ultimate stresses are found using the same assumption as

that used in section 3.3; the properties of Graphite/Epoxy are used to ratio the Kevlar/Polyester fabric properties.

From reference [20], the ratio of ultimates for Graphite/Epoxy are

$$\frac{X_t}{X_c} = \frac{130,989 \text{ psi}}{9,290 \text{ psi}} = 14.1 \quad (6.10)$$

$$\frac{Y_t}{Y_c} = \frac{197,143 \text{ psi}}{35,204 \text{ psi}} = 5.6$$

One can now divide the Kevlar/Polyester ultimate strengths,  $X_t$  and  $X_c$  (Equation 6.9), by 14.1 and 5.6 (Equation 6.10) respectively, to get the estimated  $Y_t$ ,  $Y_c$  values for Kevlar/Polyester. These values are given as

$$Y_t = 4,993 \text{ psi} \quad (6.11)$$

$$X_c = 2,321 \text{ psi}$$

With all of the Kevlar/Polyester ultimate values defined (Equations (6.9) and (6.11)), all that remains in the analysis is to determine the stresses within the laminate in the material directions.

Calculating the stresses in a ply in the material direction using STAGS presented little difficulties since STAGS gives the user the option to print out stresses in either the local or material directions. Using the same finite element model as the one used to compare experimental versus finite element solutions (see section 5), the stresses were obtained in the material directions for the inner and outer plies; potentially the highest stresses due to in-plane and bending effects. It was noted that the stresses were given for each of the surfaces on the inner and outer ply. Therefore, an average of

these values was used as the ply stress value. Also, since the inner and outer ply on the edges was a Glass/Polyester material and was not of prime concern in this analysis and since during testing it was visually verified that there was no apparent composite failure in any part of the shell, the lower edge elements were omitted from the analysis.

A Fortran program was written to enter each of the average inner and outer ply stresses and the Kevlar/Polyester ultimate stress values (Equations (6.9) and (6.11)) into the left-hand side of Equation (6.1). A Tsai-Wu value was then obtained for each inner and outer ply within an element. These values were then sorted in the program in descending order along with their respective ply and element numbers.

The highest Tsai-Wu value obtained in the analysis was 0.31 and is far below the unity value required for failure in Equation (6.1). The top nine Tsai-Wu values (0.22 to 0.31) are shown in Figure 6.1 since they show a definite pattern.



Figure 6.1 Tsai-Wu Composite Failure Analysis

All of these values are on the inside ply of the location shown in Figure 6.1. This makes sense in the analysis since the largest deflection gradient occurs on this side of the model as shown in Figure 5.1. Although these values are well below unity (failure value) they show a definite area of concern in the model if the loading is increased.

Given the assumptions used in the model, it would appear that under the loading in this analysis, failure of the composite material would not occur. But, the material values are assumptions, therefore an investigation into the true material values needs to be done to insure better confidence in the failure analysis.

## 7. Conclusions

Based on the analysis of a large, thin composite shell, with asymmetric loading, presented in this thesis, the following conclusions can be made:

1. Modeling of the structure should include:

- Taking into account the thickness variations within the structure. Modeling of the thickness variations in a structure by using an average element thickness appears to work well especially when reducing the grid size to accommodate the varying thicknesses is impractical.
- Accurate modeling of the material used in the structure whether orthotropic or isotropic. Modeling an orthotropic material as an isotropic (1 layer through the thickness) material does not work well especially when assumptions have to be made about the material properties. The layered isotropic material modeling was much too stiff for this analysis. Modeling a weave composite by splitting the individual plies in half and orienting the plies at 0 and 90 degrees produced reasonable results. Also, making assumptions about Kevlar/Polyester composite weave material properties from Graphite/Epoxy composite (orthotropic) values appeared to work well.
- Boundary conditions on a structure have a large effect on the analysis. These effects are especially true when the boundary conditions are elastically dependent. Proper

modeling of the boundary conditions on the structure especially when standard finite element boundary conditions (clamped, pinned, free, etc.) do not model the actual boundary conditions accurately.

2. Use of the QUAFF 410 element is more practical for cases involving mild geometric nonlinearities. The QUAFF 411 Element took nearly four times as long to run (over 26 CPU hours) as the QUAFF 410 element with little difference in results.
3. Visual observation after experimentation indicated no failure in the composite shell. This was concurred with analytically with a Tsai-Wu strength analysis.
4. Use of a geometric nonlinear analysis is essential to problems involving displacements as large as four times the shell thickness. The linear analysis carried out over predicted some deflections by more than 100 percent.
5. The nonlinear variable thickness model with modified boundary conditions and an orthotropic material assumption modeled the shell reasonably well.
6. STAGSC-1 with its updated Lagrangian formulation and nonlinear capabilities does a very good job in analyzing a general shell with large displacements.



## Appendix A: Derivation of the STAGSC-1 Nonlinear Strain Displacement Equations

Since one of the primary strengths of the STAGS computer program is its ability to analyze shells nonlinearly, a derivation of the nonlinear kinematics is presented.

To start the derivation a few assumptions need to be made. STAGS uses plate elements to model a shell structure. These plate elements are considered thin so that the in-plane displacements,  $u$  and  $v$ , and the normal displacement,  $w$ , is a function of only two space variables [7]. A plane stress assumption is made whereby  $\gamma_{xz}$ ,  $\gamma_{yz}$ ,  $\epsilon_z$ , and  $\sigma_z$  are considered zero. And finally, the Kirchhoff-Love hypothesis applies for strains away from the midplane. With these assumptions, the presentation can now be started.

Consider a line segment as show in Figure A.1 oriented in its undeformed and deformed (represented with an asterisk) state. From Figure A.1, it is evident that the deformed state can be related to the undeformed state by [7]

$$\begin{aligned} x^* &= x + u \\ z^* &= z + w \end{aligned} \tag{A.1}$$

and the differential change in distance by [7]

$$\begin{aligned} dx^* &= dx(1 + u_{,x}) \\ dz^* &= dx w_{,x} \\ (ds^*)^2 &= (dx^*)^2 + (dz^*)^2 \end{aligned} \tag{A.2}$$

By substituting the first two equations of Equation (A.2) into the last equation it follows that [7]

$$\left(\frac{ds}{dx}\right)^2 - 1 = 2u_{,x} + (u_{,x})^2 + (w_{,x})^2 \quad (A.3)$$

Using the definition of strain [7]

$$\epsilon_x = (ds^* - dx)/dx \quad (A.4)$$

and then rearranging it to get an alternate form [7]:

$$\epsilon_x + 1/2 \epsilon_x^2 = 1/2 \left[ \left(\frac{ds^*}{dx}\right)^2 - 1 \right] \quad (A.5)$$

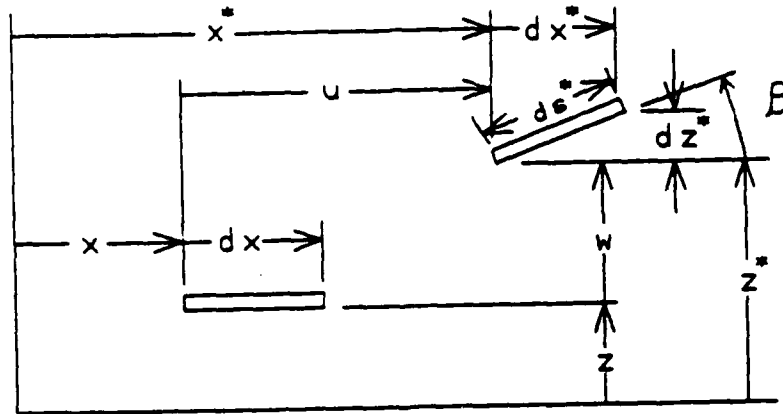


Figure A.1 Line Element in Undeformed and Deformed State [7]

Substituting Equation (A.3) into Equation (A.5) and assuming the strain is small so that  $\epsilon_x^2$  can be eliminated gives [7]

$$\epsilon_x = u_{,x} + 1/2(u_{,x}^2 + w_{,x}^2) \quad (A.6)$$

So far the analysis for this line element has been only in one plane. If this line element is in the midplane of a plate element, the rotation of this line element about the normal has to be

considered. If this rotation is included in Equation (A.6), as in Sanders' nonlinear shell equations, and rewritten to reflect midplane strain, the result is

$$\epsilon_x^0 = u_{,x} + 1/2(u_{,x}^2 + w_{,x}^2 + \phi^2) \quad (A.7)$$

where in Sanders' equations [3]

$$\phi = 1/2(u_{,y} - v_{,x}) \quad (A.8)$$

The term that should be included in Equation (A.7) to represent this rotation in the x-direction about the normal, for a flat plate, is  $v_{,x}$ . This does not imply the use of Sanders' equation, just the importance of defining a normal rotation term for flat plates representing a shell. Substituting this term in Equation (A.7) results in [7].

$$\epsilon_x^0 = u_{,x} + 1/2(u_{,x}^2 + w_{,x}^2 + v_{,x}^2) \quad (A.9)$$

Following this same line of reasoning, the other two midplane strain terms,  $\epsilon_y^0$  and  $\gamma_{xy}^0$ , can be written as [7]

$$\epsilon_y^0 = v_{,y} + 1/2(u_{,y}^2 + w_{,y}^2 + v_{,y}^2) \quad (A.10)$$

$$\gamma_{xy}^0 = u_{,y} + v_{,x} + (u_{,x}u_{,y} + v_{,x}v_{,y} + w_{,x}w_{,y})$$

Now, if the Kirchhoff hypothesis is included, where strains away from the midplane are due to the following curvatures

$$\begin{aligned} \kappa_x &= -w_{,xx} \\ \kappa_y &= -w_{,yy} \\ \kappa_{xy} &= -w_{,xy} \end{aligned} \quad (A.11)$$

the full expression for strain in the plate element can be written

from Equations (A.9), (A.10), and (A.11) as

$$\begin{aligned}\epsilon_x &= \epsilon_x^0 - z \kappa_x \\ \epsilon_y &= \epsilon_y^0 - z \kappa_y \\ \gamma_{xy} &= \gamma_{xy}^0 - 2z \kappa_{xy}\end{aligned}\tag{A.12}$$

This kinematic formulation allows for large displacements and moderate rotations (due to the Kirchhoff hypothesis).

## Appendix B: Variational Formulation

STAGSC-1 is an energy based finite element program dependent on a variational formulation. Therefore a presentation of this formulation is given for better understanding.

For the static case where the motion of the system can be ignored, the total potential energy of a system,  $\Pi$ , can be given as

$$\Pi = U - W \quad (B.1)$$

where  $U$  is the internal strain energy of the system and  $W$  is the external work due to applied forces. For a conservative system, the change in the total potential energy is independent of path [7]. The equations of equilibrium can then be derived from the first variation of the total potential energy [7]. In equation form, the principle of virtual work is

$$\delta\Pi = \delta U - \delta W = 0 \quad (B.2)$$

The expression for the internal strain energy is [6]

$$U = \int_V \{\epsilon\}^T [D] \{\epsilon\} dVol \quad (B.3)$$

where  $\{\epsilon\}$  is the strain vector for the body and  $[D]$  is the material matrix. Taking the variation of Equation (B.3) results in

$$\delta U = 1/2 \int_V \delta\{\epsilon\}^T [D] \{\epsilon\} dVol + 1/2 \int_V \{\epsilon\}^T [D] \delta\{\epsilon\} dVol \quad (B.4)$$

or alternatively by taking the transpose of the last expression in Equation (B.4) and adding it to the remaining term results in

$$\delta U = \int_V \delta\{\epsilon\}^T \{\sigma\} dVol \quad (B.5)$$

Now one defines a differential operator,  $[L]$ , which acts on the general displacements,  $\{u\}$ , to get [8]

$$\{\epsilon\} = [L]\{u\} \quad (\text{B.6})$$

Next one can define the shape functions,  $[N]$ , to describe the general displacements in terms of nodal displacements (parameters),  $\{a\}$ , of the element where

$$\{u\} = [N]\{a\} \quad (\text{B.7})$$

If one substitutes Equation (B.7) into Equation (B.6) the results give

$$\{\epsilon\} = [L][N]\{a\} \quad (\text{B.8})$$

Or alternatively, defining a matrix  $[B]$  such that [8]

$$[B] = [L][N] \quad (\text{B.9})$$

Equation (B.8) can now be written as

$$\{\epsilon\} = [B]\{a\} \quad (\text{B.10})$$

Finally one can take the variation of Equation (B.10), transpose it, and substitute it into Equation (B.5) resulting in

$$\delta U = \delta\{a\}^T \int_V [B]^T \{\sigma\} dVol \quad (\text{B.11})$$

In order to get the full expression for the variation of the potential energy, assume that the work term has been defined in terms of nodal displacements,  $\{a\}$ , and forces,  $\{f\}$ , such that

$$W = \{a\}^T \{f\} \quad (\text{B.12})$$

Taking the variation of Equation (B.12), combining it with Equation (B.11), and substituting these equations into Equation (B.2) results in

$$\delta \Pi = \delta\{a\}^T \left\{ \int_V [B]^T \{\sigma\} dVol - \{f\} \right\} = 0 \quad (\text{B.13})$$

Finally, define a term,  $\{\Psi\}$ , which represents the sum of external and internal forces (inside braces, Equation (B.13)) [8]

$$\{\Psi\} - \int_V [B]^T(\sigma) \, dVol - \{f\} = 0 \quad (B.14)$$

or alternatively after integration

$$\{\Psi\} - [K]\{a\} - \{f\} = 0 \quad (B.15)$$

where  $[K]$  is the stiffness matrix.

## Appendix C: Classical Laminated Plate Theory

The shell analyzed in this thesis is made of composite materials. STAGSC-1, the computer program used in the analysis, uses flat plates to model a shell surface. Because of this, a review of composite plate theory is presented.

To start the formulation, a few of the classical laminated plate assumptions need to be made. The laminate is assumed to consist of perfectly bonded plies where this bond is assumed infinitesimally thin and does not allow shear deformation within itself (i.e. the displacements between plies is continuous; no slip between plies) [14]. Also, the laminate is thin so that the in-plane displacements,  $u$  and  $v$ , as well as the normal displacement,  $w$ , are functions of only two in-plane space variables ( $x$  and  $y$ ) [7]. A plane stress assumption is assumed to where  $\gamma_{xz}$ ,  $\gamma_{yz}$ ,  $\epsilon_z$ , and  $\sigma_z$  are assumed to equal zero. Finally, out of plane strains are due to the curvatures as in the Kirchhoff hypotheses for plates.

Figure C.1 shows the coordinate system, the associated displacements, and the force and moment resultants ( $N_x$ ,  $M_x$ , etc. respectively) on the laminate [14]. The  $x$ - $y$  plane of Figure C.1 coincides with the reference axis. From these assumptions, a general expression can be written for the strains in the laminate using the Kirchhoff hypothesis as

$$\begin{Bmatrix} \epsilon_x \\ \epsilon_y \\ \gamma_{xy} \end{Bmatrix} = \begin{Bmatrix} \epsilon_x^0 \\ \epsilon_y^0 \\ \gamma_{xy}^0 \end{Bmatrix} - z \begin{Bmatrix} \kappa_x \\ \kappa_y \\ \kappa_{xy} \end{Bmatrix} \quad (C.1)$$

where  $\epsilon_x^0$ ,  $\epsilon_y^0$ , and  $\gamma_{xy}^0$  represent in-plane strains and the terms  $\kappa_x$ ,



$\kappa_y$ , and  $\kappa_{xy}$  are curvatures. The curvature terms are defined as

$$\begin{Bmatrix} \kappa_x \\ \kappa_y \\ \kappa_{xy} \end{Bmatrix} = \begin{Bmatrix} w_{,xx} \\ w_{,yy} \\ 2w_{,xy} \end{Bmatrix} \quad (C.2)$$

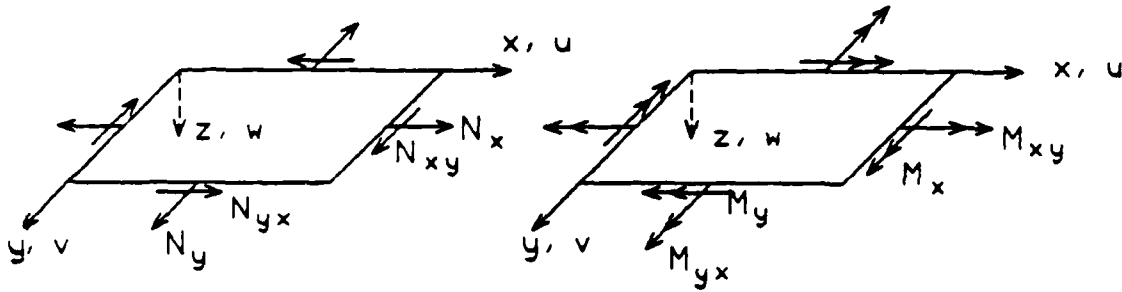


Figure C.1 Coordinate System, Displacements, and Force and Moment Resultants

The kinematic relations for the laminate (Equation C.1) can be substituted into the constitutive equation for the laminate resulting in [14]

$$\begin{Bmatrix} \sigma_x \\ \sigma_y \\ \tau_{xy} \end{Bmatrix} = \begin{bmatrix} \bar{Q}_{11} & \bar{Q}_{12} & \bar{Q}_{16} \\ \bar{Q}_{12} & \bar{Q}_{22} & \bar{Q}_{26} \\ \bar{Q}_{16} & \bar{Q}_{26} & \bar{Q}_{66} \end{bmatrix}_k \begin{Bmatrix} \epsilon_x^0 \\ \epsilon_y^0 \\ \gamma_{xy}^0 \end{Bmatrix} + z \begin{Bmatrix} \kappa_x \\ \kappa_y \\ \kappa_{xy} \end{Bmatrix} \quad (C.3)$$

where the subscript k refers to the ply layer and the  $\bar{Q}$  quantities are defined as follows [14]:

$$\begin{aligned} \bar{Q}_{11} &= Q_{11} \cos^4 \theta + 2(Q_{12} + 2Q_{66}) \sin^2 \theta \cos^2 \theta + Q_{22} \sin^4 \theta \\ \bar{Q}_{12} &= (Q_{11} + Q_{22} - 4Q_{66}) \sin^2 \theta \cos^2 \theta + Q_{12} (\sin^4 \theta + \cos^4 \theta) \end{aligned} \quad (C.4)$$

$$\begin{aligned}
\bar{Q}_{22} &= Q_{11} \sin^4 \theta + 2(Q_{12} + 2Q_{66}) \sin^2 \theta \cos^2 \theta + Q_{22} \cos^4 \theta \\
\bar{Q}_{16} &= (Q_{11} - Q_{12} - 2Q_{66}) \sin \theta \cos^3 \theta + (Q_{12} - Q_{22} + Q_{66}) \sin^3 \theta \cos \theta \\
\bar{Q}_{26} &= (Q_{11} - Q_{12} - 2Q_{66}) \sin^3 \theta \cos \theta + (Q_{12} - Q_{22} + Q_{66}) \sin \theta \cos^3 \theta \\
\bar{Q}_{66} &= (Q_{11} - Q_{22} - 2Q_{16} - 2Q_{66}) \sin^2 \theta \cos^2 \theta + Q_{66} (\sin^4 \theta + \cos^4 \theta)
\end{aligned} \tag{C.4}$$

(cont)

The  $Q$  terms in Equation (C.4) are functions of the material properties as follows [14]

$$\begin{aligned}
Q_{11} &= \frac{E_1}{1 - \nu_{12} \nu_{21}} \\
Q_{12} &= \frac{\nu_{12} E_2}{1 - \nu_{12} \nu_{21}} = \frac{\nu_{21} E_1}{1 - \nu_{12} \nu_{21}} \\
Q_{22} &= \frac{E_2}{1 - \nu_{12} \nu_{21}} \\
Q_{66} &= G_{12}
\end{aligned} \tag{C.5}$$

The angle  $\theta$  in Equation (C.4) is the angle between the principle axis ( $x, y, z$ ) and the material axis (1, 2, 3) as in Figure C.2

The force and moment resultants (forces and moments per unit length) acting on a composite plate can be found by integrating the stresses in each ply through the plate thickness, for example [14]

$$\begin{aligned}
N_x &= \int_{-t/2}^{t/2} \sigma_x dz \\
M_x &= \int_{-t/2}^{t/2} \sigma_x z dz
\end{aligned} \tag{C.6}$$

These force and moment resultants are shown in Figure C.1. All of the force and moment resultants are put in vector form for an

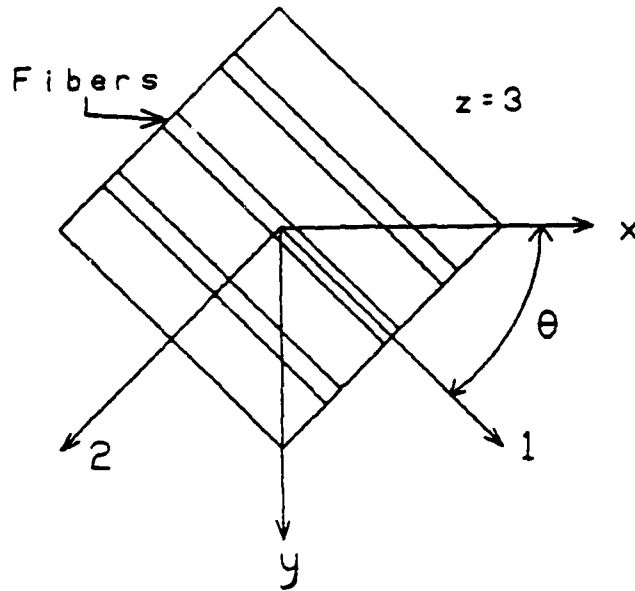


Figure C.2 Principal (x,y,z) and Material (1,2,3) Axis Systems

N-layered laminate and the results are [14]

$$\begin{Bmatrix} N_x \\ N_y \\ N_{xy} \end{Bmatrix} = \int_{-t/2}^{t/2} \begin{Bmatrix} \sigma_x \\ \sigma_y \\ \tau_{xy} \end{Bmatrix} dz = \sum_{k=1}^N \int_{z_{k-1}}^{z_k} \begin{Bmatrix} \sigma_x \\ \sigma_y \\ \tau_{xy} \end{Bmatrix}_k dz \quad (C.7)$$

and

$$\begin{Bmatrix} M_x \\ M_y \\ M_{xy} \end{Bmatrix} = \int_{-t/2}^{t/2} \begin{Bmatrix} \sigma_x \\ \sigma_y \\ \tau_{xy} \end{Bmatrix} z dz = \sum_{k=1}^N \int_{z_{k-1}}^{z_k} \begin{Bmatrix} \sigma_x \\ \sigma_y \\ \tau_{xy} \end{Bmatrix}_k z dz \quad (C.8)$$

where  $z_k$  and  $z_{k-1}$  are defined in Figure C.3.

Substituting Equation (C.3) into Equations (C.7) and (C.8), results

in

$$\begin{Bmatrix} N_x \\ N_y \\ N_{xy} \end{Bmatrix} = \sum_{k=1}^N \begin{bmatrix} \bar{Q}_{11} & \bar{Q}_{12} & \bar{Q}_{16} \\ \bar{Q}_{12} & \bar{Q}_{22} & \bar{Q}_{26} \\ \bar{Q}_{16} & \bar{Q}_{26} & \bar{Q}_{66} \end{bmatrix}_k \left\{ \int_{z_{k-1}}^{z_k} \begin{Bmatrix} \epsilon_x^0 \\ \epsilon_y^0 \\ \gamma_{xy}^0 \end{Bmatrix} dz - \int_{z_{k-1}}^{z_k} \begin{Bmatrix} \kappa_x \\ \kappa_y \\ \kappa_{xy} \end{Bmatrix} z dz \right\} \quad (C.9)$$

$$\begin{Bmatrix} M_x \\ M_y \\ M_{xy} \end{Bmatrix} = \sum_{k=1}^N \begin{bmatrix} \bar{Q}_{11} & \bar{Q}_{12} & \bar{Q}_{16} \\ \bar{Q}_{12} & \bar{Q}_{22} & \bar{Q}_{26} \\ \bar{Q}_{16} & \bar{Q}_{26} & \bar{Q}_{66} \end{bmatrix}_k \left\{ \int_{z_{k-1}}^{z_k} \begin{Bmatrix} \epsilon_x^0 \\ \epsilon_y^0 \\ \gamma_{xy}^0 \end{Bmatrix} z dz - \int_{z_{k-1}}^{z_k} \begin{Bmatrix} \kappa_x \\ \kappa_y \\ \kappa_{xy} \end{Bmatrix} z^2 dz \right\}$$

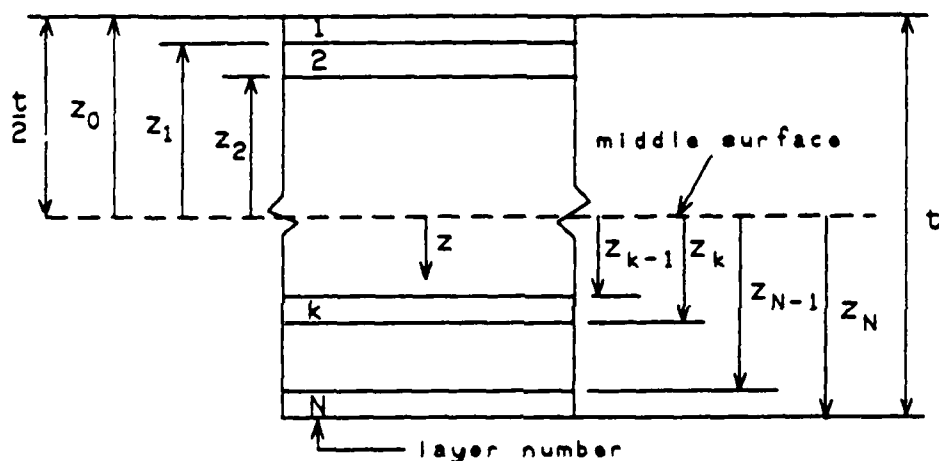


Figure C.3 Geometry of an N-Layered Laminate [14]

The stiffness matrix  $[\bar{Q}]$  has been removed from the integrals in Equations (C.9) because it is constant within a lamina but must be included within the summation of force and moment resultants for each ply [14]. Since the strain and curvature terms in Equations (C.9) are not functions of  $z$  but are midplane values they can be removed from the integration and summation signs [14]. After integrating the remaining terms, the results are

$$\begin{Bmatrix} N_x \\ N_y \\ N_{xy} \\ M_x \\ M_y \\ M_{xy} \end{Bmatrix} = \begin{bmatrix} [A] & [B] \\ [B] & [D] \end{bmatrix} \begin{Bmatrix} \epsilon_x \\ \epsilon_y \\ \gamma_{xy} \\ \kappa_x \\ \kappa_y \\ \kappa_{xy} \end{Bmatrix} \quad (C.10)$$

where

$$\begin{aligned} A_{ij} &= \sum_{k=1}^N (\bar{Q}_{ij})_k (z_k - z_{k-1}) \\ B_{ij} &= 1/2 \sum_{k=1}^N (\bar{Q}_{ij})_k (z_k^2 - z_{k-1}^2) \\ D_{ij} &= 1/3 \sum_{k=1}^N (\bar{Q}_{ij})_k (z_k^3 - z_{k-1}^3) \end{aligned} \quad (C.11)$$

## Appendix D: Surface Normal Calculations

In order to compare the global displacements calculated by STAGS with the normal displacements from experimentation, the STAGS displacements had to be transformed into surface normal displacements. To do this an approximate unit normal was calculated at each node point on the finite element model and multiplied (scalar product) by the global displacements (in vector form) resulting in a normal displacement.

An example of a unit normal calculation for a hypothetical node (node 5) in Figure D.1 is shown.

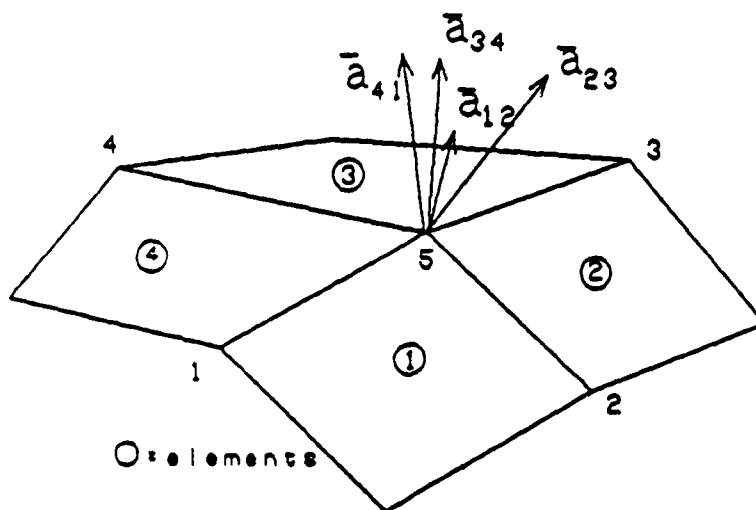


Figure D.1 Hypothetical Finite Element Surface

First, the element dividing lines radiating from node 5 to the adjacent nodes are converted into vectors. For example, to get a vector from node 5 to node 1 ( $\vec{b}_{s1}$ ) the global coordinates of node 1

$(\bar{g}_1)$  are subtracted as a vector from the global coordinates of node 5  $(\bar{g}_5)$  as in

$$\bar{b}_{51} = \bar{g}_1 - \bar{g}_5 \quad (D.1)$$

Next, the vectors radiating out from node 5 are multiplied (cross product) for each element (numbers circled in Figure D.1) to find a normal for the element. For example, for element 4

$$\bar{a}_{41} = \bar{b}_{54} \times \bar{b}_{51} \quad (D.2)$$

where the resulting vector  $\bar{a}_{41}$  is an outward normal.

The four vectors ( $\bar{a}_{12}$ ,  $\bar{a}_{23}$ ,  $\bar{a}_{34}$ , and  $\bar{a}_{41}$ ) are then normalized, added together, and divided by four resulting in a normal vector radiating from the node. Finally, this vector is then normalized and multiplied (scalar product) by the global displacements (in vector form) resulting in an approximate normal displacement.

A Fortran program was written to calculate the surface unit normals for the finite element model and stored in a file. As the displacement solutions were available, they, as well as the unit normals, were used as input files to another Fortran program that calculated normal displacements for the entire shell.

## Appendix E: Convergence Model: 1 to 1 Aspect Ratio

The following input data deck was used for the 1 to 1 aspect ratio convergence model. The reader is directed to the STAGS users manual [16] for specifics on the data deck. The letters immediately following the dollar sign in each row can be cross referenced to specific cards in the STAGS users manual.

[illegible]



1 0.0042500 0.0	\$K2 LAYERED WALL RECORD
1 0.0042500 90.0	\$K2 LAYERED WALL RECORD
1 0.0042500 0.0	\$K2 LAYERED WALL RECORD
1 0.0042500 90.0	\$K2 LAYERED WALL RECORD
1 0.0042500 0.0	\$K2 LAYERED WALL RECORD
1 0.0042500 90.0	\$K2 LAYERED WALL RECORD
1 0.0042500 0.0	\$K2 LAYERED WALL RECORD
1 0.0042500 90.0	\$K2 LAYERED WALL RECORD
1 0.0018000 0.0	\$K2 LAYERED WALL RECORD
1 0.0018000 90.0 1	\$K2 LAYERED WALL RECORD
11 0	\$M1
0. 180. 0. 180. 108. 26.	\$M2A
1	\$M5
410 -1	\$N1
0. 2.87 5.73 7.5 9.26 10.98 12.7 14.42 16.14 18.65 21.16 24.5,	
27.81 33.71 39.6 49.8 60. 75. 90. 105. 120. 130.2 140.4 146.3,	
152.19 155.52 158.84 161.35 163.86 165.58 167.3 169.02 170.7,	
172.5 174.27 177.13 180.	\$N4
2	\$P1
2	\$P1
2	\$P1
2	\$P1
1	\$Q1
1 0 2	\$Q2
0	\$R1

## Appendix F: UPRESS Subroutine for Convergence Test

The following subroutine was used for applying the pressure loading in the convergence test. The subroutine is written using guidelines in the STAGS users manual [16]. The subroutine is then compiled and linked to the main program before execution.

```
      subroutine upress(t,pa,pb,iunit,ielt,x,y,z,live,press)
c
c  Pressure distribution subroutine for
c  convergence test. Pressures are fed back to the main
c  program depending on element x and y coordinates.
c  loads.dat is the pressure distribution data file
c  that has the twenty loads, one on each line
c
      integer i
      real c(20)
      open(unit=1,file='loads.dat',status='old')
      live=1
      do 20 i=1,20
        read(1,30) c(i)
20    continue
30    format(f15.7)
      rewind(unit=1)
c
      if (x.le.16.14) then
        if (y.le.90.) then
          press=c(1)*pa
        elseif (y.le.180.) then
          press=c(11)*pa
        endif
      elseif (x.le.39.6) then
        if (y.le.45.) then
          press=c(3)*pa
        elseif (y.le.90.) then
          press=c(2)*pa
        elseif (y.le.135.) then
          press=c(12)*pa
        elseif (y.le.180.) then
          press=c(13)*pa
        endif
      elseif (x.le.90.) then
        if (y.le.45.) then
          press=c(5)*pa
        elseif (y.le.90.) then
          press=c(4)*pa
        elseif (y.le.135.) then
          press=c(14)*pa

```

```

elseif (y.le.180.) then
  press=c(15)*pa
endif
elseif (x.le.140.4) then
  if (y.le.45.) then
    press=c(7)*pa
  elseif (y.le.90.) then
    press=c(6)*pa
  elseif (y.le.135.) then
    press=c(16)*pa
  elseif (y.le.180.) then
    press=c(17)*pa
  endif
elseif (x.le.163.86) then
  if (y.le.45.) then
    press=c(9)*pa
  elseif (y.le.90.) then
    press=c(8)*pa
  elseif (y.le.135.) then
    press=c(18)*pa
  elseif (y.le.180.) then
    press=c(19)*pa
  endif
elseif (x.le.180.) then
  if (y.le.90.) then
    press=c(10)*pa
  elseif (y.le.180.) then
    press=c(20)*pa
  endif
endif
return
endg

```

## Appendix G: Finite Element Model (Model 6)

The following input data deck was used for the Model 6 (see section 3.3) finite element run. The reader is directed to the STAGS users manual [16] for specifics on the data deck. The letters immediately following the dollar sign in each row can be cross referenced to specific cards in the STAGS users manual.

[illegible]

[illegible][illegible]

[illegible][illegible]

1	0.0042500	90.0	
1	0.0042500	0.0	
1	0.0042500	90.0	
1	0.0042500	0.0	
1	0.0042500	90.0	
1	0.0042500	0.0	
1	0.0042500	90.0	
1	0.0042500	0.0	
1	0.0042500	90.0	
1	0.0042500	0.0	
1	0.0042500	90.0	
1	0.0042500	0.0	
1	0.0042500	90.0	
1	0.0018000	0.0	
1	0.0018000	90.0	1
5	1	36	
1	0.0012250	0.0	1
1	0.0012250	90.0	
1	0.0012250	0.0	
1	0.0012250	90.0	
1	0.0042500	0.0	
1	0.0042500	90.0	
1	0.0042500	0.0	
1	0.0042500	90.0	
1	0.0042500	0.0	
1	0.0042500	90.0	
1	0.0042500	0.0	
1	0.0042500	90.0	
1	0.0042500	0.0	
1	0.0042500	90.0	
1	0.0042500	0.0	
1	0.0042500	90.0	
1	0.0042500	0.0	
1	0.0042500	90.0	
1	0.0042500	0.0	
1	0.0042500	90.0	
1	0.0042500	0.0	
1	0.0042500	90.0	
1	0.0042500	0.0	
1	0.0042500	90.0	
1	0.0042500	0.0	
1	0.0042500	90.0	
1	0.0042500	0.0	
1	0.0042500	90.0	
1	0.0042500	0.0	
1	0.0042500	90.0	
1	0.0042500	0.0	
1	0.0042500	90.0	
1	0.0042500	0.0	
1	0.0042500	90.0	
1	0.0042500	0.0	
1	0.0042500	90.0	
1	0.0018000	0.0	
1	0.0018000	90.0	1
6	1	36	
1	0.0014750	0.0	1

[illegible]

[illegible][illegible]





124

[illegible][illegible]

[illegible][illegible]

13 1 40

### SK1 SHELL WALL RECORD

128

[illegible][illegible]

130



```

2 0.0085000 0.0 1
19 1 42

```

\$K2 LAYERED WALL RECORD  
\$K1 SHELL WALL RECORD

20 1 42

SK1 SHELL WALL RECORD

[illegible][illegible]

22 1 42

## SK1 SHELL WALL RECORD

24 1

\$K1\$ \$S\$

[illegible][illegible]

137

1 0.0018000 0.0			\$K2 LAYERED WALL RECORD
1 0.0018000 90.0			\$K2 LAYERED WALL RECORD
2 0.0085000 0.0 1			\$K2 LAYERED WALL RECORD
27 1 1			\$K1 SHELL WALL RECORD (BOUNDARY)
3 0.1250000 0.0			\$K2 LAYERED WALL RECORD
1 0 0 0 .0000 .0000		.0000 111 111	\$S1 USER PT RCD
2 0 0 0 .9543 2.6429		.0000 111 111	\$S1 USER PT RCD
3 0 0 0 1.7067 2.6154		2.4038 111 111	\$S1 USER PT RCD
4 0 0 0 1.7067 .0000		3.4593 111 111	\$S1 USER PT RCD
5 0 0 0 1.7067 2.6154		-2.4038 111 111	\$S1 USER PT RCD
6 0 0 0 1.7067 .0000		-3.4593 111 111	\$S1 USER PT RCD
7 0 0 0 5.8027 9.2129		.0000 111 111	\$S1 USER PT RCD
8 0 0 0 5.8027 8.0588		2.7373 111 111	\$S1 USER PT RCD
9 0 0 0 5.8027 5.8590		4.8204 111 111	\$S1 USER PT RCD
10 0 0 0 5.8027 2.4660		6.7054 111 111	\$S1 USER PT RCD
11 0 0 0 5.8027 -.1554		6.9066 111 111	\$S1 USER PT RCD
12 0 0 0 5.8027 8.0588		-2.7373 111 111	\$S1 USER PT RCD
13 0 0 0 5.8027 5.8590		-4.8204 111 111	\$S1 USER PT RCD
14 0 0 0 5.8027 2.4660		-6.7054 111 111	\$S1 USER PT RCD
15 0 0 0 5.8027 -.1554		-6.9066 111 111	\$S1 USER PT RCD
16 0 0 0 11.6267 13.1878		.0000 111 111	\$S1 USER PT RCD
17 0 0 0 11.6267 12.5106		2.7447 111 111	\$S1 USER PT RCD
18 0 0 0 11.6267 10.9231		5.1033 111 111	\$S1 USER PT RCD
19 0 0 0 11.6267 8.8064		7.0056 111 111	\$S1 USER PT RCD
20 0 0 0 11.6267 6.3305		8.4114 111 111	\$S1 USER PT RCD
21 0 0 0 11.6267 2.2535		9.4921 111 111	\$S1 USER PT RCD
22 0 0 0 11.6267 -.3141		9.8173 111 111	\$S1 USER PT RCD
23 0 0 0 11.6267 12.5106		-2.7447 111 111	\$S1 USER PT RCD
24 0 0 0 11.6267 10.9231		-5.1033 111 111	\$S1 USER PT RCD
25 0 0 0 11.6267 8.8064		-7.0056 111 111	\$S1 USER PT RCD
26 0 0 0 11.6267 6.3305		-8.4114 111 111	\$S1 USER PT RCD
27 0 0 0 11.6267 2.2535		-9.4921 111 111	\$S1 USER PT RCD
28 0 0 0 11.6267 -.3141		-9.8173 111 111	\$S1 USER PT RCD
29 0 0 0 17.4507 16.4566		.0000 111 111	\$S1 USER PT RCD
30 0 0 0 17.4507 16.1636		2.2341 111 111	\$S1 USER PT RCD
31 0 0 0 17.4507 15.3482		4.3357 111 111	\$S1 USER PT RCD
32 0 0 0 17.4507 13.2931		7.0699 111 111	\$S1 USER PT RCD
33 0 0 0 17.4507 10.5753		9.1282 111 111	\$S1 USER PT RCD
34 0 0 0 17.4507 7.4389		10.5816 111 111	\$S1 USER PT RCD
35 0 0 0 17.4507 2.0410		11.6746 111 111	\$S1 USER PT RCD
36 0 0 0 17.4507 -.4632		11.9202 111 111	\$S1 USER PT RCD
37 0 0 0 17.4507 16.1636		-2.2341 111 111	\$S1 USER PT RCD
38 0 0 0 17.4507 15.3482		-4.3357 111 111	\$S1 USER PT RCD
39 0 0 0 17.4507 13.2931		-7.0699 111 111	\$S1 USER PT RCD
40 0 0 0 17.4507 10.5753		-9.1282 111 111	\$S1 USER PT RCD
41 0 0 0 17.4507 7.4389		-10.5816 111 111	\$S1 USER PT RCD
42 0 0 0 17.4507 2.0410		-11.6746 111 111	\$S1 USER PT RCD
43 0 0 0 17.4507 -.4632		-11.9202 111 111	\$S1 USER PT RCD
44 0 0 0 23.2533 19.3166		.0000 111 111	\$S1 USER PT RCD
45 0 0 0 23.2533 18.9387		2.9493 111 111	\$S1 USER PT RCD
46 0 0 0 23.2533 17.7758		5.6968 111 111	\$S1 USER PT RCD
47 0 0 0 23.2533 15.1888		8.6430 111 111	\$S1 USER PT RCD
48 0 0 0 23.2533 11.9307		10.7546 111 111	\$S1 USER PT RCD
49 0 0 0 23.2533 8.2676		12.2041 111 111	\$S1 USER PT RCD



50	0	0	0	23.2533	4.1848	13.0923	111	111	\$\$1	USER	PT	RCD
51	0	0	0	23.2533	1.9000	13.4892	111	111	\$\$1	USER	PT	RCD
52	0	0	0	23.2533	-.5935	13.4892	111	111	\$\$1	USER	PT	RCD
53	0	0	0	23.2533	18.9387	-2.9493	111	111	\$\$1	USER	PT	RCD
54	0	0	0	23.2533	17.7758	-5.6968	111	111	\$\$1	USER	PT	RCD
55	0	0	0	23.2533	15.1888	-8.6430	111	111	\$\$1	USER	PT	RCD
56	0	0	0	23.2533	11.9307	-10.7546	111	111	\$\$1	USER	PT	RCD
57	0	0	0	23.2533	8.2676	-12.2041	111	111	\$\$1	USER	PT	RCD
58	0	0	0	23.2533	4.1848	-13.0923	111	111	\$\$1	USER	PT	RCD
59	0	0	0	23.2533	1.9000	-13.4892	111	111	\$\$1	USER	PT	RCD
60	0	0	0	23.2533	-.5935	-13.4892	111	111	\$\$1	USER	PT	RCD
61	0	0	0	34.9013	23.9924	.0000	111	111	\$\$1	USER	PT	RCD
62	0	0	0	34.9012	23.4369	4.1085	111	111	\$\$1	USER	PT	RCD
63	0	0	0	34.9012	21.6871	7.8900	111	111	\$\$1	USER	PT	RCD
64	0	0	0	34.9012	18.4749	11.3699	111	111	\$\$1	USER	PT	RCD
65	0	0	0	34.9012	14.2577	13.5470	111	111	\$\$1	USER	PT	RCD
66	0	0	0	34.9012	9.3745	14.3713	111	111	\$\$1	USER	PT	RCD
67	0	0	0	34.9012	4.4698	15.0336	111	111	\$\$1	USER	PT	RCD
68	0	0	0	34.9012	1.6900	15.7464	111	111	\$\$1	USER	PT	RCD
69	0	0	0	34.9012	-.8093	15.7464	111	111	\$\$1	USER	PT	RCD
70	0	0	0	34.9012	23.4369	-4.1085	111	111	\$\$1	USER	PT	RCD
71	0	0	0	34.9012	21.6871	-7.8900	111	111	\$\$1	USER	PT	RCD
72	0	0	0	34.9012	18.4749	-11.3699	111	111	\$\$1	USER	PT	RCD
73	0	0	0	34.9012	14.2577	-13.5470	111	111	\$\$1	USER	PT	RCD
74	0	0	0	34.9012	9.3745	-14.3713	111	111	\$\$1	USER	PT	RCD
75	0	0	0	34.9012	4.4698	-15.0336	111	111	\$\$1	USER	PT	RCD
76	0	0	0	34.9012	1.6900	-15.7464	111	111	\$\$1	USER	PT	RCD
77	0	0	0	34.9012	-.8093	-15.7464	111	111	\$\$1	USER	PT	RCD
78	0	0	0	46.5493	27.3530	.0000	111	111	\$\$1	USER	PT	RCD
79	0	0	0	46.5493	26.6173	4.9282	111	111	\$\$1	USER	PT	RCD
80	0	0	0	46.5493	24.4760	9.4544	111	111	\$\$1	USER	PT	RCD
81	0	0	0	46.5493	20.7198	13.2326	111	111	\$\$1	USER	PT	RCD
82	0	0	0	46.5493	15.7233	15.3057	111	111	\$\$1	USER	PT	RCD
83	0	0	0	46.5493	10.2022	15.9920	111	111	\$\$1	USER	PT	RCD
84	0	0	0	46.5493	4.7007	16.6059	111	111	\$\$1	USER	PT	RCD
85	0	0	0	46.5493	1.5300	17.2388	111	111	\$\$1	USER	PT	RCD
86	0	0	0	46.5493	-.9704	17.2388	111	111	\$\$1	USER	PT	RCD
87	0	0	0	46.5493	26.6173	-4.9282	111	111	\$\$1	USER	PT	RCD
88	0	0	0	46.5493	24.4760	-9.4544	111	111	\$\$1	USER	PT	RCD
89	0	0	0	46.5493	20.7198	-13.2326	111	111	\$\$1	USER	PT	RCD
90	0	0	0	46.5493	15.7233	-15.3057	111	111	\$\$1	USER	PT	RCD
91	0	0	0	46.5493	10.2022	-15.9920	111	111	\$\$1	USER	PT	RCD
92	0	0	0	46.5493	4.7007	-16.6059	111	111	\$\$1	USER	PT	RCD
93	0	0	0	46.5493	1.5300	-17.2388	111	111	\$\$1	USER	PT	RCD
94	0	0	0	46.5493	-.9704	-17.2388	111	111	\$\$1	USER	PT	RCD
95	0	0	0	58.1760	29.6612	.0000	111	111	\$\$1	USER	PT	RCD
96	0	0	0	58.1759	28.7711	5.4832	111	111	\$\$1	USER	PT	RCD
97	0	0	0	58.1759	26.3311	10.4938	111	111	\$\$1	USER	PT	RCD
98	0	0	0	58.1859	21.9052	14.2165	111	111	\$\$1	USER	PT	RCD
99	0	0	0	58.1759	16.4688	16.2003	111	111	\$\$1	USER	PT	RCD
100	0	0	0	58.1759	10.6657	16.8997	111	111	\$\$1	USER	PT	RCD
101	0	0	0	58.1759	4.8376	17.5387	111	111	\$\$1	USER	PT	RCD
102	0	0	0	58.1759	1.4200	18.1876	111	111	\$\$1	USER	PT	RCD
103	0	0	0	58.1759	-1.0806	18.1876	111	111	\$\$1	USER	PT	RCD

104	0	0	0	58.1759	28.7711	-5.4832	111	111	\$\$1	USER	PT	RCD
105	0	0	0	58.1759	26.3311	-10.4938	111	111	\$\$1	USER	PT	RCD
106	0	0	0	58.1759	21.9052	-14.2165	111	111	\$\$1	USER	PT	RCD
107	0	0	0	58.1759	16.4688	-16.2003	111	111	\$\$1	USER	PT	RCD
108	0	0	0	58.1759	10.6657	-16.8997	111	111	\$\$1	USER	PT	RCD
109	0	0	0	58.1759	4.8376	-17.5387	111	111	\$\$1	USER	PT	RCD
110	0	0	0	58.1759	1.4200	-18.1876	111	111	\$\$1	USER	PT	RCD
111	0	0	0	58.1759	-1.0806	-18.1876	111	111	\$\$1	USER	PT	RCD
112	0	0	0	69.8240	31.2109	.0000	111	111	\$\$1	USER	PT	RCD
113	0	0	0	69.8239	30.2019	5.8520	111	111	\$\$1	USER	PT	RCD
114	0	0	0	69.8239	27.3508	11.0656	111	111	\$\$1	USER	PT	RCD
115	0	0	0	69.8539	22.6940	14.8710	111	111	\$\$1	USER	PT	RCD
116	0	0	0	69.8239	16.9340	16.7585	111	111	\$\$1	USER	PT	RCD
117	0	0	0	69.8239	10.9299	17.4168	111	111	\$\$1	USER	PT	RCD
118	0	0	0	69.8239	4.9165	18.0761	111	111	\$\$1	USER	PT	RCD
119	0	0	0	69.8239	1.3500	18.7409	111	111	\$\$1	USER	PT	RCD
120	0	0	0	69.8239	-1.1476	18.7409	111	111	\$\$1	USER	PT	RCD
121	0	0	0	69.8239	30.2019	-5.8520	111	111	\$\$1	USER	PT	RCD
122	0	0	0	69.8239	27.3508	-11.0656	111	111	\$\$1	USER	PT	RCD
123	0	0	0	69.8239	22.6940	-14.8710	111	111	\$\$1	USER	PT	RCD
124	0	0	0	69.8239	16.9340	-16.7585	111	111	\$\$1	USER	PT	RCD
125	0	0	0	69.8239	10.9299	-17.4168	111	111	\$\$1	USER	PT	RCD
126	0	0	0	69.8239	4.9165	-18.0761	111	111	\$\$1	USER	PT	RCD
127	0	0	0	69.8239	1.3500	-18.7409	111	111	\$\$1	USER	PT	RCD
128	0	0	0	69.8239	-1.1476	-18.7409	111	111	\$\$1	USER	PT	RCD
129	0	0	0	75.6273	31.6500	.0000	111	111	\$\$1	USER	PT	RCD
130	0	0	0	75.6373	30.5637	5.9453	111	111	\$\$1	USER	PT	RCD
131	0	0	0	75.6373	27.5961	11.2032	111	111	\$\$1	USER	PT	RCD
132	0	0	0	75.6373	22.8776	15.0234	111	111	\$\$1	USER	PT	RCD
133	0	0	0	75.6373	17.0874	16.9425	111	111	\$\$1	USER	PT	RCD
134	0	0	0	75.6373	11.0153	17.5839	111	111	\$\$1	USER	PT	RCD
135	0	0	0	75.6373	4.9385	18.2258	111	111	\$\$1	USER	PT	RCD
136	0	0	0	75.6373	1.3400	18.8704	111	111	\$\$1	USER	PT	RCD
137	0	0	0	75.6373	-1.1636	18.8704	111	111	\$\$1	USER	PT	RCD
138	0	0	0	75.6373	30.5637	-5.9453	111	111	\$\$1	USER	PT	RCD
139	0	0	0	75.6373	27.5961	-11.2032	111	111	\$\$1	USER	PT	RCD
140	0	0	0	75.6373	22.8776	-15.0234	111	111	\$\$1	USER	PT	RCD
141	0	0	0	75.6373	17.0874	-16.9425	111	111	\$\$1	USER	PT	RCD
142	0	0	0	75.6373	11.0153	-17.5839	111	111	\$\$1	USER	PT	RCD
143	0	0	0	75.6373	4.9385	-18.2258	111	111	\$\$1	USER	PT	RCD
144	0	0	0	75.6373	1.3400	-18.8704	111	111	\$\$1	USER	PT	RCD
145	0	0	0	75.6373	-1.1636	-18.8704	111	111	\$\$1	USER	PT	RCD
146	0	0	0	81.4506	31.9999	.0000	111	111	\$\$1	USER	PT	RCD
147	0	0	0	81.4506	30.9256	6.0385	111	111	\$\$1	USER	PT	RCD
148	0	0	0	81.4506	27.8414	11.3408	111	111	\$\$1	USER	PT	RCD
149	0	0	0	81.4506	23.0612	15.1759	111	111	\$\$1	USER	PT	RCD
150	0	0	0	81.4506	17.2408	17.1266	111	111	\$\$1	USER	PT	RCD
151	0	0	0	81.4506	11.1006	17.7510	111	111	\$\$1	USER	PT	RCD
152	0	0	0	81.4506	4.9605	18.3755	111	111	\$\$1	USER	PT	RCD
153	0	0	0	81.4506	1.3200	18.9999	111	111	\$\$1	USER	PT	RCD
154	0	0	0	81.4506	-1.1797	18.9999	111	111	\$\$1	USER	PT	RCD
155	0	0	0	81.4506	30.9256	-6.0385	111	111	\$\$1	USER	PT	RCD
156	0	0	0	81.4506	27.8414	-11.3408	111	111	\$\$1	USER	PT	RCD
157	0	0	0	81.4506	23.0612	-15.1759	111	111	\$\$1	USER	PT	RCD

158	0	0	0	81.4506	17.2408	-17.1266	111	111	\$\$1	USER	PT	RCD
159	0	0	0	81.4506	11.1006	-17.7510	111	111	\$\$1	USER	PT	RCD
160	0	0	0	81.4506	4.9605	-18.3755	111	111	\$\$1	USER	PT	RCD
161	0	0	0	81.4506	1.3200	-18.9999	111	111	\$\$1	USER	PT	RCD
162	0	0	0	81.4506	-1.1797	-18.9999	111	111	\$\$1	USER	PT	RCD
163	0	0	0	90.8613	32.0000	.0000	111	111	\$\$1	USER	PT	RCD
164	0	0	0	90.8613	30.8852	6.0320	111	111	\$\$1	USER	PT	RCD
165	0	0	0	90.8613	27.7692	11.3113	111	111	\$\$1	USER	PT	RCD
166	0	0	0	90.8613	23.0409	15.1589	111	111	\$\$1	USER	PT	RCD
167	0	0	0	90.8613	17.2351	17.1560	111	111	\$\$1	USER	PT	RCD
168	0	0	0	90.8613	11.1349	17.7957	111	111	\$\$1	USER	PT	RCD
169	0	0	0	90.8613	4.9926	18.4399	111	111	\$\$1	USER	PT	RCD
170	0	0	0	90.8613	1.3100	18.9331	111	111	\$\$1	USER	PT	RCD
171	0	0	0	90.8613	-1.1880	19.0881	111	111	\$\$1	USER	PT	RCD
172	0	0	0	90.8613	30.8852	-6.0320	111	111	\$\$1	USER	PT	RCD
173	0	0	0	90.8613	27.7692	-11.3113	111	111	\$\$1	USER	PT	RCD
174	0	0	0	90.8613	23.0409	-15.1589	111	111	\$\$1	USER	PT	RCD
175	0	0	0	90.8613	17.2351	-17.1560	111	111	\$\$1	USER	PT	RCD
176	0	0	0	90.8613	11.1349	-17.7957	111	111	\$\$1	USER	PT	RCD
177	0	0	0	90.8613	4.9926	-18.4399	111	111	\$\$1	USER	PT	RCD
178	0	0	0	90.8613	1.3100	-18.9331	111	111	\$\$1	USER	PT	RCD
179	0	0	0	90.8613	-1.1880	-19.0881	111	111	\$\$1	USER	PT	RCD
180	0	0	0	98.5000	32.0000	.0000	111	111	\$\$1	USER	PT	RCD
181	0	0	0	98.5000	30.8852	6.0320	111	111	\$\$1	USER	PT	RCD
182	0	0	0	98.5000	27.7692	11.3113	111	111	\$\$1	USER	PT	RCD
183	0	0	0	98.5000	23.0409	15.1589	111	111	\$\$1	USER	PT	RCD
184	0	0	0	98.5000	17.2351	17.1560	111	111	\$\$1	USER	PT	RCD
185	0	0	0	98.5000	11.1349	17.7957	111	111	\$\$1	USER	PT	RCD
186	0	0	0	98.5000	4.9926	18.4399	111	111	\$\$1	USER	PT	RCD
187	0	0	0	98.5000	1.1300	18.9331	111	111	\$\$1	USER	PT	RCD
188	0	0	0	98.5000	-1.1880	19.0881	111	111	\$\$1	USER	PT	RCD
189	0	0	0	98.5000	30.8852	-6.0320	111	111	\$\$1	USER	PT	RCD
190	0	0	0	98.5000	27.7692	-11.3113	111	111	\$\$1	USER	PT	RCD
191	0	0	0	98.5000	23.0409	-15.1589	111	111	\$\$1	USER	PT	RCD
192	0	0	0	98.5000	17.2351	-17.1560	111	111	\$\$1	USER	PT	RCD
193	0	0	0	98.5000	11.1349	-17.7957	111	111	\$\$1	USER	PT	RCD
194	0	0	0	98.5000	4.9926	-18.4399	111	111	\$\$1	USER	PT	RCD
195	0	0	0	98.5000	1.3100	-18.9331	111	111	\$\$1	USER	PT	RCD
196	0	0	0	98.5000	-1.1880	-19.0881	111	111	\$\$1	USER	PT	RCD
197	0	0	0	103.8900	31.9687	.0000	111	111	\$\$1	USER	PT	RCD
198	0	0	0	103.8900	30.8852	6.0320	111	111	\$\$1	USER	PT	RCD
199	0	0	0	103.8900	27.7692	11.3113	111	111	\$\$1	USER	PT	RCD
200	0	0	0	103.8900	23.0409	15.1589	111	111	\$\$1	USER	PT	RCD
201	0	0	0	103.8900	17.2351	17.1560	111	111	\$\$1	USER	PT	RCD
202	0	0	0	103.8900	11.1349	17.7957	111	111	\$\$1	USER	PT	RCD
203	0	0	0	103.8900	4.9926	18.4399	111	111	\$\$1	USER	PT	RCD
204	0	0	0	103.8900	1.3100	18.9331	111	111	\$\$1	USER	PT	RCD
205	0	0	0	103.8900	-1.1880	19.0881	111	111	\$\$1	USER	PT	RCD
206	0	0	0	103.8900	30.8852	-6.0320	111	111	\$\$1	USER	PT	RCD
207	0	0	0	103.8900	27.7692	-11.3113	111	111	\$\$1	USER	PT	RCD
208	0	0	0	103.8900	23.0409	-15.1589	111	111	\$\$1	USER	PT	RCD
209	0	0	0	103.8900	17.2351	-17.1560	111	111	\$\$1	USER	PT	RCD
210	0	0	0	103.8900	11.1349	-17.7957	111	111	\$\$1	USER	PT	RCD
211	0	0	0	103.8900	4.9926	-18.4399	111	111	\$\$1	USER	PT	RCD

212	0	0	0	103.8900	1.3100	-18.9331	111	111	\$\$1	USER	PT	RCD
213	0	0	0	103.8900	-1.1880	-19.0881	111	111	\$\$1	USER	PT	RCD
214	0	0	0	113.3800	31.4000	.0000	111	111	\$\$1	USER	PT	RCD
215	0	0	0	113.3800	30.2179	5.9301	111	111	\$\$1	USER	PT	RCD
216	0	0	0	113.3800	27.2238	11.0903	111	111	\$\$1	USER	PT	RCD
217	0	0	0	113.3800	22.7083	14.8830	111	111	\$\$1	USER	PT	RCD
218	0	0	0	113.3800	17.0730	16.9586	111	111	\$\$1	USER	PT	RCD
219	0	0	0	113.3800	11.0068	17.6280	111	111	\$\$1	USER	PT	RCD
220	0	0	0	113.3800	4.9016	18.2567	111	111	\$\$1	USER	PT	RCD
221	0	0	0	113.3800	1.3300	18.7300	111	111	\$\$1	USER	PT	RCD
222	0	0	0	113.3800	-1.1686	18.8819	111	111	\$\$1	USER	PT	RCD
223	0	0	0	113.3800	30.2179	-5.9301	111	111	\$\$1	USER	PT	RCD
224	0	0	0	113.3800	27.2238	-11.0904	111	111	\$\$1	USER	PT	RCD
225	0	0	0	113.3800	22.7083	-14.8831	111	111	\$\$1	USER	PT	RCD
226	0	0	0	113.3800	17.0730	-16.9586	111	111	\$\$1	USER	PT	RCD
227	0	0	0	113.3800	11.0068	-17.6280	111	111	\$\$1	USER	PT	RCD
228	0	0	0	113.3800	4.9016	-18.2567	111	111	\$\$1	USER	PT	RCD
229	0	0	0	113.3800	1.3300	-18.7300	111	111	\$\$1	USER	PT	RCD
230	0	0	0	113.3800	-1.1686	-18.8819	111	111	\$\$1	USER	PT	RCD
231	0	0	0	122.8700	30.5737	.0000	111	111	\$\$1	USER	PT	RCD
232	0	0	0	122.8700	29.5506	5.8281	111	111	\$\$1	USER	PT	RCD
233	0	0	0	122.8700	26.6784	10.8694	111	111	\$\$1	USER	PT	RCD
234	0	0	0	122.8700	22.3758	14.6072	111	111	\$\$1	USER	PT	RCD
235	0	0	0	122.8700	16.9109	16.7612	111	111	\$\$1	USER	PT	RCD
236	0	0	0	122.8700	10.8788	17.4604	111	111	\$\$1	USER	PT	RCD
237	0	0	0	122.8700	4.8107	18.0735	111	111	\$\$1	USER	PT	RCD
238	0	0	0	122.8700	1.3500	18.5269	111	111	\$\$1	USER	PT	RCD
239	0	0	0	122.8700	-1.1492	18.6758	111	111	\$\$1	USER	PT	RCD
240	0	0	0	122.8700	29.5506	-5.8281	111	111	\$\$1	USER	PT	RCD
241	0	0	0	122.8700	26.6784	-10.8694	111	111	\$\$1	USER	PT	RCD
242	0	0	0	122.8700	22.3758	-14.6072	111	111	\$\$1	USER	PT	RCD
243	0	0	0	122.8700	16.9109	-16.7612	111	111	\$\$1	USER	PT	RCD
244	0	0	0	122.8700	10.8788	-17.4604	111	111	\$\$1	USER	PT	RCD
245	0	0	0	122.8700	4.8107	-18.0735	111	111	\$\$1	USER	PT	RCD
246	0	0	0	122.8700	1.3500	-18.5269	111	111	\$\$1	USER	PT	RCD
247	0	0	0	122.8700	-1.1492	-18.6758	111	111	\$\$1	USER	PT	RCD
248	0	0	0	136.1700	28.2630	.0000	111	111	\$\$1	USER	PT	RCD
249	0	0	0	136.1700	27.3259	5.4883	111	111	\$\$1	USER	PT	RCD
250	0	0	0	136.1700	24.8112	10.1130	111	111	\$\$1	USER	PT	RCD
251	0	0	0	136.1700	21.1503	13.5906	111	111	\$\$1	USER	PT	RCD
252	0	0	0	136.1700	16.2183	15.9177	111	111	\$\$1	USER	PT	RCD
253	0	0	0	136.1700	10.3390	16.7532	111	111	\$\$1	USER	PT	RCD
254	0	0	0	136.1700	4.4403	17.3274	111	111	\$\$1	USER	PT	RCD
255	0	0	0	136.1700	1.4500	17.7217	111	111	\$\$1	USER	PT	RCD
256	0	0	0	136.1740	-1.0464	17.8586	111	111	\$\$1	USER	PT	RCD
257	0	0	0	136.1700	27.3259	-5.4883	111	111	\$\$1	USER	PT	RCD
258	0	0	0	136.1700	24.8112	-10.1130	111	111	\$\$1	USER	PT	RCD
259	0	0	0	136.1700	21.1503	-13.5906	111	111	\$\$1	USER	PT	RCD
260	0	0	0	136.1700	16.2183	-15.9177	111	111	\$\$1	USER	PT	RCD
261	0	0	0	136.1700	10.3390	-16.7532	111	111	\$\$1	USER	PT	RCD
262	0	0	0	136.1700	4.4403	-17.3274	111	111	\$\$1	USER	PT	RCD
263	0	0	0	136.1700	1.4500	-17.7217	111	111	\$\$1	USER	PT	RCD
264	0	0	0	136.1740	-1.0464	-17.8586	111	111	\$\$1	USER	PT	RCD
265	0	0	0	149.4800	24.9563	.0000	111	111	\$\$1	USER	PT	RCD

266	0	0	0	149.4800	24.1245	4.9995	111	111	\$\$1	USER	PT	RCD
267	0	0	0	149.4800	22.0625	8.9998	111	111	\$\$1	USER	PT	RCD
268	0	0	0	149.4800	19.2328	11.9998	111	111	\$\$1	USER	PT	RCD
269	0	0	0	149.4800	15.0000	14.4343	111	111	\$\$1	USER	PT	RCD
270	0	0	0	149.4800	9.3972	15.5198	111	111	\$\$1	USER	PT	RCD
271	0	0	0	149.4800	3.8030	16.0437	111	111	\$\$1	USER	PT	RCD
272	0	0	0	149.4800	1.5600	16.3084	111	111	\$\$1	USER	PT	RCD
273	0	0	0	149.4800	-.9436	16.4880	111	111	\$\$1	USER	PT	RCD
274	0	0	0	149.4800	24.1245	-4.9995	111	111	\$\$1	USER	PT	RCD
275	0	0	0	149.4800	22.0625	-8.9998	111	111	\$\$1	USER	PT	RCD
276	0	0	0	149.4800	19.2328	-11.9998	111	111	\$\$1	USER	PT	RCD
277	0	0	0	149.4800	15.0000	-14.4343	111	111	\$\$1	USER	PT	RCD
278	0	0	0	149.4800	9.3972	-15.5198	111	111	\$\$1	USER	PT	RCD
279	0	0	0	149.4800	3.8030	-16.0437	111	111	\$\$1	USER	PT	RCD
280	0	0	0	149.4800	1.5600	-16.3084	111	111	\$\$1	USER	PT	RCD
281	0	0	0	149.4800	-.9436	-16.4880	111	111	\$\$1	USER	PT	RCD
282	0	0	0	162.7800	20.8424	.0000	111	111	\$\$1	USER	PT	RCD
283	0	0	0	162.7800	20.1915	4.2271	111	111	\$\$1	USER	PT	RCD
284	0	0	0	162.7800	18.6665	7.5112	111	111	\$\$1	USER	PT	RCD
285	0	0	0	162.7800	16.3676	10.2830	111	111	\$\$1	USER	PT	RCD
286	0	0	0	162.7800	12.8861	12.6611	111	111	\$\$1	USER	PT	RCD
287	0	0	0	162.7800	8.1095	13.9902	111	111	\$\$1	USER	PT	RCD
288	0	0	0	162.7800	1.7300	14.5972	111	111	\$\$1	USER	PT	RCD
289	0	0	0	162.7800	-.7750	14.7893	111	111	\$\$1	USER	PT	RCD
290	0	0	0	162.7800	20.1915	-4.2271	111	111	\$\$1	USER	PT	RCD
291	0	0	0	162.7800	18.6665	-7.5112	111	111	\$\$1	USER	PT	RCD
292	0	0	0	162.7800	16.3676	-10.2830	111	111	\$\$1	USER	PT	RCD
293	0	0	0	162.7800	12.8861	-12.6611	111	111	\$\$1	USER	PT	RCD
294	0	0	0	162.7800	8.1095	-13.9902	111	111	\$\$1	USER	PT	RCD
295	0	0	0	162.7800	1.7300	-14.5972	111	111	\$\$1	USER	PT	RCD
296	0	0	0	162.7800	-.7750	-14.7893	111	111	\$\$1	USER	PT	RCD
297	0	0	0	176.0900	16.2070	.0000	111	111	\$\$1	USER	PT	RCD
298	0	0	0	176.0900	15.7459	3.3538	111	111	\$\$1	USER	PT	RCD
299	0	0	0	176.0900	14.7690	5.8030	111	111	\$\$1	USER	PT	RCD
300	0	0	0	176.0900	13.0393	8.2886	111	111	\$\$1	USER	PT	RCD
301	0	0	0	176.0900	10.3600	10.5422	111	111	\$\$1	USER	PT	RCD
302	0	0	0	176.0900	6.4710	12.1328	111	111	\$\$1	USER	PT	RCD
303	0	0	0	176.0900	1.9200	12.6490	111	111	\$\$1	USER	PT	RCD
304	0	0	0	176.0900	-.5825	12.8499	111	111	\$\$1	USER	PT	RCD
305	0	0	0	176.0900	15.7459	-3.3538	111	111	\$\$1	USER	PT	RCD
306	0	0	0	176.0900	14.7690	-5.8030	111	111	\$\$1	USER	PT	RCD
307	0	0	0	176.0900	13.0393	-8.2886	111	111	\$\$1	USER	PT	RCD
308	0	0	0	176.0900	10.3600	-10.5422	111	111	\$\$1	USER	PT	RCD
309	0	0	0	176.0900	6.4710	-12.1328	111	111	\$\$1	USER	PT	RCD
310	0	0	0	176.0900	1.9200	-12.6490	111	111	\$\$1	USER	PT	RCD
311	0	0	0	176.0900	-.5825	-12.8499	111	111	\$\$1	USER	PT	RCD
312	0	0	0	189.3900	11.4580	.0000	111	111	\$\$1	USER	PT	RCD
313	0	0	0	189.3900	11.1631	2.4536	111	111	\$\$1	USER	PT	RCD
314	0	0	0	189.3900	10.6543	3.9995	111	111	\$\$1	USER	PT	RCD
315	0	0	0	189.3900	9.5424	5.9995	111	111	\$\$1	USER	PT	RCD
316	0	0	0	189.3900	7.4991	8.1426	111	111	\$\$1	USER	PT	RCD
317	0	0	0	189.3900	4.4203	9.8081	111	111	\$\$1	USER	PT	RCD
318	0	0	0	189.3900	2.1100	10.3972	111	111	\$\$1	USER	PT	RCD
319	0	0	0	189.3900	-.3881	10.5117	111	111	\$\$1	USER	PT	RCD

320	0	0	0	189.3900	11.1631	-2.4536	111	111	\$\$1	USER	PT	RCD
321	0	0	0	189.3900	10.6543	-3.9995	111	111	\$\$1	USER	PT	RCD
322	0	0	0	189.3900	9.5424	-5.9995	111	111	\$\$1	USER	PT	RCD
323	0	0	0	189.3900	7.4991	-8.1426	111	111	\$\$1	USER	PT	RCD
324	0	0	0	189.3900	4.4203	-9.8081	111	111	\$\$1	USER	PT	RCD
325	0	0	0	189.3900	2.1100	-10.3972	111	111	\$\$1	USER	PT	RCD
326	0	0	0	189.3900	-.3881	-10.5117	111	111	\$\$1	USER	PT	RCD
327	0	0	0	196.0500	9.0705	.0000	111	111	\$\$1	USER	PT	RCD
328	0	0	0	196.0500	8.8519	2.0000	111	111	\$\$1	USER	PT	RCD
329	0	0	0	196.0500	8.0001	4.3208	111	111	\$\$1	USER	PT	RCD
330	0	0	0	196.0500	6.0001	6.8855	111	111	\$\$1	USER	PT	RCD
331	0	0	0	196.0500	3.7709	8.3677	111	111	\$\$1	USER	PT	RCD
332	0	0	0	196.0500	2.1900	9.0000	111	111	\$\$1	USER	PT	RCD
333	0	0	0	196.0500	-.3097	9.2942	111	111	\$\$1	USER	PT	RCD
334	0	0	0	196.0500	8.8519	-2.0000	111	111	\$\$1	USER	PT	RCD
335	0	0	0	196.0500	8.0001	-4.3208	111	111	\$\$1	USER	PT	RCD
336	0	0	0	196.0500	6.0001	-6.8855	111	111	\$\$1	USER	PT	RCD
337	0	0	0	196.0500	3.7709	-8.3677	111	111	\$\$1	USER	PT	RCD
338	0	0	0	196.0500	2.1900	-9.0000	111	111	\$\$1	USER	PT	RCD
339	0	0	0	196.0500	-.3097	-9.2942	111	111	\$\$1	USER	PT	RCD
340	0	0	0	202.7000	6.7899	.0000	111	111	\$\$1	USER	PT	RCD
341	0	0	0	202.7000	6.1991	2.9995	111	111	\$\$1	USER	PT	RCD
342	0	0	0	202.7000	5.0311	4.9995	111	111	\$\$1	USER	PT	RCD
343	0	0	0	202.7000	2.2800	7.3000	111	111	\$\$1	USER	PT	RCD
344	0	0	0	202.7000	-.2170	7.8560	111	111	\$\$1	USER	PT	RCD
345	0	0	0	202.7000	6.1991	-2.9995	111	111	\$\$1	USER	PT	RCD
346	0	0	0	202.7000	5.0311	-4.9995	111	111	\$\$1	USER	PT	RCD
347	0	0	0	202.7000	2.2800	-7.3000	111	111	\$\$1	USER	PT	RCD
348	0	0	0	202.7000	-.2170	-7.8560	111	111	\$\$1	USER	PT	RCD
349	0	0	0	209.3600	4.3978	.0000	111	111	\$\$1	USER	PT	RCD
350	0	0	0	209.3600	4.0000	2.4407	111	111	\$\$1	USER	PT	RCD
351	0	0	0	209.3600	2.3261	5.0000	111	111	\$\$1	USER	PT	RCD
352	0	0	0	209.3600	-.1730	6.2522	111	111	\$\$1	USER	PT	RCD
353	0	0	0	209.3600	4.0000	-2.4407	111	111	\$\$1	USER	PT	RCD
354	0	0	0	209.3600	2.3261	-5.0000	111	111	\$\$1	USER	PT	RCD
355	0	0	0	209.3600	-.1730	-6.2522	111	111	\$\$1	USER	PT	RCD
356	0	0	0	212.7610	3.0416	.0000	111	111	\$\$1	USER	PT	RCD
357	0	0	0	215.5260	1.3518	.0000	111	111	\$\$1	USER	PT	RCD
358	0	0	0	215.5260	1.3518	2.9995	111	111	\$\$1	USER	PT	RCD
359	0	0	0	215.5260	-.1112	3.9998	111	111	\$\$1	USER	PT	RCD
360	0	0	0	215.5260	1.3518	-2.9995	111	111	\$\$1	USER	PT	RCD
361	0	0	0	215.5260	-.1112	-3.9998	111	111	\$\$1	USER	PT	RCD
362	0	0	0	216.0100	.0000	.0000	111	111	\$\$1	USER	PT	RCD
363	0	0	0	0.0000	-0.5000	0.0000	001	000	\$\$1	USER	PT	RCD
364	0	0	0	1.7067	-0.5000	3.4593	001	000	\$\$1	USER	PT	RCD
365	0	0	0	1.7067	-0.5000	-3.4593	001	000	\$\$1	USER	PT	RCD
366	0	0	0	5.8027	-0.6554	6.9066	001	000	\$\$1	USER	PT	RCD
367	0	0	0	5.8027	-0.6554	-6.9066	001	000	\$\$1	USER	PT	RCD
368	0	0	0	11.6267	-0.8141	9.8173	001	000	\$\$1	USER	PT	RCD
369	0	0	0	11.6267	-0.8141	-9.8173	001	000	\$\$1	USER	PT	RCD
370	0	0	0	17.4507	-0.9632	11.9202	001	000	\$\$1	USER	PT	RCD
371	0	0	0	17.4507	-0.9632	-11.9202	001	000	\$\$1	USER	PT	RCD
372	0	0	0	23.2533	-1.0935	13.4892	001	000	\$\$1	USER	PT	RCD
373	0	0	0	23.2533	-1.0935	-13.4892	001	000	\$\$1	USER	PT	RCD

374	0	0	0	34.9012	-1.3093	15.7464	001	000	\$S1	USER	PT	RCD
375	0	0	0	34.9012	-1.3093	-15.7464	001	000	\$S1	USER	PT	RCD
376	0	0	0	46.5493	-1.4704	17.2388	001	000	\$S1	USER	PT	RCD
377	0	0	0	46.5493	-1.4704	-17.2388	001	000	\$S1	USER	PT	RCD
378	0	0	0	58.1759	-1.5806	18.1876	001	000	\$S1	USER	PT	RCD
379	0	0	0	58.1759	-1.5806	-18.1876	001	000	\$S1	USER	PT	RCD
380	0	0	0	69.8239	-1.6476	18.7409	001	000	\$S1	USER	PT	RCD
381	0	0	0	69.8239	-1.6476	-18.7409	001	000	\$S1	USER	PT	RCD
382	0	0	0	75.6373	-1.6636	18.8704	001	000	\$S1	USER	PT	RCD
383	0	0	0	75.6373	-1.6636	-18.8704	001	000	\$S1	USER	PT	RCD
384	0	0	0	81.4506	-1.6797	18.9999	001	000	\$S1	USER	PT	RCD
385	0	0	0	81.4506	-1.6797	-18.9999	001	000	\$S1	USER	PT	RCD
386	0	0	0	90.8613	-1.6880	19.0881	001	000	\$S1	USER	PT	RCD
387	0	0	0	90.8613	-1.6880	-19.0881	001	000	\$S1	USER	PT	RCD
388	0	0	0	98.5000	-1.6880	19.0881	001	000	\$S1	USER	PT	RCD
389	0	0	0	98.5000	-1.6880	-19.0881	001	000	\$S1	USER	PT	RCD
390	0	0	0	103.8900	-1.6880	19.0881	001	000	\$S1	USER	PT	RCD
391	0	0	0	103.8900	-1.6880	-19.0881	001	000	\$S1	USER	PT	RCD
392	0	0	0	113.3800	-1.6686	18.8819	001	000	\$S1	USER	PT	RCD
393	0	0	0	113.3800	-1.6686	-18.8819	001	000	\$S1	USER	PT	RCD
394	0	0	0	122.8700	-1.6492	18.6758	001	000	\$S1	USER	PT	RCD
395	0	0	0	122.8700	-1.6492	-18.6758	001	000	\$S1	USER	PT	RCD
396	0	0	0	136.1740	-1.5464	17.8586	001	000	\$S1	USER	PT	RCD
397	0	0	0	136.1740	-1.5464	-17.8586	001	000	\$S1	USER	PT	RCD
398	0	0	0	149.4800	-1.4436	16.4880	001	000	\$S1	USER	PT	RCD
399	0	0	0	149.4800	-1.4436	-16.4880	001	000	\$S1	USER	PT	RCD
400	0	0	0	162.7800	-1.2750	14.7893	001	000	\$S1	USER	PT	RCD
401	0	0	0	162.7800	-1.2750	-14.7893	001	000	\$S1	USER	PT	RCD
402	0	0	0	176.0900	-1.0825	12.8499	001	000	\$S1	USER	PT	RCD
403	0	0	0	176.0900	-1.0825	-12.8499	001	000	\$S1	USER	PT	RCD
404	0	0	0	189.3900	-0.8881	10.5117	001	000	\$S1	USER	PT	RCD
405	0	0	0	189.3900	-0.8881	-10.5117	001	000	\$S1	USER	PT	RCD
406	0	0	0	196.0500	-0.8097	9.2942	001	000	\$S1	USER	PT	RCD
407	0	0	0	196.0500	-0.8097	-9.2942	001	000	\$S1	USER	PT	RCD
408	0	0	0	202.7000	-0.7170	7.8560	001	000	\$S1	USER	PT	RCD
409	0	0	0	202.7000	-0.7170	-7.8560	001	000	\$S1	USER	PT	RCD
410	0	0	0	209.3600	-0.6730	6.2522	001	000	\$S1	USER	PT	RCD
411	0	0	0	209.3600	-0.6730	-6.2522	001	000	\$S1	USER	PT	RCD
412	0	0	0	215.5260	-0.6112	3.9998	001	000	\$S1	USER	PT	RCD
413	0	0	0	215.5260	-0.6112	-3.9998	001	000	\$S1	USER	PT	RCD
414	0	0	0	216.0100	-0.5000	0.0000	001	000	\$S1	USER	PT	RCD
415	0	0	0	0.0000	-0.8770	0.0000	000	000	\$S1	USER	PT	RCD
416	0	0	0	1.7067	-0.8770	3.4593	000	000	\$S1	USER	PT	RCD
417	0	0	0	1.7067	-0.8770	-3.4593	000	000	\$S1	USER	PT	RCD
418	0	0	0	5.8027	-1.0324	6.9066	000	000	\$S1	USER	PT	RCD
419	0	0	0	5.8027	-1.0324	-6.9066	000	000	\$S1	USER	PT	RCD
420	0	0	0	11.6267	-1.1911	9.8173	000	000	\$S1	USER	PT	RCD
421	0	0	0	11.6267	-1.1911	-9.8173	000	000	\$S1	USER	PT	RCD
422	0	0	0	17.4507	-1.3402	11.9202	000	000	\$S1	USER	PT	RCD
423	0	0	0	17.4507	-1.3402	-11.9202	000	000	\$S1	USER	PT	RCD
424	0	0	0	23.2533	-1.4705	13.4892	000	000	\$S1	USER	PT	RCD
425	0	0	0	23.2533	-1.4705	-13.4892	000	000	\$S1	USER	PT	RCD
426	0	0	0	34.9012	-1.6863	15.7464	000	000	\$S1	USER	PT	RCD
427	0	0	0	34.9012	-1.6863	-15.7464	000	000	\$S1	USER	PT	RCD

428	0	0	0	46.5493	-1.8474	17.2388	000	000	\$\$1	USER	PT	RCD
429	0	0	0	46.5493	-1.8474	-17.2388	000	000	\$\$1	USER	PT	RCD
430	0	0	0	58.1759	-1.9576	18.1876	000	000	\$\$1	USER	PT	RCD
431	0	0	0	58.1759	-1.9576	-18.1876	000	000	\$\$1	USER	PT	RCD
432	0	0	0	69.8239	-2.0246	18.7409	000	000	\$\$1	USER	PT	RCD
433	0	0	0	69.8239	-2.0246	-18.7409	000	000	\$\$1	USER	PT	RCD
434	0	0	0	75.6373	-2.0406	18.8704	000	000	\$\$1	USER	PT	RCD
435	0	0	0	75.6373	-2.0406	-18.8704	000	000	\$\$1	USER	PT	RCD
436	0	0	0	81.4506	-2.0567	18.9999	000	000	\$\$1	USER	PT	RCD
437	0	0	0	81.4506	-2.0567	-18.9999	000	000	\$\$1	USER	PT	RCD
438	0	0	0	90.8613	-2.0650	19.0881	000	000	\$\$1	USER	PT	RCD
439	0	0	0	90.8613	-2.0650	-19.0881	000	000	\$\$1	USER	PT	RCD
440	0	0	0	98.5000	-2.0650	19.0881	000	000	\$\$1	USER	PT	RCD
441	0	0	0	98.5000	-2.0650	-19.0881	000	000	\$\$1	USER	PT	RCD
442	0	0	0	103.8900	-2.0650	19.0881	000	000	\$\$1	USER	PT	RCD
443	0	0	0	103.8900	-2.0650	-19.0881	000	000	\$\$1	USER	PT	RCD
444	0	0	0	113.3800	-2.0456	18.8819	000	000	\$\$1	USER	PT	RCD
445	0	0	0	113.3800	-2.0456	-18.8819	000	000	\$\$1	USER	PT	RCD
446	0	0	0	122.8700	-2.0262	18.6758	000	000	\$\$1	USER	PT	RCD
447	0	0	0	122.8700	-2.0262	-18.6758	000	000	\$\$1	USER	PT	RCD
448	0	0	0	136.1740	-1.9234	17.8586	000	000	\$\$1	USER	PT	RCD
449	0	0	0	136.1740	-1.9234	-17.8586	000	000	\$\$1	USER	PT	RCD
450	0	0	0	149.4800	-1.8206	16.4880	000	000	\$\$1	USER	PT	RCD
451	0	0	0	149.4800	-1.8206	-16.4880	000	000	\$\$1	USER	PT	RCD
452	0	0	0	162.7800	-1.6520	14.7893	000	000	\$\$1	USER	PT	RCD
453	0	0	0	162.7800	-1.6520	-14.7893	000	000	\$\$1	USER	PT	RCD
454	0	0	0	176.0900	-1.4595	12.8499	000	000	\$\$1	USER	PT	RCD
455	0	0	0	176.0900	-1.4595	-12.8499	000	000	\$\$1	USER	PT	RCD
456	0	0	0	189.3900	-1.2651	10.5117	000	000	\$\$1	USER	PT	RCD
457	0	0	0	189.3900	-1.2651	-10.5117	000	000	\$\$1	USER	PT	RCD
458	0	0	0	196.0500	-1.1867	9.2942	000	000	\$\$1	USER	PT	RCD
459	0	0	0	196.0500	-1.1867	-9.2942	000	000	\$\$1	USER	PT	RCD
460	0	0	0	202.7000	-1.0940	7.8560	000	000	\$\$1	USER	PT	RCD
461	0	0	0	202.7000	-1.0940	-7.8560	000	000	\$\$1	USER	PT	RCD
462	0	0	0	209.3600	-1.0500	6.2522	000	000	\$\$1	USER	PT	RCD
463	0	0	0	209.3600	-1.0500	-6.2522	000	000	\$\$1	USER	PT	RCD
464	0	0	0	215.5260	-0.9882	3.9998	000	000	\$\$1	USER	PT	RCD
465	0	0	0	215.5260	-0.9882	-3.9998	000	000	\$\$1	USER	PT	RCD
466	0	0	0	216.0100	-0.8770	0.0000	000	000	\$\$1	USER	PT	RCD
363	415	365	210	1	0.0	0.0	0.0	1	0	\$T2	BEAM	ELEM
364	416	363	210	1	0.0	0.0	0.0	1	0	\$T2	BEAM	ELEM
366	418	364	210	1	0.0	0.0	0.0	1	0	\$T2	BEAM	ELEM
368	420	366	210	1	0.0	0.0	0.0	1	0	\$T2	BEAM	ELEM
370	422	368	210	1	0.0	0.0	0.0	1	0	\$T2	BEAM	ELEM
372	424	370	210	1	0.0	0.0	0.0	1	0	\$T2	BEAM	ELEM
374	426	372	210	1	0.0	0.0	0.0	1	0	\$T2	BEAM	ELEM
376	428	374	210	1	0.0	0.0	0.0	1	0	\$T2	BEAM	ELEM
378	430	376	210	1	0.0	0.0	0.0	1	0	\$T2	BEAM	ELEM
380	432	378	210	1	0.0	0.0	0.0	1	0	\$T2	BEAM	ELEM
382	434	380	210	1	0.0	0.0	0.0	1	0	\$T2	BEAM	ELEM
384	436	382	210	1	0.0	0.0	0.0	1	0	\$T2	BEAM	ELEM
386	438	384	210	1	0.0	0.0	0.0	1	0	\$T2	BEAM	ELEM
388	440	386	210	1	0.0	0.0	0.0	1	0	\$T2	BEAM	ELEM
390	442	388	210	1	0.0	0.0	0.0	1	0	\$T2	BEAM	ELEM



392	444	390	210	1	0.0	0.0	0.0	1	0	\$T2	BEAM	ELEM
394	446	392	210	1	0.0	0.0	0.0	1	0	\$T2	BEAM	ELEM
396	448	394	210	1	0.0	0.0	0.0	1	0	\$T2	BEAM	ELEM
398	450	396	210	1	0.0	0.0	0.0	1	0	\$T2	BEAM	ELEM
400	452	398	210	1	0.0	0.0	0.0	1	0	\$T2	BEAM	ELEM
402	454	400	210	1	0.0	0.0	0.0	1	0	\$T2	BEAM	ELEM
404	456	402	210	1	0.0	0.0	0.0	1	0	\$T2	BEAM	ELEM
406	458	404	210	1	0.0	0.0	0.0	1	0	\$T2	BEAM	ELEM
408	460	406	210	1	0.0	0.0	0.0	1	0	\$T2	BEAM	ELEM
410	462	408	210	1	0.0	0.0	0.0	1	0	\$T2	BEAM	ELEM
412	464	410	210	1	0.0	0.0	0.0	1	0	\$T2	BEAM	ELEM
414	466	412	210	1	0.0	0.0	0.0	1	0	\$T2	BEAM	ELEM
413	465	414	210	1	0.0	0.0	0.0	1	0	\$T2	BEAM	ELEM
411	463	413	210	1	0.0	0.0	0.0	1	0	\$T2	BEAM	ELEM
409	461	411	210	1	0.0	0.0	0.0	1	0	\$T2	BEAM	ELEM
407	459	409	210	1	0.0	0.0	0.0	1	0	\$T2	BEAM	ELEM
405	457	407	210	1	0.0	0.0	0.0	1	0	\$T2	BEAM	ELEM
403	455	405	210	1	0.0	0.0	0.0	1	0	\$T2	BEAM	ELEM
401	453	403	210	1	0.0	0.0	0.0	1	0	\$T2	BEAM	ELEM
399	451	401	210	1	0.0	0.0	0.0	1	0	\$T2	BEAM	ELEM
397	449	399	210	1	0.0	0.0	0.0	1	0	\$T2	BEAM	ELEM
395	447	397	210	1	0.0	0.0	0.0	1	0	\$T2	BEAM	ELEM
393	445	395	210	1	0.0	0.0	0.0	1	0	\$T2	BEAM	ELEM
391	443	393	210	1	0.0	0.0	0.0	1	0	\$T2	BEAM	ELEM
389	441	391	210	1	0.0	0.0	0.0	1	0	\$T2	BEAM	ELEM
387	439	389	210	1	0.0	0.0	0.0	1	0	\$T2	BEAM	ELEM
385	437	387	210	1	0.0	0.0	0.0	1	0	\$T2	BEAM	ELEM
383	435	385	210	1	0.0	0.0	0.0	1	0	\$T2	BEAM	ELEM
381	433	383	210	1	0.0	0.0	0.0	1	0	\$T2	BEAM	ELEM
379	431	381	210	1	0.0	0.0	0.0	1	0	\$T2	BEAM	ELEM
377	429	379	210	1	0.0	0.0	0.0	1	0	\$T2	BEAM	ELEM
375	427	377	210	1	0.0	0.0	0.0	1	0	\$T2	BEAM	ELEM
373	425	375	210	1	0.0	0.0	0.0	1	0	\$T2	BEAM	ELEM
371	423	373	210	1	0.0	0.0	0.0	1	0	\$T2	BEAM	ELEM
369	421	371	210	1	0.0	0.0	0.0	1	0	\$T2	BEAM	ELEM
367	419	369	210	1	0.0	0.0	0.0	1	0	\$T2	BEAM	ELEM
365	417	367	210	1	0.0	0.0	0.0	1	0	\$T2	BEAM	ELEM
1	3	2	320	26	\$T3	TRI	ELEM					
1	4	3	320	26	\$T3	TRI	ELEM					
1	2	5	320	26	\$T3	TRI	ELEM					
1	5	6	320	26	\$T3	TRI	ELEM					
2	8	7	320	15	\$T3	TRI	ELEM					
2	9	8	320	15	\$T3	TRI	ELEM					
2	3	9	320	15	\$T3	TRI	ELEM					
3	10	9	320	15	\$T3	TRI	ELEM					
2	7	12	320	15	\$T3	TRI	ELEM					
2	12	13	320	15	\$T3	TRI	ELEM					
2	13	5	320	15	\$T3	TRI	ELEM					
5	13	14	320	15	\$T3	TRI	ELEM					
7	17	16	320	15	\$T3	TRI	ELEM					
9	20	19	320	15	\$T3	TRI	ELEM					
10	20	9	320	15	\$T3	TRI	ELEM					
10	21	20	320	15	\$T3	TRI	ELEM					
7	16	23	320	15	\$T3	TRI	ELEM					

13	25	26	320	15	\$T3	TRI	ELEM
14	13	26	320	15	\$T3	TRI	ELEM
14	26	27	320	15	\$T3	TRI	ELEM
16	30	29	320	15	\$T3	TRI	ELEM
20	21	34	320	15	\$T3	TRI	ELEM
21	35	34	320	15	\$T3	TRI	ELEM
16	29	37	320	15	\$T3	TRI	ELEM
26	41	27	320	15	\$T3	TRI	ELEM
27	41	42	320	15	\$T3	TRI	ELEM
34	50	49	320	15	\$T3	TRI	ELEM
34	35	50	320	15	\$T3	TRI	ELEM
35	51	50	320	15	\$T3	TRI	ELEM
41	57	58	320	15	\$T3	TRI	ELEM
41	58	42	320	15	\$T3	TRI	ELEM
42	58	59	320	15	\$T3	TRI	ELEM
271	272	288	320	15	\$T3	TRI	ELEM
279	295	280	320	15	\$T3	TRI	ELEM
314	328	313	320	15	\$T3	TRI	ELEM
321	320	334	320	15	\$T3	TRI	ELEM
328	340	327	320	15	\$T3	TRI	ELEM
331	332	343	320	15	\$T3	TRI	ELEM
334	327	340	320	15	\$T3	TRI	ELEM
337	347	338	320	15	\$T3	TRI	ELEM
342	350	341	320	15	\$T3	TRI	ELEM
346	345	353	320	15	\$T3	TRI	ELEM
350	356	349	320	15	\$T3	TRI	ELEM
358	356	350	320	15	\$T3	TRI	ELEM
358	350	351	320	15	\$T3	TRI	ELEM
353	349	356	320	15	\$T3	TRI	ELEM
360	353	356	320	15	\$T3	TRI	ELEM
360	354	353	320	15	\$T3	TRI	ELEM
358	357	356	320	15	\$T3	TRI	ELEM
360	356	357	320	15	\$T3	TRI	ELEM
357	358	362	320	26	\$T3	TRI	ELEM
358	359	362	320	26	\$T3	TRI	ELEM
357	362	360	320	26	\$T3	TRI	ELEM
360	362	361	320	26	\$T3	TRI	ELEM
4	11	10	3	410	26	\$T4	QUAD ELEM
6	5	14	15	410	26	\$T4	QUAD ELEM
7	8	18	17	410	15	\$T4	QUAD ELEM
8	9	19	18	410	15	\$T4	QUAD ELEM
10	11	22	21	410	26	\$T4	QUAD ELEM
7	23	24	12	410	15	\$T4	QUAD ELEM
12	24	25	13	410	15	\$T4	QUAD ELEM
14	27	28	15	410	26	\$T4	QUAD ELEM
16	17	31	30	410	15	\$T4	QUAD ELEM
17	18	32	31	410	15	\$T4	QUAD ELEM
18	19	33	32	410	15	\$T4	QUAD ELEM
19	20	34	33	410	15	\$T4	QUAD ELEM
21	22	36	35	410	26	\$T4	QUAD ELEM
16	37	38	23	410	15	\$T4	QUAD ELEM
23	38	39	24	410	15	\$T4	QUAD ELEM
24	39	40	25	410	15	\$T4	QUAD ELEM
25	40	41	26	410	15	\$T4	QUAD ELEM

27	42	43	28	410	26	\$T4	QUAD	ELEM
29	30	45	44	410	15	\$T4	QUAD	ELEM
30	31	46	45	410	15	\$T4	QUAD	ELEM
31	32	47	46	410	15	\$T4	QUAD	ELEM
32	33	48	47	410	15	\$T4	QUAD	ELEM
33	34	49	48	410	15	\$T4	QUAD	ELEM
35	36	52	51	410	26	\$T4	QUAD	ELEM
29	44	53	37	410	15	\$T4	QUAD	ELEM
37	53	54	38	410	15	\$T4	QUAD	ELEM
38	54	55	39	410	15	\$T4	QUAD	ELEM
39	55	56	40	410	15	\$T4	QUAD	ELEM
40	56	57	41	410	15	\$T4	QUAD	ELEM
42	59	60	43	410	26	\$T4	QUAD	ELEM
44	45	62	61	410	15	\$T4	QUAD	ELEM
45	46	63	62	410	15	\$T4	QUAD	ELEM
46	47	64	63	410	15	\$T4	QUAD	ELEM
47	48	65	64	410	15	\$T4	QUAD	ELEM
48	49	66	65	410	15	\$T4	QUAD	ELEM
49	50	67	66	410	15	\$T4	QUAD	ELEM
50	51	68	67	410	15	\$T4	QUAD	ELEM
51	52	69	68	410	26	\$T4	QUAD	ELEM
44	61	70	53	410	15	\$T4	QUAD	ELEM
53	70	71	54	410	15	\$T4	QUAD	ELEM
54	71	72	55	410	15	\$T4	QUAD	ELEM
55	72	73	56	410	15	\$T4	QUAD	ELEM
56	73	74	57	410	15	\$T4	QUAD	ELEM
57	74	75	58	410	15	\$T4	QUAD	ELEM
58	75	76	59	410	15	\$T4	QUAD	ELEM
59	76	77	60	410	26	\$T4	QUAD	ELEM
61	62	79	78	410	15	\$T4	QUAD	ELEM
62	63	80	79	410	15	\$T4	QUAD	ELEM
63	64	81	80	410	15	\$T4	QUAD	ELEM
64	65	82	81	410	15	\$T4	QUAD	ELEM
65	66	83	82	410	15	\$T4	QUAD	ELEM
66	67	84	83	410	15	\$T4	QUAD	ELEM
67	68	85	84	410	15	\$T4	QUAD	ELEM
68	69	86	85	410	25	\$T4	QUAD	ELEM
61	78	87	70	410	15	\$T4	QUAD	ELEM
70	87	88	71	410	15	\$T4	QUAD	ELEM
71	88	89	72	410	15	\$T4	QUAD	ELEM
72	89	90	73	410	15	\$T4	QUAD	ELEM
73	90	91	74	410	15	\$T4	QUAD	ELEM
74	91	92	75	410	15	\$T4	QUAD	ELEM
75	92	93	76	410	15	\$T4	QUAD	ELEM
76	93	94	77	410	25	\$T4	QUAD	ELEM
78	79	96	95	410	12	\$T4	QUAD	ELEM
79	80	97	96	410	12	\$T4	QUAD	ELEM
80	81	98	97	410	12	\$T4	QUAD	ELEM
81	82	99	98	410	13	\$T4	QUAD	ELEM
82	83	100	99	410	14	\$T4	QUAD	ELEM
83	84	101	100	410	15	\$T4	QUAD	ELEM
84	85	102	101	410	15	\$T4	QUAD	ELEM
85	86	103	102	410	23	\$T4	QUAD	ELEM
78	95	104	87	410	12	\$T4	QUAD	ELEM

87	104	105	88	410	12	\$T4	QUAD	ELEM
88	105	106	89	410	12	\$T4	QUAD	ELEM
89	106	107	90	410	13	\$T4	QUAD	ELEM
90	107	108	91	410	14	\$T4	QUAD	ELEM
91	108	109	92	410	15	\$T4	QUAD	ELEM
92	109	110	93	410	15	\$T4	QUAD	ELEM
93	110	111	94	410	23	\$T4	QUAD	ELEM
95	96	113	112	410	10	\$T4	QUAD	ELEM
96	97	114	113	410	10	\$T4	QUAD	ELEM
97	98	115	114	410	10	\$T4	QUAD	ELEM
98	99	116	115	410	10	\$T4	QUAD	ELEM
99	100	117	116	410	11	\$T4	QUAD	ELEM
100	101	118	117	410	12	\$T4	QUAD	ELEM
101	102	119	118	410	12	\$T4	QUAD	ELEM
102	103	120	119	410	19	\$T4	QUAD	ELEM
95	112	121	104	410	10	\$T4	QUAD	ELEM
104	121	122	105	410	10	\$T4	QUAD	ELEM
105	122	123	106	410	10	\$T4	QUAD	ELEM
106	123	124	107	410	10	\$T4	QUAD	ELEM
107	124	125	108	410	11	\$T4	QUAD	ELEM
108	125	126	109	410	12	\$T4	QUAD	ELEM
109	126	127	110	410	12	\$T4	QUAD	ELEM
110	127	128	111	410	19	\$T4	QUAD	ELEM
112	113	130	129	410	5	\$T4	QUAD	ELEM
113	114	131	130	410	5	\$T4	QUAD	ELEM
114	115	132	131	410	5	\$T4	QUAD	ELEM
115	116	133	132	410	6	\$T4	QUAD	ELEM
116	117	134	133	410	7	\$T4	QUAD	ELEM
117	118	135	134	410	8	\$T4	QUAD	ELEM
118	119	136	135	410	10	\$T4	QUAD	ELEM
119	120	137	136	410	18	\$T4	QUAD	ELEM
129	130	147	146	410	1	\$T4	QUAD	ELEM
130	131	148	147	410	1	\$T4	QUAD	ELEM
131	132	149	148	410	1	\$T4	QUAD	ELEM
132	133	150	149	410	1	\$T4	QUAD	ELEM
133	134	151	150	410	1	\$T4	QUAD	ELEM
134	135	152	151	410	4	\$T4	QUAD	ELEM
135	136	153	152	410	7	\$T4	QUAD	ELEM
136	137	154	153	410	21	\$T4	QUAD	ELEM
112	129	138	121	410	5	\$T4	QUAD	ELEM
121	138	139	122	410	5	\$T4	QUAD	ELEM
122	139	140	123	410	5	\$T4	QUAD	ELEM
123	140	141	124	410	6	\$T4	QUAD	ELEM
124	141	142	125	410	7	\$T4	QUAD	ELEM
125	142	143	126	410	8	\$T4	QUAD	ELEM
126	143	144	127	410	10	\$T4	QUAD	ELEM
127	144	145	128	410	18	\$T4	QUAD	ELEM
129	146	155	138	410	1	\$T4	QUAD	ELEM
138	155	156	139	410	1	\$T4	QUAD	ELEM
139	156	157	140	410	1	\$T4	QUAD	ELEM
140	157	158	141	410	1	\$T4	QUAD	ELEM
141	158	159	142	410	1	\$T4	QUAD	ELEM
142	159	160	143	410	4	\$T4	QUAD	ELEM
143	160	161	144	410	7	\$T4	QUAD	ELEM

144	161	162	145	410	21	\$T4	QUAD	ELEM
146	147	164	163	410	1	\$T4	QUAD	ELEM
147	148	165	164	410	1	\$T4	QUAD	ELEM
148	149	166	165	410	1	\$T4	QUAD	ELEM
149	150	167	166	410	1	\$T4	QUAD	ELEM
150	151	168	167	410	1	\$T4	QUAD	ELEM
151	152	169	168	410	1	\$T4	QUAD	ELEM
152	153	170	169	410	3	\$T4	QUAD	ELEM
153	154	171	170	410	17	\$T4	QUAD	ELEM
146	163	172	155	410	1	\$T4	QUAD	ELEM
155	172	173	156	410	1	\$T4	QUAD	ELEM
156	173	174	157	410	1	\$T4	QUAD	ELEM
157	174	175	158	410	1	\$T4	QUAD	ELEM
158	175	176	159	410	1	\$T4	QUAD	ELEM
159	176	177	160	410	1	\$T4	QUAD	ELEM
160	177	178	161	410	3	\$T4	QUAD	ELEM
161	178	179	162	410	17	\$T4	QUAD	ELEM
163	164	181	180	410	1	\$T4	QUAD	ELEM
164	165	182	181	410	1	\$T4	QUAD	ELEM
165	166	183	182	410	1	\$T4	QUAD	ELEM
166	167	184	183	410	1	\$T4	QUAD	ELEM
167	168	185	184	410	1	\$T4	QUAD	ELEM
168	169	186	185	410	1	\$T4	QUAD	ELEM
169	170	187	186	410	3	\$T4	QUAD	ELEM
170	171	188	187	410	17	\$T4	QUAD	ELEM
180	181	198	197	410	1	\$T4	QUAD	ELEM
181	182	199	198	410	1	\$T4	QUAD	ELEM
182	183	200	199	410	1	\$T4	QUAD	ELEM
183	184	201	200	410	1	\$T4	QUAD	ELEM
184	185	202	201	410	1	\$T4	QUAD	ELEM
185	186	203	202	410	2	\$T4	QUAD	ELEM
186	187	204	203	410	7	\$T4	QUAD	ELEM
187	188	205	204	410	17	\$T4	QUAD	ELEM
163	180	189	172	410	1	\$T4	QUAD	ELEM
172	189	190	173	410	1	\$T4	QUAD	ELEM
173	190	191	174	410	1	\$T4	QUAD	ELEM
174	191	192	175	410	1	\$T4	QUAD	ELEM
175	192	193	176	410	1	\$T4	QUAD	ELEM
176	193	194	177	410	1	\$T4	QUAD	ELEM
177	194	195	178	410	3	\$T4	QUAD	ELEM
178	195	196	179	410	17	\$T4	QUAD	ELEM
180	197	206	189	410	1	\$T4	QUAD	ELEM
189	206	207	190	410	1	\$T4	QUAD	ELEM
190	207	208	191	410	1	\$T4	QUAD	ELEM
191	208	209	192	410	1	\$T4	QUAD	ELEM
192	209	210	193	410	1	\$T4	QUAD	ELEM
193	210	211	194	410	2	\$T4	QUAD	ELEM
194	211	212	195	410	7	\$T4	QUAD	ELEM
195	212	213	196	410	17	\$T4	QUAD	ELEM
197	198	215	214	410	6	\$T4	QUAD	ELEM
198	199	216	215	410	5	\$T4	QUAD	ELEM
199	200	217	216	410	6	\$T4	QUAD	ELEM
200	201	218	217	410	6	\$T4	QUAD	ELEM
201	202	219	218	410	7	\$T4	QUAD	ELEM

202	203	220	219	410	9	\$T4	QUAD	ELEM
203	204	221	220	410	10	\$T4	QUAD	ELEM
204	205	222	221	410	16	\$T4	QUAD	ELEM
214	215	232	231	410	10	\$T4	QUAD	ELEM
215	216	233	232	410	11	\$T4	QUAD	ELEM
216	217	234	233	410	11	\$T4	QUAD	ELEM
217	218	235	234	410	11	\$T4	QUAD	ELEM
218	219	236	235	410	11	\$T4	QUAD	ELEM
219	220	237	236	410	11	\$T4	QUAD	ELEM
220	221	238	237	410	12	\$T4	QUAD	ELEM
221	222	239	238	410	20	\$T4	QUAD	ELEM
197	214	223	206	410	6	\$T4	QUAD	ELEM
206	223	224	207	410	5	\$T4	QUAD	ELEM
207	224	225	208	410	6	\$T4	QUAD	ELEM
208	225	226	209	410	6	\$T4	QUAD	ELEM
209	226	227	210	410	7	\$T4	QUAD	ELEM
210	227	228	211	410	9	\$T4	QUAD	ELEM
211	228	229	212	410	10	\$T4	QUAD	ELEM
212	229	230	213	410	16	\$T4	QUAD	ELEM
214	231	240	223	410	10	\$T4	QUAD	ELEM
223	240	241	224	410	11	\$T4	QUAD	ELEM
224	241	242	225	410	11	\$T4	QUAD	ELEM
225	242	243	226	410	11	\$T4	QUAD	ELEM
226	243	244	227	410	11	\$T4	QUAD	ELEM
227	244	245	228	410	11	\$T4	QUAD	ELEM
228	245	246	229	410	12	\$T4	QUAD	ELEM
229	246	247	230	410	20	\$T4	QUAD	ELEM
231	232	249	248	410	12	\$T4	QUAD	ELEM
232	233	250	249	410	12	\$T4	QUAD	ELEM
233	234	251	250	410	12	\$T4	QUAD	ELEM
234	235	252	251	410	13	\$T4	QUAD	ELEM
235	236	253	252	410	14	\$T4	QUAD	ELEM
236	237	254	253	410	15	\$T4	QUAD	ELEM
237	238	255	254	410	15	\$T4	QUAD	ELEM
238	239	256	255	410	22	\$T4	QUAD	ELEM
231	248	257	240	410	12	\$T4	QUAD	ELEM
240	257	258	241	410	12	\$T4	QUAD	ELEM
241	258	259	242	410	12	\$T4	QUAD	ELEM
242	259	260	243	410	13	\$T4	QUAD	ELEM
243	260	261	244	410	14	\$T4	QUAD	ELEM
244	261	262	245	410	15	\$T4	QUAD	ELEM
245	262	263	246	410	15	\$T4	QUAD	ELEM
246	263	264	247	410	22	\$T4	QUAD	ELEM
248	249	266	265	410	15	\$T4	QUAD	ELEM
249	250	267	266	410	15	\$T4	QUAD	ELEM
250	251	268	267	410	15	\$T4	QUAD	ELEM
251	252	269	268	410	15	\$T4	QUAD	ELEM
252	253	270	269	410	15	\$T4	QUAD	ELEM
253	254	271	270	410	15	\$T4	QUAD	ELEM
254	255	272	271	410	15	\$T4	QUAD	ELEM
255	256	273	272	410	24	\$T4	QUAD	ELEM
248	265	274	257	410	15	\$T4	QUAD	ELEM
257	274	275	258	410	15	\$T4	QUAD	ELEM
258	275	276	259	410	15	\$T4	QUAD	ELEM

259	276	277	260	410	15	\$T4	QUAD	ELEM
260	277	278	261	410	15	\$T4	QUAD	ELEM
261	278	279	262	410	15	\$T4	QUAD	ELEM
262	279	280	263	410	15	\$T4	QUAD	ELEM
263	280	281	264	410	24	\$T4	QUAD	ELEM
265	266	283	282	410	15	\$T4	QUAD	ELEM
266	267	284	283	410	15	\$T4	QUAD	ELEM
267	268	285	284	410	15	\$T4	QUAD	ELEM
268	269	286	285	410	15	\$T4	QUAD	ELEM
269	270	287	286	410	15	\$T4	QUAD	ELEM
270	271	288	287	410	15	\$T4	QUAD	ELEM
272	273	289	288	410	26	\$T4	QUAD	ELEM
265	282	290	274	410	15	\$T4	QUAD	ELEM
274	290	291	275	410	15	\$T4	QUAD	ELEM
275	291	292	276	410	15	\$T4	QUAD	ELEM
276	292	293	277	410	15	\$T4	QUAD	ELEM
277	293	294	278	410	15	\$T4	QUAD	ELEM
278	294	295	279	410	15	\$T4	QUAD	ELEM
280	295	296	281	410	26	\$T4	QUAD	ELEM
282	283	298	297	410	15	\$T4	QUAD	ELEM
283	284	299	298	410	15	\$T4	QUAD	ELEM
284	285	300	299	410	15	\$T4	QUAD	ELEM
285	286	301	300	410	15	\$T4	QUAD	ELEM
286	287	302	301	410	15	\$T4	QUAD	ELEM
287	288	303	302	410	15	\$T4	QUAD	ELEM
288	289	304	303	410	26	\$T4	QUAD	ELEM
282	297	305	290	410	15	\$T4	QUAD	ELEM
290	305	306	291	410	15	\$T4	QUAD	ELEM
291	306	307	292	410	15	\$T4	QUAD	ELEM
292	307	308	293	410	15	\$T4	QUAD	ELEM
293	308	309	294	410	15	\$T4	QUAD	ELEM
294	309	310	295	410	15	\$T4	QUAD	ELEM
295	310	311	296	410	26	\$T4	QUAD	ELEM
297	298	313	312	410	15	\$T4	QUAD	ELEM
298	299	314	313	410	15	\$T4	QUAD	ELEM
299	300	315	314	410	15	\$T4	QUAD	ELEM
300	301	316	315	410	15	\$T4	QUAD	ELEM
301	302	317	316	410	15	\$T4	QUAD	ELEM
303	318	317	302	410	15	\$T4	QUAD	ELEM
303	304	319	318	410	26	\$T4	QUAD	ELEM
297	312	320	305	410	15	\$T4	QUAD	ELEM
305	320	321	306	410	15	\$T4	QUAD	ELEM
306	321	322	307	410	15	\$T4	QUAD	ELEM
307	322	323	308	410	15	\$T4	QUAD	ELEM
308	323	324	309	410	15	\$T4	QUAD	ELEM
310	309	324	325	410	15	\$T4	QUAD	ELEM
310	325	326	311	410	26	\$T4	QUAD	ELEM
312	313	328	327	410	15	\$T4	QUAD	ELEM
315	329	328	314	410	15	\$T4	QUAD	ELEM
316	330	329	315	410	15	\$T4	QUAD	ELEM
317	331	330	316	410	15	\$T4	QUAD	ELEM
318	332	331	317	410	15	\$T4	QUAD	ELEM
319	333	332	318	410	26	\$T4	QUAD	ELEM
312	327	334	320	410	15	\$T4	QUAD	ELEM

322	321	334	335	410	15	\$T4	QUAD	ELEM
323	322	335	336	410	15	\$T4	QUAD	ELEM
324	323	336	337	410	15	\$T4	QUAD	ELEM
325	324	337	338	410	15	\$T4	QUAD	ELEM
326	325	338	339	410	26	\$T4	QUAD	ELEM
328	329	341	340	410	15	\$T4	QUAD	ELEM
329	330	342	341	410	15	\$T4	QUAD	ELEM
331	343	342	330	410	15	\$T4	QUAD	ELEM
333	344	343	332	410	26	\$T4	QUAD	ELEM
334	340	345	335	410	15	\$T4	QUAD	ELEM
335	345	346	336	410	15	\$T4	QUAD	ELEM
337	336	346	347	410	15	\$T4	QUAD	ELEM
339	338	347	348	410	26	\$T4	QUAD	ELEM
340	341	350	349	410	15	\$T4	QUAD	ELEM
343	351	350	342	410	15	\$T4	QUAD	ELEM
344	352	351	343	410	26	\$T4	QUAD	ELEM
340	349	353	345	410	15	\$T4	QUAD	ELEM
347	346	353	354	410	15	\$T4	QUAD	ELEM
348	347	354	355	410	26	\$T4	QUAD	ELEM
352	359	358	351	410	26	\$T4	QUAD	ELEM
355	354	360	361	410	26	\$T4	QUAD	ELEM
4	1	363	364	410	27	\$T4	QUAD	ELEM
1	6	365	363	410	27	\$T4	QUAD	ELEM
11	4	364	366	410	27	\$T4	QUAD	ELEM
6	15	367	365	410	27	\$T4	QUAD	ELEM
22	11	366	368	410	27	\$T4	QUAD	ELEM
15	28	369	367	410	27	\$T4	QUAD	ELEM
36	22	368	370	410	27	\$T4	QUAD	ELEM
28	43	371	369	410	27	\$T4	QUAD	ELEM
52	36	370	372	410	27	\$T4	QUAD	ELEM
43	60	373	371	410	27	\$T4	QUAD	ELEM
69	52	372	374	410	27	\$T4	QUAD	ELEM
60	77	375	373	410	27	\$T4	QUAD	ELEM
86	69	374	376	410	27	\$T4	QUAD	ELEM
77	94	377	375	410	27	\$T4	QUAD	ELEM
103	86	376	378	410	27	\$T4	QUAD	ELEM
94	111	379	377	410	27	\$T4	QUAD	ELEM
120	103	378	380	410	27	\$T4	QUAD	ELEM
111	128	381	379	410	27	\$T4	QUAD	ELEM
137	120	380	382	410	27	\$T4	QUAD	ELEM
128	145	383	381	410	27	\$T4	QUAD	ELEM
154	137	382	384	410	27	\$T4	QUAD	ELEM
145	162	385	383	410	27	\$T4	QUAD	ELEM
171	154	384	386	410	27	\$T4	QUAD	ELEM
162	179	387	385	410	27	\$T4	QUAD	ELEM
188	171	386	388	410	27	\$T4	QUAD	ELEM
179	196	389	387	410	27	\$T4	QUAD	ELEM
205	188	388	390	410	27	\$T4	QUAD	ELEM
196	213	391	389	410	27	\$T4	QUAD	ELEM
222	205	390	392	410	27	\$T4	QUAD	ELEM
213	230	393	391	410	27	\$T4	QUAD	ELEM
239	222	392	394	410	27	\$T4	QUAD	ELEM
230	247	395	393	410	27	\$T4	QUAD	ELEM
256	239	394	396	410	27	\$T4	QUAD	ELEM



247	264	397	395	410	27	\$T4	QUAD	ELEM
273	256	396	398	410	27	\$T4	QUAD	ELEM
264	281	399	397	410	27	\$T4	QUAD	ELEM
289	273	398	400	410	27	\$T4	QUAD	ELEM
281	296	401	399	410	27	\$T4	QUAD	ELEM
304	289	400	402	410	27	\$T4	QUAD	ELEM
296	311	403	401	410	27	\$T4	QUAD	ELEM
319	304	402	404	410	27	\$T4	QUAD	ELEM
311	326	405	403	410	27	\$T4	QUAD	ELEM
333	319	404	406	410	27	\$T4	QUAD	ELEM
326	339	407	405	410	27	\$T4	QUAD	ELEM
344	333	406	408	410	27	\$T4	QUAD	ELEM
339	348	409	407	410	27	\$T4	QUAD	ELEM
352	344	408	410	410	27	\$T4	QUAD	ELEM
348	355	411	409	410	27	\$T4	QUAD	ELEM
359	352	410	412	410	27	\$T4	QUAD	ELEM
355	361	413	411	410	27	\$T4	QUAD	ELEM
362	359	412	414	410	27	\$T4	QUAD	ELEM
361	362	414	413	410	27	\$T4	QUAD	ELEM
1	0	0				\$U1	LOAD	RECORD SUMMARY
1	0	2				\$U2	LOAD	SET RECORD
0	0	0	0	0	0	\$V1	OUTPUT	CONTROL

## Appendix H: UPRESS Subroutine for Finite Element

### Models 6 and 7

The following subroutine was used for applying the pressure loading in the Model 6 and 7 finite element runs. The subroutine is written using guidelines in the STAGS users manual [16]. The subroutine is then compiled and linked to the main program before execution.

```
SUBROUTINE UPRESS(T,PA,PB,IUNIT,IELT,X,Y,Z,LIVE,PRESS)
c
c   Pressure distribution subroutine for the modified
c   boundary conditions. Uses element number to determine
c   element pressure loading. Modified from Models 1-5
c   because of the addition of the 52 rubber beam elements
c   (not loaded) in models 6 and 7. The 52 beams are
c   elements 1 through 52. The next 362 elements correspond
c   to the original finite element model. All elements
c   after this are plate elements used to model the aluminum
c   plate in the modified boundary conditions.
c   Needs input file 'loads.dat' which contains the twenty
c   loads written one on each line.
c
  INTEGER I,NIELT
  REAL C(20),PA
  OPEN (UNIT=1,FILE='LOADS.DAT',STATUS='OLD')
  LIVE=1
    DO 20 I=1,20
      READ(1,30) C(I)
20    CONTINUE
30    FORMAT(F15.7)
  REWIND (UNIT=1)
  IF ((IELT.LE.52).OR.(IELT.GE.415)) THEN
    PRESS=0.0
  C
    ELSE
      NIELT=IELT-52
      IF ((NIELT.LE. 2)
+ .OR.(NIELT.GE. 5.AND.NIELT.LE. 8)
+ .OR.(NIELT.EQ. 55)
+ .OR.(NIELT.EQ. 13)
+ .OR.(NIELT.GE. 57.AND.NIELT.LE. 59)
+ .OR.(NIELT.GE. 14.AND.NIELT.LE. 16)
+ .OR.(NIELT.EQ. 21)
+ .OR.(NIELT.GE. 63.AND.NIELT.LE. 67)
```

```

+.OR.(NIELT.GE. 22.AND.NIELT.LE. 23)
+.OR.(NIELT.GE. 73.AND.NIELT.LE. 78)
+.OR.(NIELT.GE. 27.AND.NIELT.LE. 29)
+.OR.(NIELT.GE. 85.AND.NIELT.LE. 92)) PRESS-C(1)*PA
C
  IF ((NIELT.GE.101.AND.NIELT.LE.104)
+.OR.(NIELT.GE.117.AND.NIELT.LE.120)
+.OR.(NIELT.GE.133.AND.NIELT.LE.136)) PRESS-C(2)*PA
C
  IF ((NIELT.GE.105.AND.NIELT.LE.108)
+.OR.(NIELT.GE.121.AND.NIELT.LE.124)
+.OR.(NIELT.GE.137.AND.NIELT.LE.140)) PRESS-C(3)*PA
C
  IF ((NIELT.GE.149.AND.NIELT.LE.152)
+.OR.(NIELT.GE.157.AND.NIELT.LE.160)
+.OR.(NIELT.GE.181.AND.NIELT.LE.184)
+.OR.(NIELT.GE.197.AND.NIELT.LE.200)
+.OR.(NIELT.GE.205.AND.NIELT.LE.208)) PRESS-C(4)*PA
C
  IF ((NIELT.GE.153.AND.NIELT.LE.156)
+.OR.(NIELT.GE.161.AND.NIELT.LE.164)
+.OR.(NIELT.GE.185.AND.NIELT.LE.188)
+.OR.(NIELT.GE.201.AND.NIELT.LE.204)
+.OR.(NIELT.GE.209.AND.NIELT.LE.212)) PRESS-C(5)*PA
C
  IF ((NIELT.GE.229.AND.NIELT.LE.232)
+.OR.(NIELT.GE.237.AND.NIELT.LE.240)
+.OR.(NIELT.GE.261.AND.NIELT.LE.264)) PRESS-C(6)*PA
C
  IF ((NIELT.GE.233.AND.NIELT.LE.236)
+.OR.(NIELT.GE.241.AND.NIELT.LE.244)
+.OR.(NIELT.GE.265.AND.NIELT.LE.268)) PRESS-C(7)*PA
C
  IF ((NIELT.GE.277.AND.NIELT.LE.281)
+.OR.(NIELT.GE.293.AND.NIELT.LE.297)
+.OR.(NIELT.GE.307.AND.NIELT.LE.310)) PRESS-C(8)*PA
C
  IF ((NIELT.GE.282.AND.NIELT.LE.284)
+.OR.(NIELT.GE.298.AND.NIELT.LE.299)
+.OR.(NIELT.EQ. 33)
+.OR.(NIELT.GE.311.AND.NIELT.LE.313)) PRESS-C(9)*PA
C
  IF ((NIELT.GE.321.AND.NIELT.LE.327)
+.OR.(NIELT.GE.335.AND.NIELT.LE.337)
+.OR.(NIELT.EQ. 35)
+.OR.(NIELT.GE.347.AND.NIELT.LE.350)
+.OR.(NIELT.GE. 37.AND.NIELT.LE. 38)
+.OR.(NIELT.GE.355.AND.NIELT.LE.357)
+.OR.(NIELT.EQ. 41)
+.OR.(NIELT.GE. 43.AND.NIELT.LE. 45)
+.OR.(NIELT.EQ.361)
+.OR.(NIELT.EQ. 49)
+.OR.(NIELT.GE. 51.AND.NIELT.LE. 52)) PRESS-C(10)*PA
C

```

```

IF ((NIELT.GE. 3.AND.NIELT.LE. 4)
+.OR.(NIELT.GE. 9.AND.NIELT.LE. 12)
+.OR.(NIELT.EQ. 56)
+.OR.(NIELT.EQ. 17)
+.OR.(NIELT.GE. 60.AND.NIELT.LE. 62)
+.OR.(NIELT.GE. 18.AND.NIELT.LE. 20)
+.OR.(NIELT.EQ. 24)
+.OR.(NIELT.GE. 68.AND.NIELT.LE. 72)
+.OR.(NIELT.GE. 25.AND.NIELT.LE. 26)
+.OR.(NIELT.GE. 79.AND.NIELT.LE. 84)
+.OR.(NIELT.GE. 30.AND.NIELT.LE. 32)
+.OR.(NIELT.GE. 93.AND.NIELT.LE.100)) PRESS=C(11)*PA

```

C

```

IF ((NIELT.GE.109.AND.NIELT.LE.112)
+.OR.(NIELT.GE.125.AND.NIELT.LE.128)
+.OR.(NIELT.GE.141.AND.NIELT.LE.144)) PRESS=C(12)*PA

```

C

```

IF ((NIELT.GE.113.AND.NIELT.LE.116)
+.OR.(NIELT.GE.129.AND.NIELT.LE.132)
+.OR.(NIELT.GE.145.AND.NIELT.LE.148)) PRESS=C(13)*PA

```

C

```

IF ((NIELT.GE.165.AND.NIELT.LE.168)
+.OR.(NIELT.GE.173.AND.NIELT.LE.176)
+.OR.(NIELT.GE.189.AND.NIELT.LE.192)
+.OR.(NIELT.GE.213.AND.NIELT.LE.216)
+.OR.(NIELT.GE.221.AND.NIELT.LE.224)) PRESS=C(14)*PA

```

C

```

IF ((NIELT.GE.169.AND.NIELT.LE.172)
+.OR.(NIELT.GE.177.AND.NIELT.LE.180)
+.OR.(NIELT.GE.193.AND.NIELT.LE.196)
+.OR.(NIELT.GE.217.AND.NIELT.LE.220)
+.OR.(NIELT.GE.225.AND.NIELT.LE.228)) PRESS=C(15)*PA

```

C

```

IF ((NIELT.GE.245.AND.NIELT.LE.248)
+.OR.(NIELT.GE.253.AND.NIELT.LE.256)
+.OR.(NIELT.GE.269.AND.NIELT.LE.272)) PRESS=C(16)*PA

```

C

```

IF ((NIELT.GE.249.AND.NIELT.LE.252)
+.OR.(NIELT.GE.257.AND.NIELT.LE.260)
+.OR.(NIELT.GE.274.AND.NIELT.LE.276)) PRESS=C(17)*PA

```

C

```

IF ((NIELT.GE.285.AND.NIELT.LE.289)
+.OR.(NIELT.GE.300.AND.NIELT.LE.304)
+.OR.(NIELT.GE.314.AND.NIELT.LE.317)) PRESS=C(18)*PA

```

C

```

IF ((NIELT.GE.290.AND.NIELT.LE.292)
+.OR.(NIELT.GE.305.AND.NIELT.LE.306)
+.OR.(NIELT.EQ. 34)
+.OR.(NIELT.GE.318.AND.NIELT.LE.320)) PRESS=C(19)*PA

```

C

```

IF ((NIELT.GE.328.AND.NIELT.LE.334)
+.OR.(NIELT.GE.341.AND.NIELT.LE.346)
+.OR.(NIELT.EQ. 36)
+.OR.(NIELT.GE.351.AND.NIELT.LE.354)

```

```
+ .OR. (NIELT. GE. 39. AND. NIELT. LE. 40)
+ .OR. (NIELT. GE. 358. AND. NIELT. LE. 360)
+ .OR. (NIELT. EQ. 42)
+ .OR. (NIELT. GE. 46. AND. NIELT. LE. 48)
+ .OR. (NIELT. EQ. 362)
+ .OR. (NIELT. EQ. 50)
+ .OR. (NIELT. GE. 53. AND. NIELT. LE. 54)) PRESS=C(20)*PA
```

C

```
ENDIF
RETURN
END
```

### Bibliography

1. Ugural, A. C. Stresses in Plates and Shells. Mc-Graw Hill Book Co., 1981.
2. Saada, A.S. Elasticity Theory and Applications. Pergamon Press, 1974.
3. Sanders, J.L. "Nonlinear Theories for Thin Shells," Qtr. of Applied Math, Vol XXI, No. 1, 1962.
4. Bauld, N.R., Jr. and K. Satyamurthy. Collapse Load Analysis for Plates and Panels. AFFDL-TR-79-3038. Air Force Flight Dynamics Laboratory, Wright-Patterson AFB OH, May 1979.
5. Dennis, Scott T. Large Displacement and Rotational Formulation for Laminated Cylindrical Shells Including Parabolic Transverse Shear. PhD dissertation. School of Engineering, Air Force Institute of Technology (AU), Wright-Patterson AFB, OH, May 1988.
6. Cook, R.D. Concepts and Applications of Finite Element Analysis (Second Edition). John Wiley and Sons, 1981.
7. Users's Manual for STAGS, Volume 1 Theory. Structural Mechanics Laboratory, Lockheed Palo Alto Research Laboratory, Palo Alto CA, 1981.
8. Zienkiewicz, O.C. The Finite Element Method (The third, expanded and revised edition of The Finite Element Method in Engineering Science). Mc Graw-Hill Book Company (UK) Limited, 1977.
9. Knight, N.F. and J.H. Starnes. "Postbuckling Behavior of Axially Compressed Graphite Epoxy Cylindrical Panels with Circular Holes," in Collapse Analysis of Structures, ed. by L.H. Sobel, ASME, PVP Vol. 84, 1984.
10. Tisler, T.W. Collapse Analysis of Cylindrical Composite Panels with Large Cutouts Under an Axial Load. M.S. Thesis GA/MS/86D-1. School of Engineering, Air Force Institute of Technology (AU), Wright-Patterson AFB, OH, 1986.
11. Lee, C.E. Numerical Determination of the Effects of Boundary Conditions on the Instability of Composite Panels with Cutouts. M.S. Thesis GA/AA83D-4. School of Engineering, Air Force Institute of Technology (AU), Wright-Patterson AFB, OH, 1983.
12. Sobel, L.H. and Kevin Thomas. Evaluation of the STAGSC-1 Shell Analysis Computer Program. WARD-10881. Westinghouse Advanced Reactors Division, Madison PA, August 1981.

13. Almroth, B.O. and F.A. Brogan. Numerical Procedures for Analysis of Structural Shells. AFWAL-TR-80-3128. Air Force Flight Dynamics Laboratory, Wright-Patterson AFB, OH, March 1981.
14. Jones, R.M. Mechanics of Composite Materials. Hemisphere Publishing Corporation, 1975.
15. Cohen, G.A. "Conservativeness of a Normal Pressure Field Acting on a Shell," AIAA Journal, Vol 4, 1966.
16. Almroth, B.O. et al. Structural Analysis of General Shells Volume II User Instructions for STAGSC-1. LMSC-D633073. Applied Mechanics Laboratory, Lockheed Palo Alto Research Laboratory, Palo Alto CA, January 1983.
17. Rankin, C.C. and F.A. Brogan. "An Element-Independent Corotational Procedure for the Treatment of Large Rotations," in Collapse Analysis of Structures, ed. by L.H. Sobel, ASME, PVP Vol. 84, 1984.
18. Rankin, C.C. et al. "Enhancements to the STAGS Computer Code." NASA Contractor Report 4000, November 1986.
19. Esbach, O.W. Handbook of Engineering Fundamentals. John Wiley and Sons, 1975.
20. Ashton, J.E. et al. Primer on Composite Materials Analysis. Technomic Publishing Co., Inc., 1969.
21. Lubin, G. Handbook of Composites. Van Nostad Reinhold Company, 1982.
22. Metallic Materials and Elements for Aerospace Vehicle Structure, Vol. 1. MIL-HDBK-5C. September 1976.
23. Tsai, S.W. and H.T. Hahn. Introduction to Composite Materials. Technomic Publishing Co., 1980.

VITA

Gregory S. Egan [REDACTED]

[REDACTED] in 1979 [REDACTED] entered the United States Air Force Academy where he received a Bachelor of Science Degree in Mechanical Engineering in 1983. He was stationed at Vandenberg AFB in July 1983 and worked as a Space Shuttle External Tank Systems Engineer in the 6595TH Shuttle Test Group. After serving 4 years at Vandenberg AFB, he was accepted into the graduate Aeronautical Engineering program at the Air Force Institute of Technology in May 1987.

[REDACTED] [REDACTED]



UNCLASSIFIED

SECURITY CLASSIFICATION OF THIS PAGE

## REPORT DOCUMENTATION PAGE

Form Approved  
OMB No. 0704-0188a. REPORT SECURITY CLASSIFICATION  
UNCLASSIFIED

1b. RESTRICTIVE MARKINGS

2a. SECURITY CLASSIFICATION AUTHORITY

3. DISTRIBUTION / AVAILABILITY OF REPORT  
Approved for public release;  
distribution unlimited

2b. DECLASSIFICATION / DOWNGRADING SCHEDULE

4. PERFORMING ORGANIZATION REPORT NUMBER(S)

5. MONITORING ORGANIZATION REPORT NUMBER(S)

AFIT/GAE/AA/88D-12

5a. NAME OF PERFORMING ORGANIZATION

School of Engineering

6b. OFFICE SYMBOL  
(If applicable)  
AFIT/ENY

7a. NAME OF MONITORING ORGANIZATION

6c. ADDRESS (City, State, and ZIP Code)

Air Force Institute of Technology  
Wright-Patterson AFB OH 45433-6583

7b. ADDRESS (City, State, and ZIP Code)

8a. NAME OF FUNDING / SPONSORING  
ORGANIZATION8b. OFFICE SYMBOL  
(If applicable)

9. PROCUREMENT INSTRUMENT IDENTIFICATION NUMBER

8c. ADDRESS (City, State, and ZIP Code)

10. SOURCE OF FUNDING NUMBERS

PROGRAM  
ELEMENT NO.PROJECT  
NO.TASK  
NO.WORK UNIT  
ACCESSION NO.

11. TITLE (Include Security Classification)

NONLINEAR FINITE ELEMENT ANALYSIS OF A GENERAL COMPOSITE SHELL

12. PERSONAL AUTHOR(S)

Gregory S. Egan, B.S., Capt, USAF

13a. TYPE OF REPORT  
MS Thesis13b. TIME COVERED  
FROM \_\_\_\_\_ TO \_\_\_\_\_14. DATE OF REPORT (Year, Month, Day)  
1988 November15. PAGE COUNT  
177

16. SUPPLEMENTARY NOTATION

17. COSATI CODES

FIELD	GROUP	SUB-GROUP
12	01	

18. SUBJECT TERMS (Continue on reverse if necessary and identify by block number)

Finite Element Analysis  
Composite Materials

19. ABSTRACT (Continue on reverse if necessary and identify by block number)

Thesis Advisor: Anthony Palazotto  
Professor  
Department of Aeronautical and Astronautical Engineering

20. DISTRIBUTION / AVAILABILITY OF ABSTRACT

☒ UNCLASSIFIED/UNLIMITED ☐ SAME AS RPT. ☐ DTIC USERS21. ABSTRACT SECURITY CLASSIFICATION  
UNCLASSIFIED

22a. NAME OF RESPONSIBLE INDIVIDUAL

Anthony Palazotto, Professor

22b. TELEPHONE (Include Area Code)  
(513) 255-299822c. OFFICE SYMBOL  
ENY

DD Form 1473, JUN 86

Previous editions are obsolete.

SECURITY CLASSIFICATION OF THIS PAGE

UNCLASSIFIED

UNCLASSIFIED

The Structural Analysis of General Shells (STAGSC-1) finite element code has the capability to consider composite shells. It also has the feature of incorporating nonlinear geometric analysis in a study. These features are considered in this research of a general composite structure. It has been found that the incorporation of the nonlinear analysis leads to displacement results which are within 15% of experimentation; linear results err by over 75% due to large displacements. The shell is loaded with equivalent aerodynamic pressures which result in an asymmetric response. This is depicted quite well by the model incorporated in the analysis.

UNCLASSIFIED